NASA Contractor Report 198379

NASA-CR-198379
19960001964

Theoretical Study of Cathode Surfaces and High-Temperature Superconductors

Wolfgang Mueller
Analatom, Inc.
Westlake, Ohio

August 1995

Prepared for
Lewis Research Center
Under Contract NAS3–25940

National Aeronautics and
Space Administration

TABLE OF CONTENTS

1. SUMMARY

A breakthrough has been achieved in the computational modeling of the work functions and emissive properties of B- and M-type cathodes. With reasonable assumptions for the bare metal work functions and a change in the structure of the BaO overlayer from square networks for cubic substrates to equi-triangular networks for hexagonal substrates, minimum work functions at 1200 K of 1.95 eV for BaO/W, 1.79 eV for BaO/Ir-W, and 1.75 eV for BaO/Os-W have been obtained that are in excellent agreement with experiment. Based on these results, a microscopic explanation is presented for the improved emission from alloy relative to tungsten cathode surfaces, which has been one of the long outstanding questions in thermionic cathode research. Other surfaces investigated with quasirelativistic cluster calculations include K and Cs on W(100) and Ba on W(100) and W(110).

A cluster embedding approach has been developed and applied to the simulation of the bulk environment in W and the surface environment of O on W. Densities of states have been generated for both systems, which show that an embedded W atom acquires bulk character and that the dominant features in inverse photoemission spectra of O/W(100) at room and elevated temperatures can be described.

The adsorption geometries of Ba and BaO on W(100) have been determined from a comparison of inverse photoemission spectra with fully relativistic embedded cluster calculations. Very good agreement is obtained between the observed two-dimensional band structures and calculated densities of unoccupied states. The height of Ba above the W(100) surface is found to be approximately 2.38 Å, and Ba and O are adsorbed on W(100) at room temperature at alternate fourfold hollow sites.

Initial calculations for models of scandate surfaces show that the surface dipoles for Sc and O on W are small, but change dramatically when Ba is added, in which case low work functions are expected. For Sc/W(100), the change in the observed band structure from half to full monolayer coverage is well described by cluster calculations.

For the $YBa_2Cu_3O_7$ superconductor, a comparison has been made between non-, quasi-, and fully relativistic Xα cluster results.

2. INTRODUCTION

The explanation of the emission enhancement in dispenser cathodes, an understanding of the mechanism for high emission from scandate surfaces, and the determination of the geometrical and electronic structure of cathode surfaces under operating conditions are among the chief questions in thermionic cathode research.

Significant accomplishments have been achieved in these areas during the course of the present theoretical study. While some previous attempts had been made to explain the observed enhancement of emission in alloy cathodes, they all failed to provide a consistent description of the whole spectrum of low-work-function surfaces. Most of the ideas were based on empirical data or considerations for pure substrate metals, and did not take into account any effects due to different crystal structures and alloy formation, which are much more difficult to address. It is, however, the alloy substrate or the combined Ba-Sc-O surface complex that provides the best emission, better than either of its components.

With the present computational cluster approach, different crystal structures and alloys have been explicitly investigated from first principles for the first time. These studies have provided the long awaited explanation for the emission enhancement in dispenser cathodes, and have enabled the determination of adsorption geometries by comparison of calculated densities of states with photoemission experiments. The theoretical approach is currently being further refined to achieve even better predictive accuracy. This is required because detailed information about the atomic surface structure is not available in most cases.

This report is organized as follows: The results for B- and M-type dispenser cathodes and the microscopic origin of the emission enhancement are discussed first. Some additional results for other low-work-function surfaces and the embedding approach are described next. The comparison of inverse photoemission spectra with fully relativistic embedded cluster results leads to the determination of the adsorption geometries of Ba and BaO on W(100). A series of calculations in preparation for the study of scandate surfaces is then presented, followed by results for the electronic structure of O/W(100) and the $YBa_2Cu_3O_7$ superconductor. A critical assessment and references conclude the first part of this report.

The major results have been described in several publications. Copies of five of these journal articles are attached and form the second part of the report.

3. EMISSION ENHANCEMENT IN DISPENSER CATHODES

One of the major accomplishments of the present theoretical study was a microscopic explanation of the emission enhancement in alloy relative to tungsten dispenser cathodes. This achievement became possible because (a) a theoretical approach for the calculation of work-function curves based on the depolarization of surface dipoles had been developed, and (b) the dependence of the dipole properties of BaO on various substrates with different crystal structures has been investigated explicitly for the first time.

The results are described in two publications which are attached to this report. In "Theoretical Modeling of Dispenser Cathode Emission Properties" (IEEE Trans. Electron Devices, pp. 399-402, 1991) the general approach is described and results are presented for BaO on Pt, W, Os, and Os-W. In "Mechanism of Emission Enhancement in Barium Dispenser Cathodes" (Proc. Tri-Service/NASA Cathode Workshop, pp. 96-100, 1992) the above systems are supplemented by the Re and Ir alloys of W, and the temperature dependence of the substrate metal work functions is included. Excellent results have been obtained for the work functions of BaO on the hexagonal alloy surfaces relative to BaO on cubic W and Pt.

In this section, the major results are highlighted and additional supporting data are presented. The calculations are based on Xα scattered-wave programs developed by Case and Yang (1980) and Cook and Case (1989). Quasirelativistic calculations have been carried out to investigate the surface electronic structure of BaO adsorbed on body-centered-cubic (bcc) W(100) and W(110), face-centered-cubic (fcc) Pt(111), hexagonal-close-packed (hcp) Os(10$\bar{1}$0), and Re, Os, and Ir alloys of W with the hcp crystal structure. For the Os-W system, a W-rich and an Os-rich substrate cluster have been considered.

The substrate is modeled with clusters which typically contain about 20 atoms in three layers. Surface-dipole properties are then calculated for clusters with 2 and 3 units of BaO, which is assumed to be adsorbed in an upright position in all cases. As an example, the $[BaO]_{2(3)}/Os_{21}$ cluster is shown in Fig. 1. Ba heights above the surface of 6.0 a_0 for W(100), 7.39 a_0 for W(110), and 6.9 a_0 for Pt(111) and all (10$\bar{1}$0) surfaces are employed. A Ba-O separation of 4.9 a_0 is used for W(100) and all (10$\bar{1}$0) surfaces, 4.95 a_0 for W(110), and 5.1 a_0 for Pt(111). (1 a_0 = 1 Bohr radius = 0.5292 Å). These geometries are based on suggestions by Tuck et al. (1986).

FIGURE 1. $[BaO]_{2(3)}/Os_{21}$ cluster.

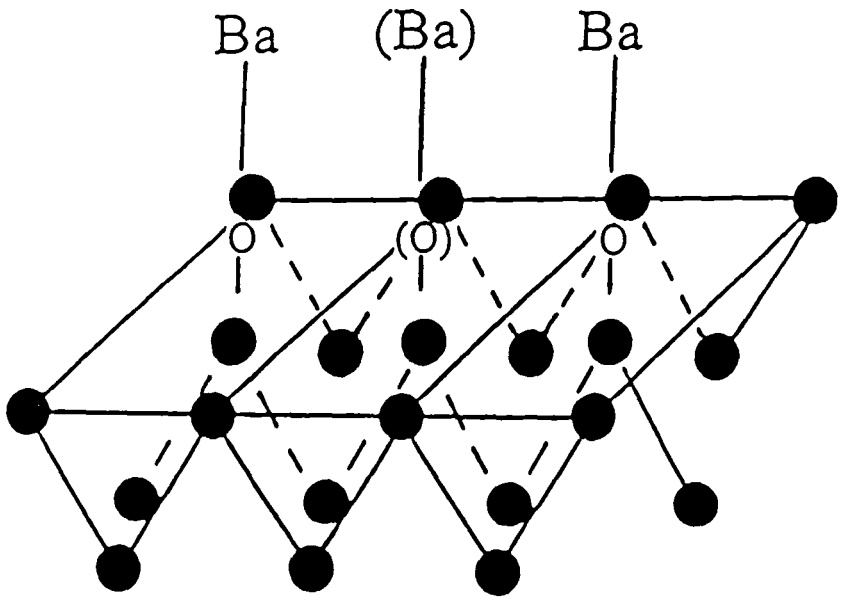

The calculated surface dipoles (μ) and net atomic charges (q) on Ba and O for the different systems are given in Table I. The surface dipoles increase in the series of BaO on bcc W(100) to the hcp $(10\bar{1}0)$ surfaces and fcc Pt(111). The net charges on Ba increase as well, while the net charges on O become smaller.

The decrease in the surface dipole per BaO from the clusters with 2 as compared to 3 BaO units is caused by the depolarization of the dipoles at smaller separations (higher coverages) and used to calculate the polarizability α of the charge distribution at a BaO site, according to

$$\alpha = \Delta\mu \; / \; f \; ,$$

where $\Delta\mu = \mu_0 - \mu_f$ is the change in the surface dipole and

$$f = 4/3 \; \mu_0 \; / \; (r^2+r_z^2)^{3/2}$$

is the additional dipole field present in the cluster with the higher surface coverage; r is the Ba-Ba distance and $r_z = \mu_0/(2q_0^{Ba})$ is 1/2 of the dipole length of the initial surface dipole. Atomic units are used in these equations, i.e., 1 a.u. (polarizability) = 0.1482 $Å^3$ and 1 a.u. (dipole moment) = 2.542 Debyes. By using the same substrate cluster, the effects of cluster size and shape on α are minimized. As a major result it is found that the polarizability exhibits a minimum for hcp substrates (see Table II below).

TABLE I.

Initial and final dipole moments μ (Debyes) per BaO and for the substrate clusters, net atomic charges q (electrons) on Ba and O, and interatomic distances r_{Ba-Ba} (Bohrs) for BaO on different substrates from quasirelativistic Xα calculations.

Cluster		μ(D)	q^{Ba}(e)	q^{O}(e)	$r_{Ba-Ba}(a_0)$
$Ba_2O_2/W_{19}(100)$	[μ_0=]	31.2	1.63 [=q_0^{Ba}]	-0.51 [=q_0^{O}]	11.96
$Ba_3O_3/W_{19}(100)$	[μ_f=]	18.0	1.25/0.86	-0.60/-0.74	5.98
$W_{19}(100)$	[μ_{sub}=]	0.0			
$Ba_2O_2/W_{23}(110)$		43.7	1.60	-0.53	11.96
$Ba_3O_3/W_{23}(110)$		25.7	1.32/0.99	-0.66/-0.77	5.98
$W_{23}(110)$		0.0			
$Ba_2O_2/Re_{11}W_{10}(10\bar{1}0)$		41.4	1.69	-0.40	10.44
$Ba_3O_3/Re_{11}W_{10}(10\bar{1}0)$		25.4	1.23/1.07	-0.47/-0.56	5.22
$Re_{11}W_{10}(10\bar{1}0)$		19.3			
$Ba_2O_2/W_{11}Os_{10}(10\bar{1}0)$		38.4	1.68	-0.40	10.36
$Ba_3O_3/W_{11}Os_{10}(10\bar{1}0)$		23.3	1.21/1.06	-0.45/-0.57	5.18
$W_{11}Os_{10}(10\bar{1}0)$		14.2			
$Ba_2O_2/Os_{11}W_{10}(10\bar{1}0)$		41.1	1.70	-0.39	10.36
$Ba_3O_3/Os_{11}W_{10}(10\bar{1}0)$		25.0	1.22/1.06	-0.45/-0.58	5.18
$Os_{11}W_{10}(10\bar{1}0)$		19.9			
$Ba_2O_2/Os_{21}(10\bar{1}0)$		40.5	1.71	-0.38	10.36
$Ba_3O_3/Os_{21}(10\bar{1}0)$		25.7	1.28/1.13	-0.46/-0.59	5.18
$Os_{21}(10\bar{1}0)$		17.6			
$Ba_2O_2/Ir_{11}W_{10}(10\bar{1}0)$		43.1	1.71	-0.36	10.48
$Ba_3O_3/Ir_{11}W_{10}(10\bar{1}0)$		27.5	1.27/1.09	-0.43/-0.60	5.24
$Ir_{11}W_{10}(10\bar{1}0)$		22.1			
$Ba_2O_2/Pt_{16}(111)$		51.9	1.82	-0.24	9.06
$Ba_2O_2/Pt_{12}(111)$		34.5	1.15	-0.27	6.04
$Pt_{16}(111)$		0.0			
$Pt_{12}(111)$		10.7			

Work-function curves are then obtained from the equation

$$\phi = \phi_0 - 1.88\, e\mu_0 n / (1+c\alpha n^{3/2})$$

where n is the coverage (in 10^{15} atoms/cm^2) and c a constant which depends on the geometrical structure of the BaO overlayer and the validity of the point-dipole approximation that is used to calculate the field of the dipole network. The constant c has been adjusted such that the minimum work function for BaO/W(100) equals 2.0 eV, which yields c=2.41. By assuming that a square network of dipoles forms on cubic substrates and an equi-triangular network on hexagonal substrates, the constants c for the two cases are related by $c_{hex} = 11/9\ c_{cubic}$, and the dimension of n_{hex} is $2/\sqrt{3}\ n_{cubic}$. It should be noted that only the work function change $\Delta\phi = \phi - \phi_0$ is obtained from calculated properties and that the minimum work functions depend critically on the bare metal work functions ϕ_0 of the different crystal faces considered. Since thermionic cathodes are operated at elevated temperatures, estimated values of ϕ_0 at operating temperature are used.

The bare metal work functions ϕ_0 given in Table II for a temperature of 1200 K are based on the empirical temperature dependencies of the polycrystalline work functions for the pure metals, which are as follows:

W : $\phi_0(T) = 4.52 + 0.6 \times 10^{-4}\ T$
Re : $\phi_0(T) = 4.93 + 0.4 \times 10^{-4}\ T$
Os : $\phi_0(T) = 5.43 - 3.9 \times 10^{-4}\ T$
Ir : $\phi_0(T) = 5.4 - 0.3 \times 10^{-4}\ T$
Pt : $\phi_0(T) = 5.3 + 2.0 \times 10^{-4}\ T$.

Since work functions for the $(10\bar{1}0)$ face of Os and the alloy substrates are not known, the following procedure has been used. For the alloy substrates, first the averages of the polycrystalline metal work functions at 1200 K have been determined and then all work functions for the hcp substrates have been increased by 0.22 eV to account for the differences between the polycrystalline and $(10\bar{1}0)$ values, as taken from the observed increase for hcp rhenium.

With these choices of ϕ_0 and an assumed change in the geometrical structure of the BaO overlayer, the calculated minimum work functions for the alloy cathodes are in excellent agreement with expectation. As shown in Table II and Fig. 2, the Os-W and Ir-W systems have a minimum work function that is up to 0.2 eV lower than for BaO/W, while ϕ_m for BaO/Pt is 0.4 eV higher. An increase in the surface concentration of W in the Os-W system, denoted in Table II as W-Os, gives rise to an increase in ϕ_m from 1.75 eV to 1.82 eV, which is consistent with the observed emission degradation with increasing life of Os-W based cathodes.

TABLE II.

Calculated initial surface dipoles μ_0(D), polarizabilities α(Å^3), work-function data ϕ(eV) at 1200 K, optimum coverages n_m(10^{15} atoms/cm^2), and Ba binding energies E^{Ba}(eV) for BaO on W, Os, Pt, and different alloys. ϕ_m for BaO/W(100) has been adjusted(*).

System	Lattice	μ_0	α	ϕ_0	$\Delta\phi$	ϕ_m	n_m	E^{Ba}
BaO/W(100)	bcc	31.2	16.6	4.65	-2.65	2.00*	0.14	5.4
BaO/W(110)	bcc	43.7	23.8	5.33	-2.92	2.41	0.11	4.8
BaO/W(poly)	bcc	(31.2)	(16.6)	4.6	-2.65	1.95	0.14	-4.8
BaO/Re-W(10$\bar{1}$0)	hcp	41.4	15.4	5.0	-3.23	1.77	0.14	5.9
BaO/W-Os(10$\bar{1}$0)	hcp	38.4	14.1	5.0	-3.18	1.82	0.15	5.8
BaO/Os-W($\bar{1}$010)	hcp	41.1	15.1	5.0	-3.25	1.75	0.15	6.0
BaO/Os(10$\bar{1}$0)	hcp	40.5	13.7	5.2	-3.42	1.78	0.16	6.5
BaO/Ir-W(10$\bar{1}$0)	hcp	43.1	15.1	5.2	-3.41	1.79	0.15	6.1
BaO/Pt(111)	fcc	51.9	27.8	5.5	-3.13	2.37	0.10	3.6

Estimates for the Ba binding energies have been calculated from the clusters with the higher surface coverage using the simple dipole expression

$$E^{Ba} = (q_{av}^{Ba})^2/r_{dip}^{Ba} = (q_{av}^{Ba})^3/\mu_f',$$

where q_{av}^{Ba} is the average net charge on Ba and $\mu_f'=(3\mu_f-\mu_{sub})/3$ the surface dipole corrected for the substrate dipole. The reasoning behind this modification is that the Ba binding energy is determined by the charge transfer from Ba to the substrate and the corresponding dipole length r_{dip}^{Ba}, and that it should not be affected by any preexisting charge transfer in the substrate. The interaction of the surface dipoles, on the other hand, *is* expected to be affected by properties of the substrate. If μ_0 and μ_f were also corrected for μ_{sub} for the determination of the polarizability and work-function data, the effect of the substrate would be largely lost. Indeed, very similar surface dipoles and almost identical work functions of about 2.0 eV would be obtained for all alloy systems.

It is possible that the calculated surface dipoles are too large. This is in part related to the nonzero μ_{sub} and to the fact that a finite cluster has a higher "work function" than a surface. Because α is calculated from the change in the surface dipole at higher coverage on the same substrate cluster, μ_0 and α are affected to a similar extent, and the calculated work-function changes are found to be highly reliable.

FIGURE 2.

Calculated work-function curves for B- and M-type cathodes.

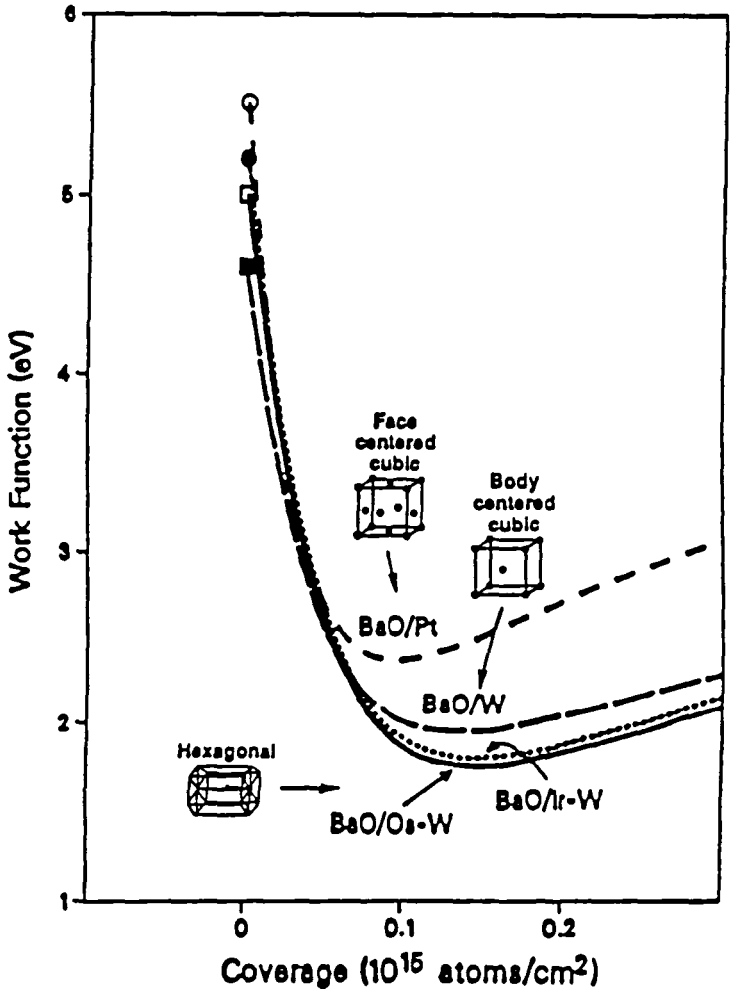

While μ_0 determines the initial slope of the work-function/coverage curve, the polarizability α governs the strength of the dipole interaction. A smaller value of α leads to a smaller depolarization and a lower final work function. The smaller polarizability of the surface dipole on hexagonal substrates with the $(10\bar{1}0)$ orientation as compared to cubic substrates is, therefore, responsible for the lowering of the work function from B- to M-type cathodes and provides the long-awaited microscopic explanation for the emission enhancement that is observed for coated and mixed-metal cathodes. The optimum for Os-W cathodes results from the combination of a sufficiently large initial surface dipole μ_0, a small polarizability α, and a not too high initial bare metal work function ϕ_0.

4. INTERACTION OF K,Cs,Ba WITH TUNGSTEN

In order to investigate the accuracy of the cluster approach as it has been used so far, quasirelativistic Xα cluster calculations have been carried out for K/W(100), Cs/W(100), and Ba on W(100) and W(110), because more detailed experimental data are available for these systems than for the more complicated BaO/W-alloy cathode surfaces.

The calculated surface-dipole properties and work-function data for K/W(100) with different K-surface distances are given in Table III. Clusters with 2 or 3 K atoms on W_{19} were used. The work-function/coverage curves are shown in Fig. 3. The best agreement between theory and experiment is obtained for a height of K above the surface of R = 4.5 a_0. The calculated work-function minimum, ϕ_m = 1.70 eV, is in reasonable agreement with the experimental values of 1.83 and 1.88 eV, and the K surface coverage, n_m = 0.28 x 10^{15} atoms/cm^2, falls in between the experimental values of 0.22 and 0.36 x 10^{15} atoms/cm^2, which apparently have a large uncertainty.

TABLE III.

Initial net charges on potassium q_0^K(electrons), initial and final surface dipoles μ_0 and μ_f(D), polarizabilities α(Å^3), work-function data φ(eV), and optimum coverages n_m(10^{15} atoms/cm^2) for K/W(100) from quasirelativistic Xα calculations with different heights R(a_0) of potassium above the surface and from experiments.

K/W(100)	q_0^K	μ_0	μ_f	α	ϕ_0	Δφ	ϕ_m	n_m
R = 3.0	0.68	11.7	9.0	8.3	4.65	-1.58	3.07	0.22
R = 4.0	0.81	14.8	12.4	6.1	4.65	-2.45	2.20	0.26
R = 4.5	0.86	16.6	14.3	5.5	4.65	-2.95	1.70	0.28
Expt.(SG,1966)		11.5	....	4.1*	4.65	-2.48	2.17	0.34
Expt.(FS,1971)		13.5	....	...	4.65	-2.77	1.88	0.22
Expt.(BBM,1975)		9.7	....	...	.....	....	1.83	0.36

* The quoted value of α (4.1) was used to calculate the work-function data. It is related to the experimental value by α = α_{exp}/8.46 due to the different choice of the parameter c in the depolarization formula.

FIGURE 3.

Calculated work-function/coverage curves for K/W(100) with different heights R(a_0) of K above the surface.

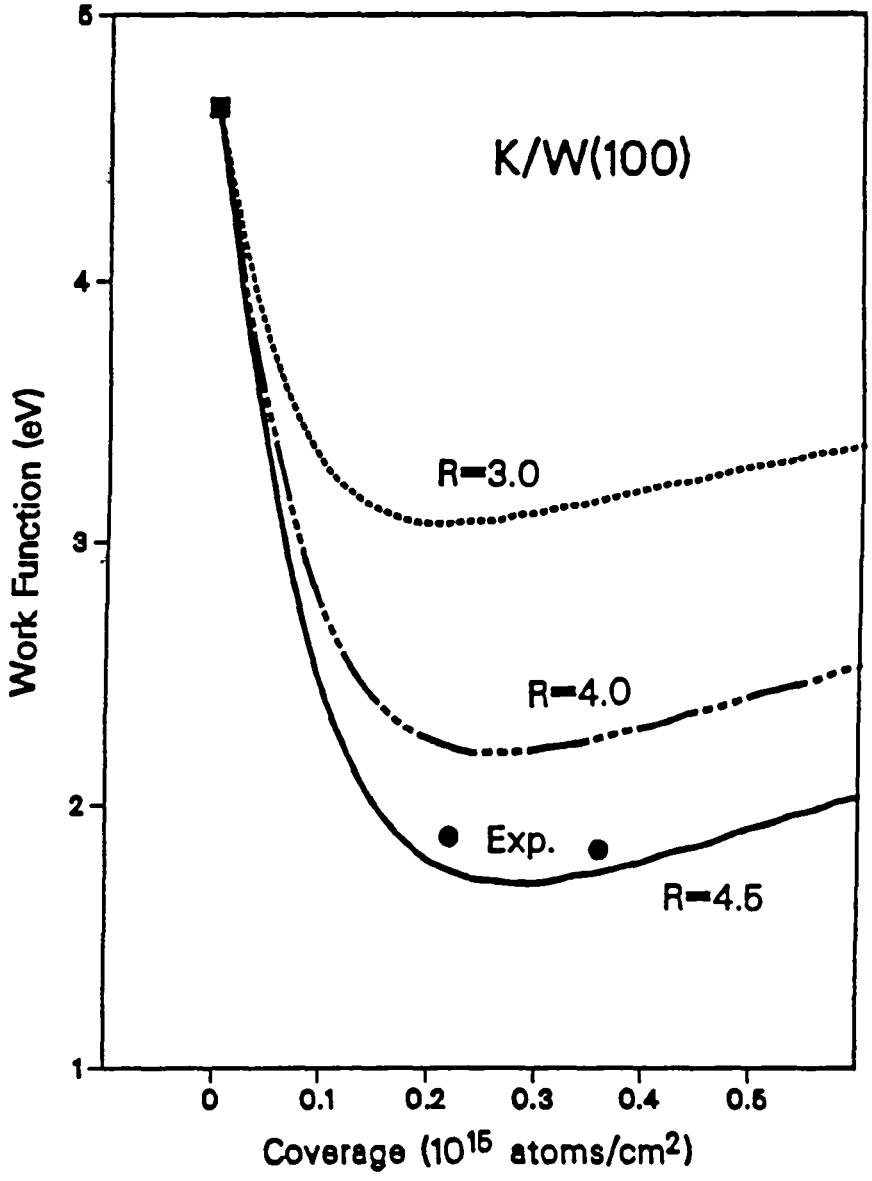

A comparison of the experimentally determined initial surface dipoles μ_0, which range from 9.7 to 13.5 Debyes, with the calculated value of 16.6 Debyes at R = 4.5 a_0 indicates, however, that the calculated μ_0 (and α) is somewhat too large. This is likely related to that fact that the finite substrate cluster has a higher "work function" than the real surface, which results in a larger charge transfer from the adsorbate to the cluster. One possibility to correct this problem is to align the cluster Fermi level with the work function of the surface. This may be accomplished by adding constant potentials in the atomic spheres of the substrate cluster. Another possibility is to investigate clusters with a significantly larger number of surface atoms, which is explored next.

For Cs/W(100), a large substrate cluster with 25 first-layer and 4 second-layer W atoms (Cs/W_{29}) has been investigated to determine the initial surface dipole μ_0. Earlier results (Müller, 1994) with substrate clusters consisting of three W layers, up to 10 W surface atoms and 2 Cs atoms gave values for μ which decreased from 19.1 to 17.7 Debyes with increasing cluster size and had not yet converged.

TABLE IV.

Total cluster dipoles μ, substrate cluster dipoles μ_{sub} of the bare substrate clusters, and adsorbate-related dipoles $\mu_{Cs}=\mu-\mu_{sub}$ (Debyes) for Cs/W(100) from quasirelativistic Xα calculations.

Cs/W_{29}		μ = 42.99	
W_{29}	Cs/W sphere radii	μ_{sub} = 31.91	μ_{Cs} = 11.08
W_{29}	standard radii	μ_{sub} = 31.70	μ_{Cs} = 11.29

Similar to the results for K/W(100), the dipole moments obtained earlier for Cs/W(100) were somewhat higher than the range of experimental values (13.3-17.7 Debyes). It was therefore expected that the larger Cs/W_{29} cluster would give a better result. Surprisingly, the dipole moment of Cs/W_{29} was calculated to be ~43 D, which is 2-3 times larger than the experimental values. This discrepancy was, however, readily resolved by realizing that the W_{29} substrate cluster, which is unsymmetrical in the direction perpendicular to the surface, has a very large dipole moment of its own. By subtracting the substrate dipole, μ_{sub} ~ 32 D, from the total cluster dipole, μ ~ 43 D, the Cs-related dipole μ_{Cs} is found to be ~ 11 D. The result that μ_{Cs} is now somewhat smaller than the

experimental values may be related to the fact that the Cs/W_{29} cluster contains only 2 substrate layers while the earlier clusters contained 3 layers, and 2 layers are probably not sufficient.

Results for Ba on W(100) and W(110) are given in Table V. For the standard Ba/W(100) system, a W_{19} substrate cluster has been employed with either 2 or 3 adsorbed Ba atoms. For the data indicated by *, different substrate clusters have been used for different Ba coverages, which is the approach that was taken previously (Müller, 1994). In the latter case, Ba_2/W_{24} and Ba_3/W_{19} were used for W(100), and Ba_2/W_{30} and Ba_3/W_{23} for W(110). The polarizability α was calculated by considering all dipole interactions in the cluster with the higher surface coverage, which led to a somewhat larger value (2.7) for the parameter c. Table V shows that the difference in treatment for Ba/W(100) has a negligibly small effect on the work-function results. The calculated Ba coverage for Ba/W(100) at the work-function minimum is, however, much smaller than expected. For a Ba height of 5.0 a_0 on W(110) very similar results are obtained.

In the future, it is planned to consider two-dimensional arrays of adsorbates on substrate clusters with up to 3 layers. This is expected to correct the deficiencies of the results from one-dimensional arrays of adsorbates with respect to the optimum Ba coverages.

TABLE V.

Initial net charges on barium μ_0^{Ba}(electrons), initial and final surface dipoles μ_0 and μ_f(D), polarizabilities α(Å^3), work-function data ϕ(eV), and optimum coverages n_m(10^{15} atoms/cm^2) for Ba/W(100) and Ba/W(110) from quasirelativistic Xα calculations with different heights R(a_0) of barium above the surface and from experiments.

System	R	q_0^{Ba}	μ_0	μ_f	α	ϕ_0	$\Delta\phi$	ϕ_m	n_m
Ba/W(100)	4.5	1.33	21.8	12.8	14.4	4.65	-2.04	2.61	0.15
Ba/W(100)*	4.5	1.30	20.5	12.8	11.8	4.65	-2.03	2.62	0.16
Expt.(LK,1992)	...	....	....	....	....	4.63	-2.00	2.63	0.50
Expt.(HS,1968)	...	....	....	....	....	4.66	-2.10	2.56	....
Ba/W(110)*	5.0	1.42	33.2	21.0	15.9	5.33	-2.69	2.64	0.13
Expt.(HS,1968)	...	....	....	....	....	5.13	-2.17	2.96	....

* Different clusters were used for different coverages (c=2.7), see text.

5. SIMULATION OF CLUSTER ENVIRONMENT

The embedding scheme for Xα scattered-wave cluster calculations has been further developed and tested for the simulation of the bulk environment of a W tungsten atom in a bcc W_9 cluster. This represents a particularly stringent test case since only one shell of nearest neighbors is present and also because these atoms all occupy surface positions in the cluster.

Three different fully relativistic calculations will be compared for this purpose. The first one is a conventional cluster calculation with standard atomic sphere radii and different atomic potentials for the inner atom and the eight equivalent outer atoms. In the second calculation, the sphere radii of the outer atoms are set equal to the radius of the inner atom (all $R_o=R_i$). In the third calculation, in addition to the radii, the potentials of the outer atoms are set equal to the potential of the inner atom (all $V_o=V_i$). The only atomic potential to be determined in this case is thus V_i, which is transferred to all outer atoms at each iteration and varied until a self-consistent solution is found. The inner atom is thereby embedded in a shell of atoms with identical potentials, as is the case in the bulk, but without long-range periodicity.

The results for the atomic charges (q), energies of the highest occupied state (ϵ_{max}), and the two dominant peaks (E) in the density of states below the Fermi level are given in Table VI.

TABLE VI.

Net atomic charges q (electrons) for inner (W_i) and outer (W_o) tungsten atoms of a body-centered-cubic W_9 cluster with and without modified atomic sphere radii and potentials, differences of the electronic charges within the atomic spheres $\Delta Q=Q(W_i)-Q(W_o)$, energies ϵ_{max} (eV) of the highest occupied state, and energies E (eV) of the two dominant peaks below the Fermi level.

Radii	Potentials	$q(W_i)$	$q(W_o)$	ΔQ	ϵ_{max}	E
Standard	$V_o \neq V_i$	-0.37	+0.05	-0.46	-5.07	-3.7/-3.0
All $R_o=R_i$	$V_o \neq V_i$	-1.93	+0.24	-1.73	-5.95	-3.3/-3.0
All $R_o=R_i$	All $V_o=V_i$	-0.28	+0.04	-0.13	-8.73	-3.0/-2.3
FLAPW Calc.	(JF,1984)	(0.0)	(0.0)	(0.0)	.....	-3.3/-2.0

The difference between the charges on the two atoms increases strongly for the calculation with identical radii, but falls back below the standard case for the calculation with identical radii *and* potentials. Because the net charges (q) contain large partitioned contributions from the electrons in the intersphere volume and because there is a large disparity between the environment of the inner and outer atoms, the difference in the charges in the atomic spheres, ΔQ, is probably a better indicator of the balance in the charge distribution. For the embedded calculation this difference is -0.13 electrons in favor of the central atom, i.e., reasonably small. ΔQ and q are, of course, zero in the bulk. The energy of the highest occupied state (ε_{max}) decreases with increasing bulk character, as expected.

The calculated densities of states (DOS) for the inner and outer W atoms in W_9 are shown in Figs. 4 and 5, respectively. The insert in the bottom panel of Fig. 4 is the calculated DOS for bulk bcc tungsten from the solid-state FLAPW calculation by Jansen and Freeman (1984). It shows two relatively sharp peaks at -3.3 and -2.0 eV and a broader feature near -5.5 eV. All of the cluster results exhibit this general pattern in the DOS below the Fermi level (E_F), with the standard calculation giving almost the best match with respect to the intensity pattern. A close inspection of the energies E of the two major peaks in Table VI, however, clearly identifies the embedded calculation as the one with the best overall agreement. The DOS for the outer atoms, shown in Fig. 5, all exhibit characteristic surface patterns, with a prominent surface peak just below and large density near E_F, in spite of the fact that the radius and potential of the embedded atom has been used in the second and third calculation, respectively.

In summary, the embedding of the central W atom in W_9 with a minimum environment of eight outer atoms proved to be quite successful for the description of the bulk tungsten environment. Contributions from this environment must, however, be excluded when computing the properties of the embedded system, since the total DOS for the entire cluster would have been dominated by surface features originating from the outer atoms.

The logical extension at this point would be the use of larger clusters, but then a solid-state band structure calculation could just as well be carried out with a similar effort and higher accuracy. The cluster embedding approach is much more useful in surface situations where band structure calculations are more difficult to do and the embedding in only two dimensions requires far fewer additional atoms than in the bulk. In cases where it is necessary to go beyond standard solid-state techniques, for example for the correct treatment of electron correlation or spin-orbit interaction and excited states, the cluster approach represents the only option.

FIGURE 4.

Densities of states for the inner "bulk" W atom in W_9 for the different calculations characterized in Table VI.

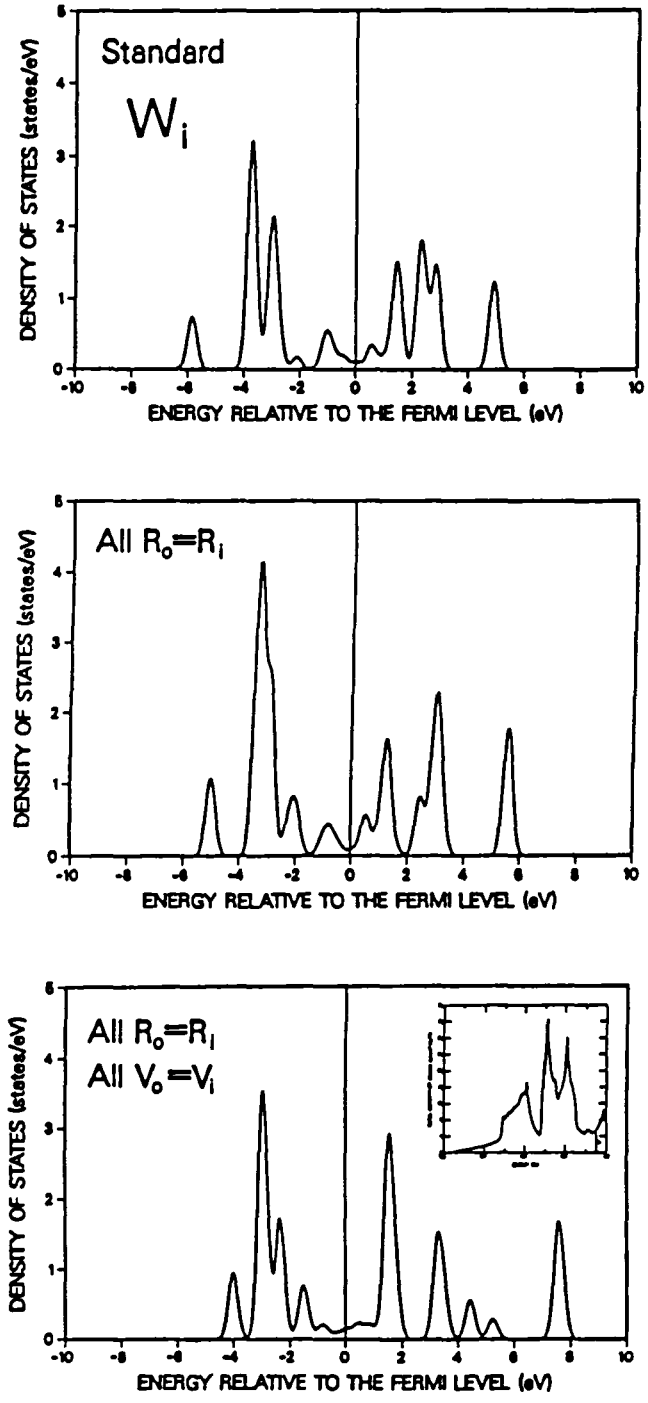

FIGURE 5.

Densities of states for the outer W atom in W_9 for the different calculations characterized in Table VI.

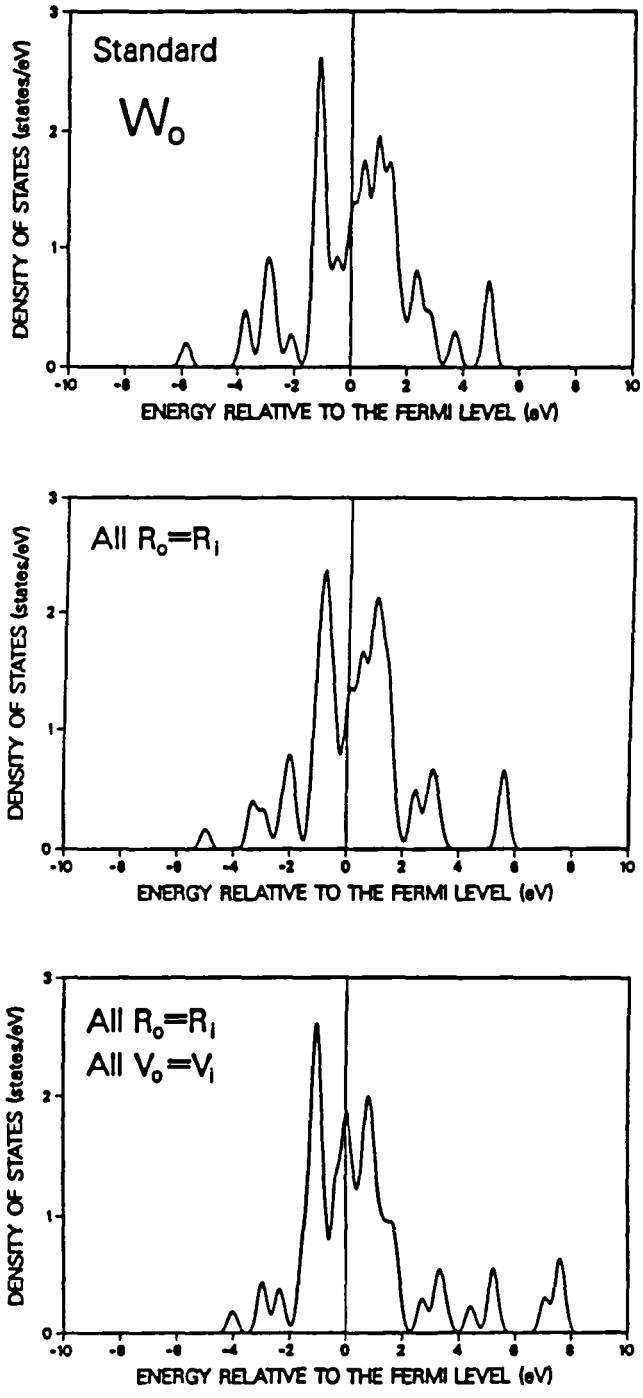

6. GEOMETRY OF Ba AND BaO ON W(100)

The presence of localized unoccupied Ba 5*d* states has been utilized to determine the geometry of adsorbed Ba and BaO on W(100). This has been achieved by comparing observed densities of unoccupied states using inverse photoemission spectroscopy (IPS) with results from fully relativistic embedded cluster calculations.

The IPS experiments were carried out by A. Lamouri and I.L. Krainsky. The measurements were performed in the isochromat mode by collecting photons at a fixed photon energy while varying the energy of the incoming electrons produced by a low-energy gun. IPS spectra were taken at different angles of electron incidence by rotating the sample, and angularly resolved spectra were obtained along two symmetry lines of the surface Brillouin zone (SBZ).

Ba and BaO adsorption on W(100) was modeled using a $W_{25}(16,9)$ substrate cluster which contains a 4x4 atom surface layer and a 3x3 atom subsurface layer. Ba is assumed to be adsorbed above alternate fourfold hollow sites of the surface layer, creating a centered (2x2) overlayer. For Ba and O adsorption, two different configurations have been considered (see Fig. 6): tilted, in which O is adsorbed above the vacant fourfold hollow sites, and upright, in which O is adsorbed directly below Ba.

FIGURE 6.

Cluster models for a c(2x2) layer of Ba and O on W(100) in the (a) tilted and (b) upright configurations. (c) illustrates the surface Brillouin zone of the clean W(100) surface (solid square) and that of the c(2x2) Ba or BaO on W(100) system (dashed square).

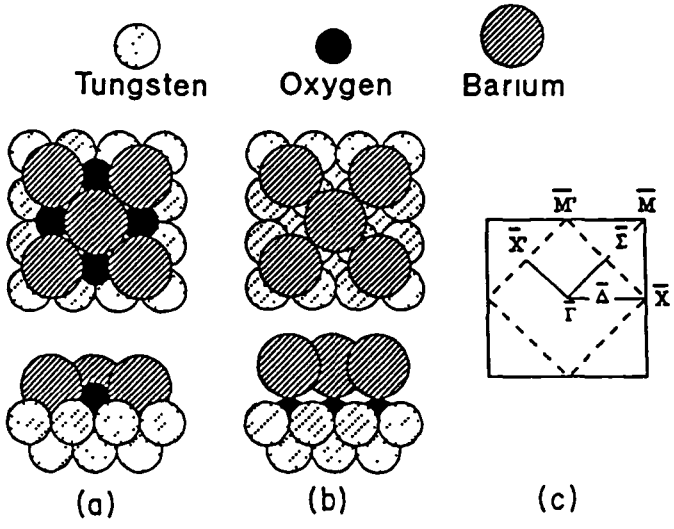

6.1 Ba/W(100)

Fully and quasirelativistic calculations have been carried out for Ba/W(100) with consideration of different levels of embedding of the central atoms in the employed cluster. The embedding is achieved by surrounding the "inner" $Ba/W_5(4,1)$ cluster with an additional shell of atoms in each layer, which leads to a $Ba_5/W_{25}(16,9)$ cluster. In embedded calculations, sphere radii and potentials are used for the outer atoms that are identical to those of the inner atoms in each layer. In a second set of calculations the modified sphere radii (but not potentials) are retained, and in the standard approach different sphere radii and potentials are used for all non symmetry-related atoms.

The computed surface dipoles and net atomic charges on Ba for the different calculations of Ba_5/W_{25} are given in Table VII. Fully relativistic embedded results have been obtained for three different heights of Ba above the surface. Both the surface dipole and the net charge on Ba are found to increase with increasing height of Ba above the surface. The comparison of the results for the different levels of embedding shows that the surface dipoles

TABLE VII.

Surface dipoles μ (Debyes) and net atomic charges q (electrons) on the inner/outer Ba atoms for Ba_5/W_{25} clusters with different heights R(Bohrs) of Ba above the surface and at different levels of calculation.

$Ba_5/W_{25}(16,9)$	$R(a_0)$	μ(D)	q^{Ba}(e)
Fully relativistic			
embedded	4.69 [2.48 Å]	33.8	1.12/0.50
embedded	4.50 [2.38 Å]	30.3	1.07/0.45
embedded	4.31 [2.28 Å]	26.8	1.02/0.41
modified radii	4.50	43.9	0.57/0.52
standard	4.50	31.0	0.45/0.45
Quasirelativistic			
embedded	4.50	51.6	1.20/1.34
modified radii	4.50	63.6	0.67/1.02
standard	4.50	55.3	0.58/1.01

(but not the net charges on the inner Ba atoms) are fairly similar for the embedded and standard calculations, while the dipole moments are larger for the calculations with modified radii. The dipole moments are also significantly larger for the set of quasirelativistic calculations which assign a much higher net charge to the outer Ba atoms.

FIGURE 7.

Fully relativistic DOS for an ordered c(2x2) Ba layer on W(100) for three different Ba heights above the surface. The total DOS are represented by solid lines and the Ba contributions by dashed lines.

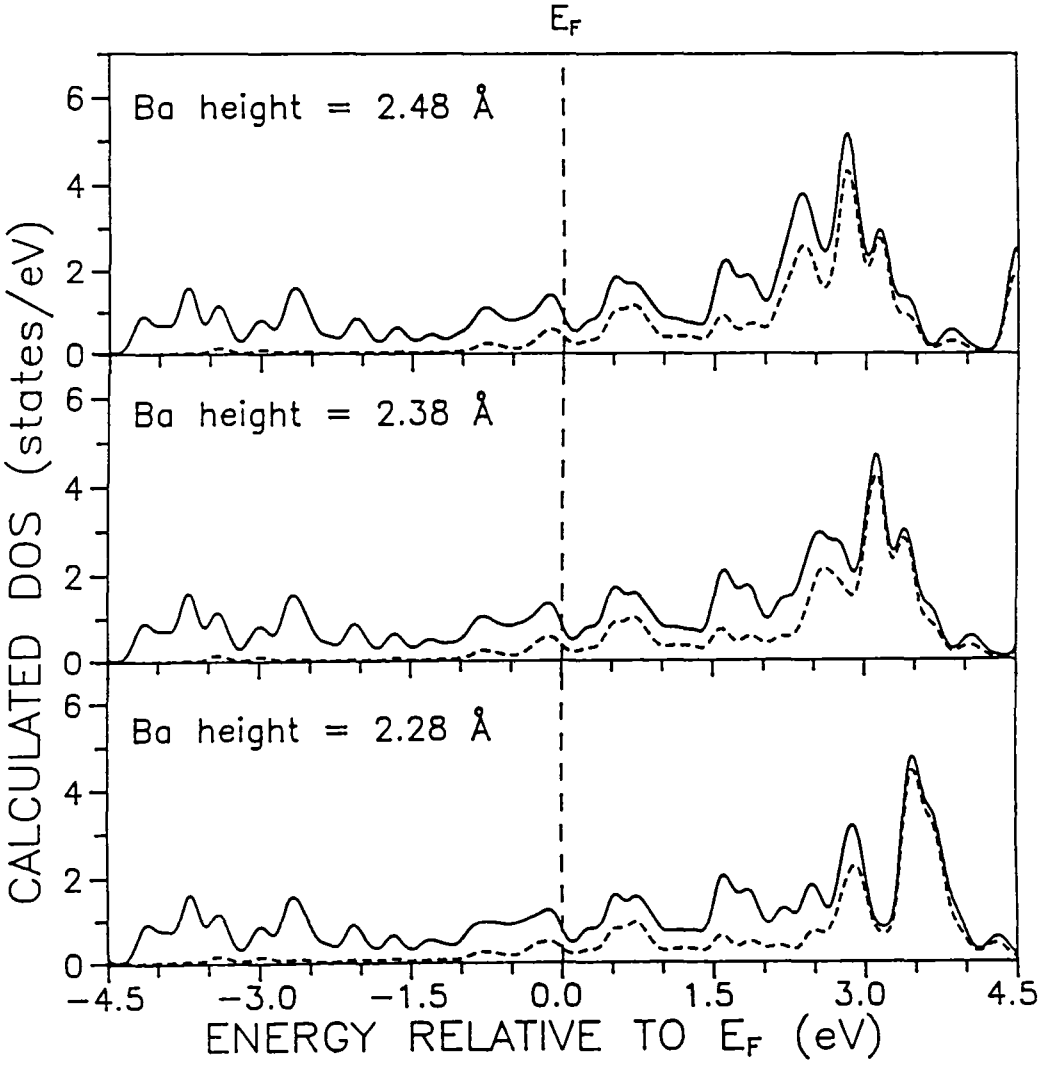

Densities of occupied and unoccupied electronic states (DOS) have been generated from the fully relativistic results for the inner Ba and W surface atoms with heights of Ba above the surface of 2.28, 2.38, and 2.48 Å. The results are shown in Fig. 7. The DOS below 2 eV are very similar in all cases and show only very small Ba contributions (as indicated by dashed lines) below the Fermi level (E_F). The DOS above E_F exhibits approximately equal contributions of Ba and W up to 2.5 eV and a dominant Ba 5*d* peak near 3 eV. The location of this peak shifts toward E_F with increasing Ba height and has been used to determine the Ba height by comparison with IPS spectra.

Fig. 8 shows on the left side the experimental DOS along the $\bar{\Gamma}\bar{\Delta}\bar{X}$ and $\bar{\Gamma}\bar{\Sigma}\bar{M}$ symmetry lines of the SBZ and on the right side the cluster DOS for a Ba height of 2.38 Å. The observed state above 3 eV is in very good agreement with the major Ba peak for this Ba height. The cluster DOS also shows the states observed near 2 5 eV (with the lower-energy state possibly shifted in the calculation), and the center of the dispersive band extending from 0.25 to 1.5 eV.

FIGURE 8.

Left panel: Experimental band structure for a c(2x2) layer of Ba on W(100). Right panel: Fully relativistic DOS for a Ba height of 2 38 Å. The solid line represents the total DOS; the short and long dashed lines represent the Ba *s+p* and *d* contributions, respectively

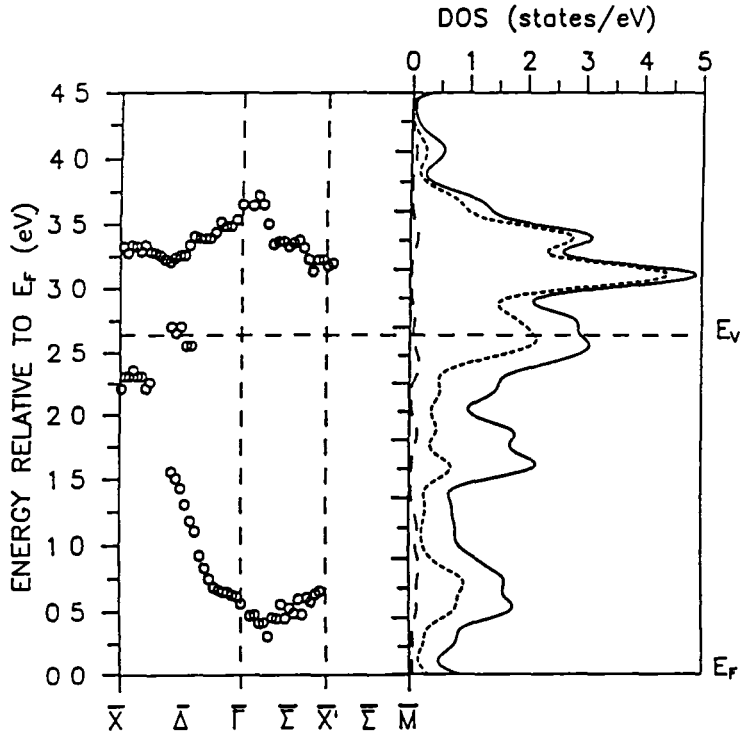

The dispersive part of the band centered near 0.6 eV and the observed states located near 2.5 eV have been found to show strong sensitivity to surface contamination and are completely quenched after oxygen adsorption exceeding 1.0 Langmuir. Because the contributions from the atomic layers to the observed spectra are expected to decay rapidly below the uppermost adsorbed layer, this observation is consistent with the large W contribution in the calculated total surface DOS in this energy range.

The state above 3 eV, on the other hand, changes only slightly with oxygen adsorption. It had previously been assigned to bulk W because a dispersive bulk W band is located in this range (Lamouri and Krainsky, 1992). Recent coverage-dependent data for Ba/W(100), however, reveal a Ba-induced feature near 3.4 eV in a region where no W states are observed. We therefore assign this peak now to Ba 5*d* and possibly W bulk states.

Since the employed W_{25} substrate cluster contains only surface atoms, no W bulk features could be expected. In order to test if subsurface W layers are partly responsible for the peak above 3 eV, a much larger calculation has been carried out for Ba/W(100). The employed Ba_{10}/W_{66} cluster consists of two Ba_5/W_{25} units that are combined bottom to bottom via a central W_{16} layer, and Ba is adsorbed on both sides of the symmetrical W_{66}(16,9,16,9,16) cluster.

The DOS for the Ba and W surface atoms of both clusters is compared in Figs. 9 (a) and (b), respectively. The contributions from the inner surface W_I, subsurface W_{II}, and central-layer W_{III} atoms are plotted in Fig. 9 (c). This figure shows that the location of the main Ba peak is affected by the symmetrical arrangement of Ba on both sides of the cluster (which is not believed to be a better model for the real surface) and that none of the W layers shows any significant DOS above 3 eV. The observed states between 0 and 2.5 eV, which contain a large W contribution, appear however to be better described.

Calculations by Hemstreet and Chubb (1993) for Ba/W(100) based on the full-potential linearized augmented-plane-wave (FLAP) method confirm the conclusions based on the cluster approach to a large extent. Their Ba height of 2.48 Å, which was derived from the minimum of the total energy, is within 5% of our optimum value of 2.38 Å.

The above results are described in a publication by A. Lamouri, W. Müller, and I.L. Krainsky in Physical Review B, vol. 50, pp. 4764-4770 (1994), entitled "Geometry and Unoccupied Electronic States of Ba and BaO on W(001)". Two previous other publications contain results for BaO/W and are entitled "Electronic Structure and Work Function Study of a Model Dispenser Cathode Surface" and "Geometry and Unoccupied Electronic States of a Model BaO Cathode Surface", copies of all of which are attached.

FIGURE 9.

Densities of states for the inner Ba and W_I surface atoms of (a) Ba_5/W_{25}, (b) Ba_{10}/W_{66}, and (c) the inner $W_{I,II,III}$ atoms of Ba_{10}/W_{66}. In (a) and (b) the solid lines represent the Ba+W_I DOS and the dashed lines the Ba contributions.

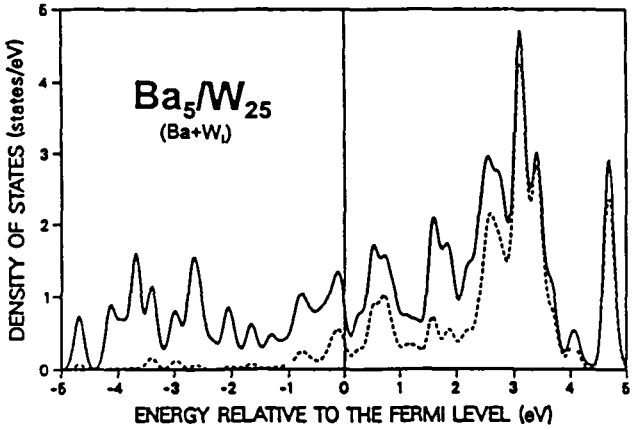

(a)

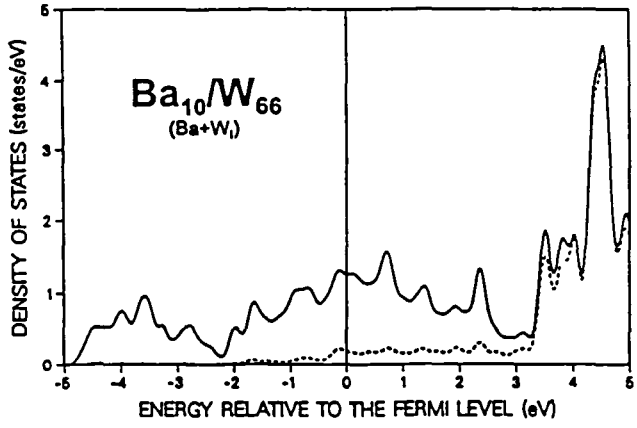

(b)

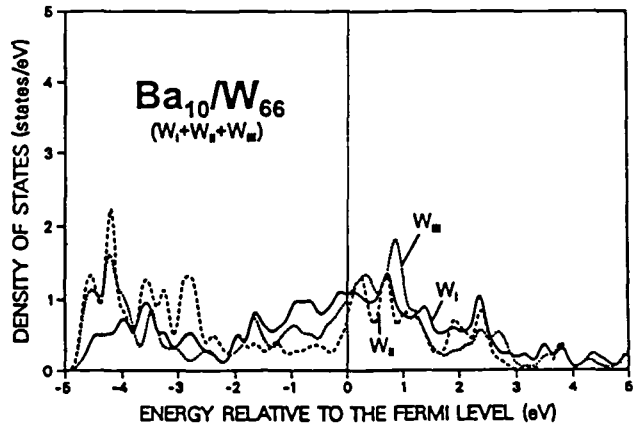

(c)

6.2 BaO/W(100)

When oxygen is added to the Ba/W(100) surface, adsorption can take place either at the vacant fourfold hollow sites or directly below Ba. These configurations are described as "tilted" or "upright" BaO, and the cluster representations have already been shown in Fig. 6 above. Fully and quasirelativistic calculations have been carried out using various heights of Ba and O above the surface.

Calculated DOS for the two different configurations are shown in Fig. 10. In the upper two panels, the results for the upright and tilted configurations are displayed, respectively, and in the lower panel, for comparison, the quasirelativistic DOS for the tilted configuration. Heights above the surface as optimized by Hemstreet et al. (1989) were used in these cases, i.e., $R^{Ba}=5.38a_0$ and $R^{O}=0.89a_0$ for the upright configuration, and $R^{Ba}=4.63a_0$ and $R^{O}=2.88a_0$ for the tilted configuration. Other heights that were considered (see Table VIII below) did not result in a better overall agreement with the mainly Ba-related unoccupied DOS from inverse photoemission spectra. A remaining discrepancy with respect to the energies of the occupied O 2*p* states, however, points to a smaller height of O above the surface for the tilted configuration.

The IPS data in Fig. 11 exhibit only two strongly localized features, one between 0.4 and 0.8 eV and one at 3.4 eV. Both states were already present in Ba/W(100), but they showed a much larger dispersion. Only the fully relativistic DOS for the tilted configuration matches the experiment, and the agreement is almost perfect. This is very strong evidence that Ba and O adsorb at room temperature at different fourfold hollow sites above the W(100) surface.

The loss of dispersion for the states of BaO/W(100) as compared to Ba/W(100) is attributed to the additional charge transfer from Ba to O. This charge transfer causes the Ba states to become more localized, thereby reducing or eliminating the mutual interaction and the dispersion along symmetry lines. The effect is clearly seen in Fig. 12, which shows the Ba-related DOS for Ba_5/W_{25} and Ba_5O_4/W_{25} (modeling the tilted configuration).

As for Ba/W(100), a calculation for a larger $Ba_{10}O_8/W_{66}$ cluster has been carried out with very similar results: the major Ba peak is shifted to higher energies away from the experimental peak, the DOS for the low-energy peak is somewhat improved, and again no significant bulk W features are found above 3 eV.

FIGURE 10.

Fully relativistic and quasirelativistic DOS for a c(2x2) BaO layer on W(100) for two different adsorption configurations (tilted and upright). Solid lines represent the total DOS; short and long dashed lines represent the Ba and O contributions, respectively.

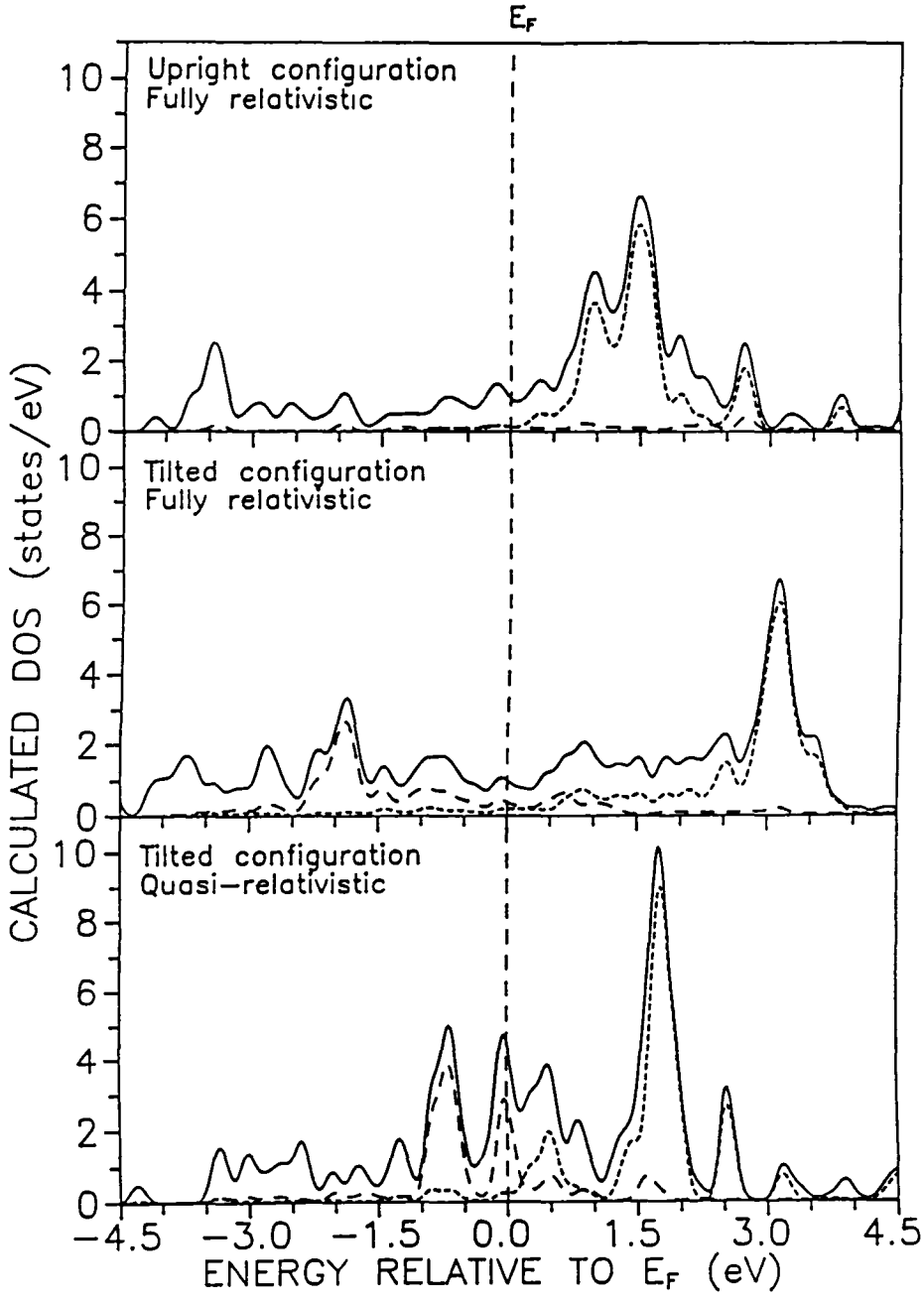

FIGURE 11.

Left panel: Experimental two-dimensional band structure for a c(2x2) layer of BaO on W(100) along two symmetry lines of the unreconstructed W(100) surface. Right panel: Fully relativistic DOS for BaO on W(100) in the tilted configuration. The solid line represents the total DOS; the short and long dashed lines represent the Ba and O contributions, respectively.

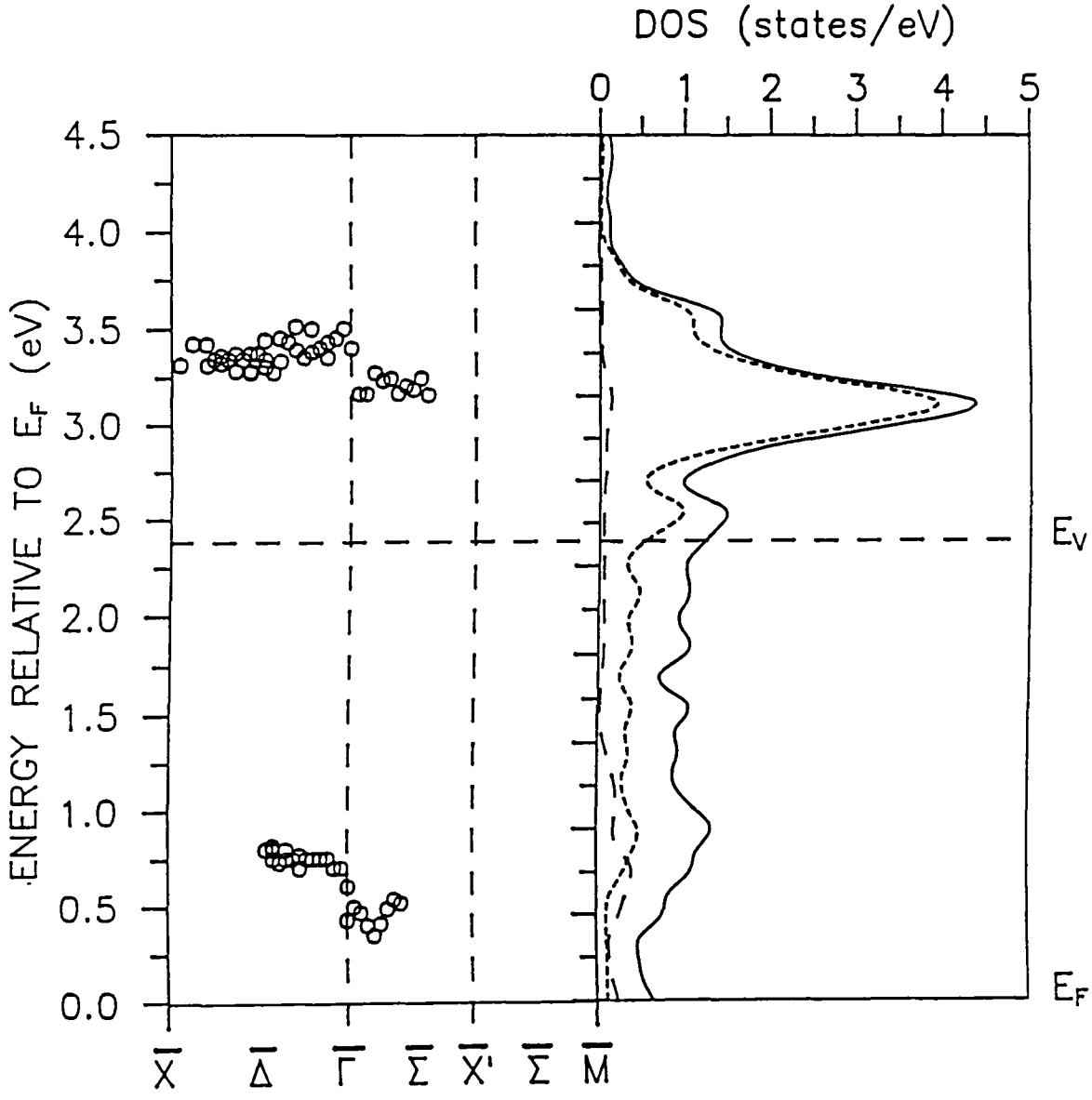

FIGURE 12.

Comparison of the Ba DOS for Ba_5/W_{25} and Ba_5O_4/W_{25}. The solid lines represent the total DOS and the dotted, short, and long dashed lines the Ba *s*, *p*, and *d* contributions, respectively.

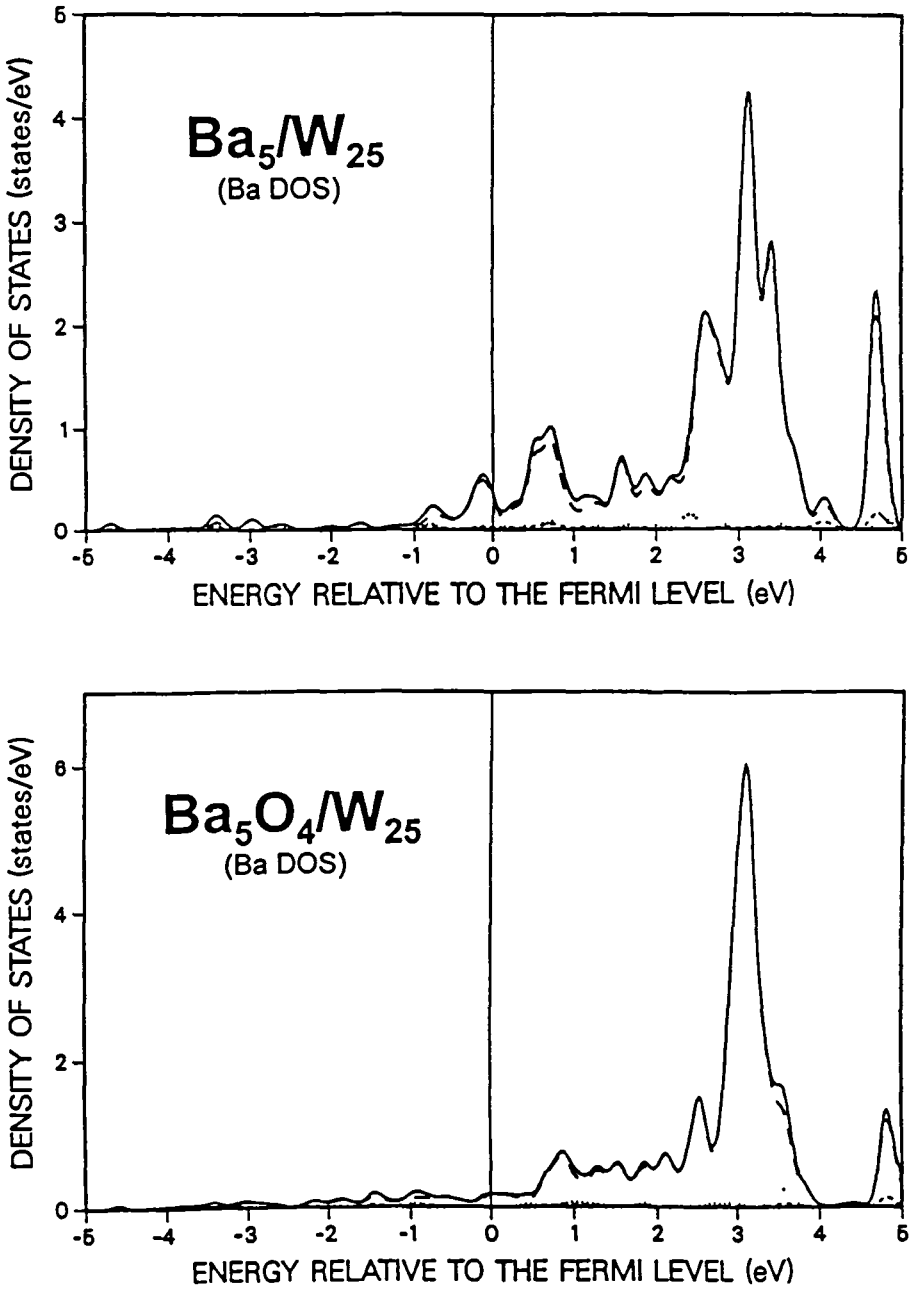

While it appears that the configuration of BaO on W(100) is now clearly established, important questions remain unresolved. The work function for one monolayer of Ba and O on W(100) as measured by Lamouri and Krainsky is about 2.4 eV (see papers with W. Müller, 1994). Hemstreet et al. (1989) calculated work functions of 2.7 eV for the tilted configuration and 2.6 eV for the upright configuration, but found that the tilted configuration is more stable. All these values are clearly too high for the W(100) surface to be considered a reasonable model for B-type surfaces with a work function of about 2.0 eV, as was claimed by Haas et al. (1983).

For the cluster study in Sec. 3 of this report, the upright configuration (with different heights of Ba and O above the surface) has provided consistent results for B- and M-type surfaces. It is, therefore, likely that the upright configuration is after all the appropriate model for cathode surfaces, and that it is realized on W(100) at elevated temperatures where the surface reconstructs. Calculations in this direction are planned for the future.

A summary of calculated surface dipoles and net adsorbate charges for Ba and O on W(100) at the fully relativistic level is presented in Table VIII. As expected, the surface dipole per Ba atom (μ^{Ba}) decreases from Ba to Ba_5 on W_{25} and is found to be very similar for standard and embedded calculations of Ba_5/W_{25}. The net charge on the inner Ba atom, however, increases significantly for the embedded cluster, and the net charge on all Ba atoms (q^{Ba}) increases again for the larger embedded Ba_{10}/W_{66} cluster, in spite of the repulsive interaction of the dipoles on both sides of the cluster. This unexpected result is related to the stabilization of the W energy levels due to the increase in bulk character brought about by embedding, which apparently has a larger effect on q^{Ba} than the repulsive dipole interaction.

For Ba and O on W(100) in the tilted configuration, as modeled by BaO_4 and Ba_5O_4 on W_{25} and $Ba_{10}O_8/W_{66}$, the surface dipoles per Ba atom are much smaller and the net charges on Ba somewhat larger. The increase in q^{Ba} does not lead to larger surface dipoles in this case because a significant amount of charge is transferred to oxygen instead of to the surface. When the reference dipole for O_4/W_{25} is taken into consideration, μ^{Ba} again decreases from BaO_4 to Ba_5O_4 on W_{25}.

For Ba and O on W(100) in the upright configuration, as modeled by Ba_5O_5/W_{25}, the surface dipole increases relative to Ba_5/W_{25} and the net charges on the adsorbates also increase. In all cases, the net charge on oxygen is relatively small and not representative of molecular or bulk BaO.

TABLE VIII.

Surface dipoles μ^{Ba} (Debyes) per Ba atom for different Ba,O/W clusters with standard or embedded radii and potentials, and net atomic charges q (electrons) on the inner/outer Ba and O atoms with heights R (Bohrs) above the surface from fully relativistic Xα calculations.

Cluster	$R^{Ba,O}(a_0)$	μ^{Ba}(D)	q^{Ba}(e)	q^{O}(e)
Ba/W_{25}	4.50,....	11.4	0.74/....	...../.....
Ba/W_{25}	4.63,....	12.1	0.78/....	...../.....
Ba_5/W_{25}	4.50,....	6.2	0.45/0.45	...../.....
Ba_5/W_{25} emb.	4.50,....	6.1	1.07/0.45	...../.....
Ba_5/W_{25} emb.	4.63,....	6.5	1.11/0.48	...../.. ..
Ba_{10}/W_{66} emb.	4.50,....	0.0	1.50/1.26	...../.....
O_4/W_{25}	....,2.88	-12.6	..../....	...../-0.51
BaO_4/W_{25}	4.63,2.88	0.7	1.13/....	...../-0.58
Ba_5O_4/W_{25} emb.	4.63,2.88	1.8	1.23/0.78	...../-0.53
Ba_5O_4/W_{25} emb.	4.63,1.89	2.9	1.28/0.72	...../-0.36
Ba_5O_4/W_{25} emb.	4.50,1.50	2.9	1.25/0.70	...../-0.28
$Ba_{10}O_8/W_{66}$ emb.	4.50,1.50	0.0	1.58/1.39	...../-0.10
Ba_5O_5/W_{25} emb.	5.38,0.89	8.9	1.44/1.42	-0.56/-0.43
Ba_5O_5/W_{25} emb.	6.00,1.10	10.6	1.48/1.43	-0.63/-0.52
W_{25}	....,....	4.6	..../....	...../.....
W_{25} emb.	....,....	-2.0	..../....	...../.....

7. MODELS FOR SCANDATE CATHODES

A series of calculations has been initiated which will lead, step by step, to the modeling of possible surface structures of scandate and oxide cathodes. The following basic systems have been investigated: Sc/W(100), O/W(100), ScO/W(100), Ba/ScO/W(100), and small clusters for barium scandium oxide and scandium tungstate.

For Sc on W(100) fully relativistic and embedded calculations have been carried out for clusters of Sc, Sc_5, and Sc_9 on W_{25}. The latter two cases represent half monolayer, c(2x2), and full monolayer coverages, respectively. Heights of Sc of 3.00 and 3.25 a_0 above the surface have been considered, and the results for a height of 3.25 a_0 will be used for a comparison with available IPS spectra by Lamouri and Krainsky.

In Fig. 13 calculated DOS are compared for Sc_5/W_{25} and Sc_9/W_{25}, representing half and full monolayer coverages, respectively. For Sc_5/W_{25} the DOS above the Fermi level exhibits a series of distinct and clearly separated peaks, with the strongest peak appearing at 2.0 eV. For Sc_9/W_{25} the peak that was located just above E_F has moved below the Fermi level and a broad peak has developed around 1 eV, which is indicative of a dispersive band.

The experimental band structure as derived from IPS data for half and full monolayer coverage is compared with the calculated DOS for Sc_9/W_{25} in Fig. 14 and shows exactly the described behavior. For the half monolayer coverage in the upper panel several distinct, non-dispersive bands are observed with a possible bulk W contribution above 3 eV. For the full monolayer coverage, a strongly dispersive band has developed which extends from the Fermi level to almost 2 eV above E_F. The calculated DOS for Sc_9/W_{25} closely matches the features in the observed band structure and also displays peaks near 3.5 and 4.5 where IPS features are observed. The loss of dispersion for Sc/W(100) from full to half monolayer coverage parallels the Ba,O/W(100) results where the dispersion is lost due to the additonal charge transfer from Ba to O.

Linear muffin-tin orbital (LMTO) calculations by A.G. Petukhov et al. (1994) for Sc/W(100) very nicely trace the dispersion of the IPS peak below 2 eV. Because the separation of the Sc layer from the surface was chosen to be the same as between the W layers (3.0 a_0), the calculated peak is, however, shifted by 1 eV to higher energies. From the present results it appears that a Sc height of 3.25 a_0 above the surface is more appropriate.

FIGURE 13.

Densities of states for the inner Sc and W_I surface atoms of (a) Sc_5/W_{25} and (b) $Sc_9/W25$. The solid lines represent the Sc+W_I DOS and the dashed lines the Sc contributions.

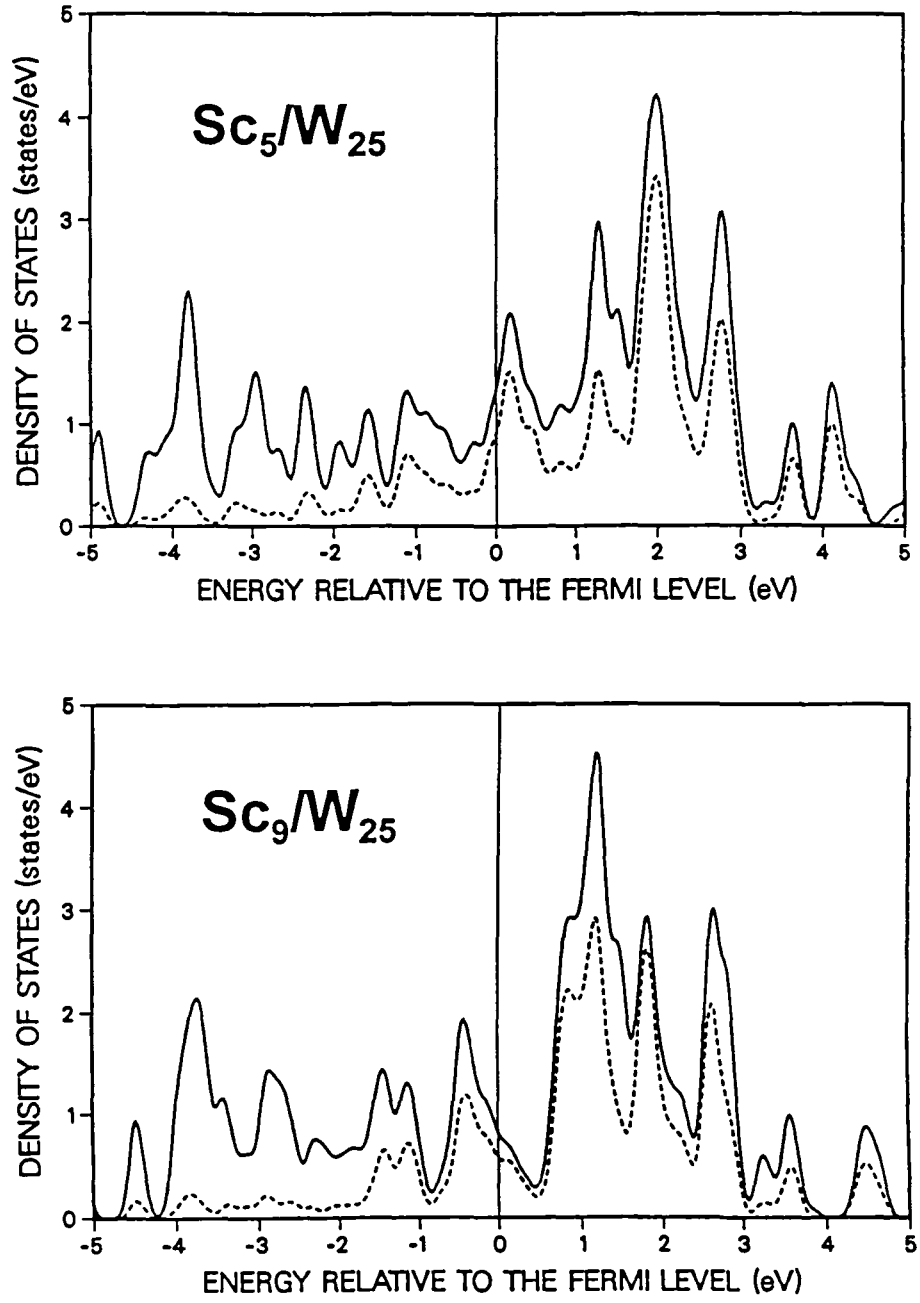

FIGURE 14.

Experimental two-dimensional band structure for half a monolayer (upper panel) and a full monolayer (middle panel) of Sc on W(100), and fully relativistic DOS for Sc_9/W_{25} (lower panel). The solid line represents the total DOS and the dashed line the Sc contribution.

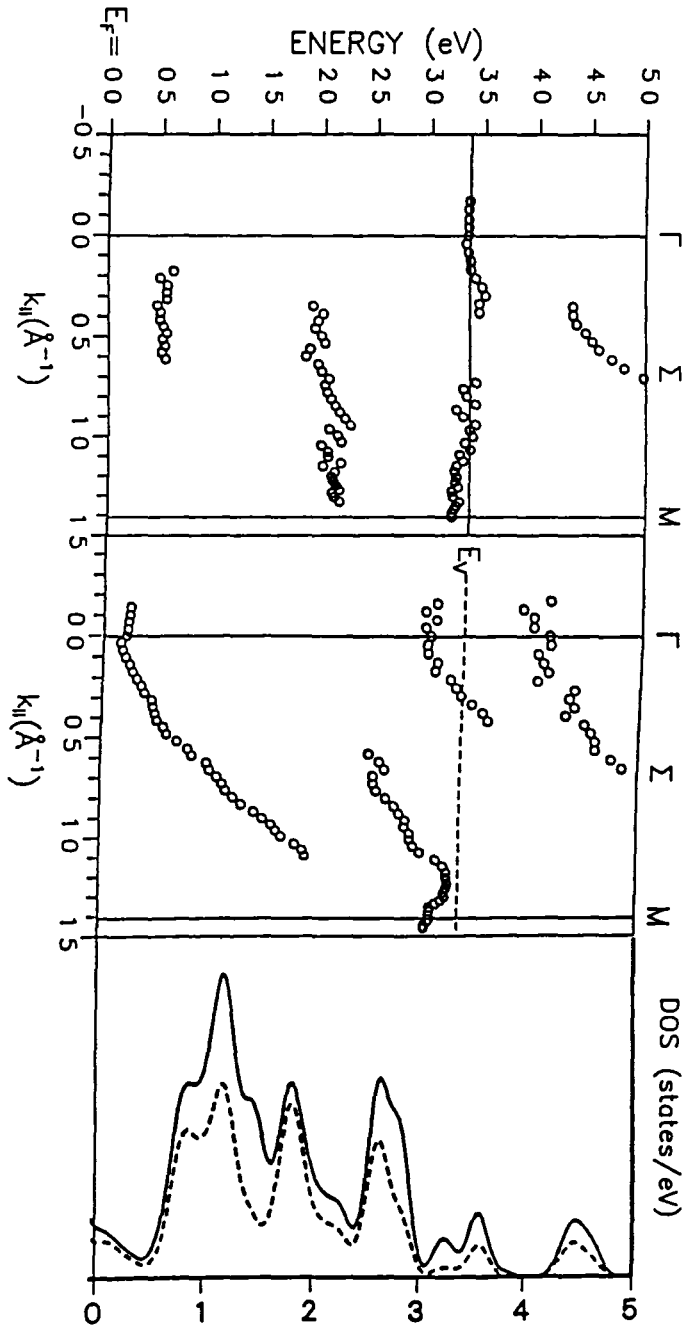

The results for the surface dipoles and adsorbate charges of Sc, O, ScO, and Ba on ScO on W_{25} are given in Table IX. Note that the dipole moments listed here are those for the entire cluster; for Sc_5 and Sc_9 on W_{25} the given values would have to be divided by the number of Sc atoms to arrive at the surface dipoles per Sc atom. Because the dipole moments for the substrate clusters are of similar magnitude, their effect may have to be considered. If μ_{sub} is subtracted, the remaining net surface dipoles are so small that a different treatment of low and high coverages (i.e., standard and embedded) is no longer justified. More calculations are needed to arrive at a numerically stable and consistent set of dipole properties which can then be used to derive work-function data for these systems.

As a general result it is found that the surface dipoles for Sc, O, and ScO on W(100) are small, and only modest changes in the respective work functions are expected. The small surface dipoles have their origin in the relatively small net charges on Sc, even in the presence of O. Only when Ba is added to ScO on W does the

TABLE IX.

Surface dipoles μ (Debyes) for different Ba,Sc,O/W_{25} clusters and net atomic charges q (electrons) on the adsorbates with heights R (Bohrs) above the surface from fully relativistic Xα calculations.

Cluster	$R^{Ads}(a_0)$			μ(D)	q^{Ads}(e)		
	Ba	Sc	O		Ba	Sc	O
Sc/W_{25}		3.00		5.0		0.17	
Sc/W_{25}		3.25		5.5		0.22	
Sc_5/W_{25} emb.		3.00		4.1		0.03	
Sc_5/W_{25} emb.		3.25		5.9		0.12	
Sc_9/W_{25} emb.		3.25		4.1		0.24	
O_4/W_{25}			1.50	-0.3			-0.38
Sc_5O_4/W_{25} emb.		3.25	1.50	-12.3		0.17	-0.27
Sc_4O_5/W_{25}		3.25	1.50	-0.1		0.27	-0.44
Sc_4O_5/W_{25} emb.		3.25	1.50	0.9		0.96	-0.53
$Ba/Sc_4O_4/W_{25}$ emb.	4.50	3.25	1.50	30.9	1.17	1.34	-0.29
W_{25}				4.6			
W_{25} emb.				-2.0			

surface dipole increase very strongly. Low work functions can therefore be expected when Ba, Sc, and O are present on the surface.

In addition to the $Ba,Sc,O/W_{25}$ clusters, some unsupported oxide clusters have been studied with quasirelativistic calculations. The latter may be considered as simple models for the oxide-like characteristics of scandate cathodes. The investigated clusters include Sc_5O_6, $Ba\text{-}Sc_5O_6$, and a tungstate cluster, Sc_4WO_6. The $Ba\text{-}Sc_5O_6$ cluster consists of Ba on $Sc_4/O_4/Sc/O_2$; in Sc_4WO_6, the third-layer Sc atom was replaced by a W atom. The calculations, however, did not converge, and self-consistent solutions for the ground states could not be found.

The problems arise from the difficulty to design small and yet structurally reasonable clusters for oxide systems that are balanced with respect to the formal oxidation levels of the atoms involved. With the formal oxidation level for scandium being +III and for oxygen -II, the Sc_5O_6 cluster is unbalanced in that respect and possesses 3 "excess" electrons. Sc_4O_6 would, of course, be balanced but does not have a structurally viable (balanced and symmetrical) cluster representation that would be compatible with the cubic crystal or surface structure.

The three "excess" electrons in Sc_5O_6 occupy electronic states above the oxide gap, which causes their energies to fluctuate strongly with their occupation and which thereby prevents convergence. The preliminary results obtained for this cluster show net charges of +0.8 for the Sc atoms at the surface and +1.3 for the Sc atoms in the oxide lattice. The net charge on the oxygen atoms is -0.7 to -0.8 electrons. All of these charges are significantly larger than those for Sc and ScO on W. The calculations for Sc_4WO_5 and $Ba\text{-}Sc_5O_6$ proved to be somewhat more stable, but ran essentially into the same convergence problems.

Much larger clusters and further software developments are required for the study of scandate-like surfaces. An extension of the embedding approach to include a self-consistent ionic environment and balancing charges in Watson spheres may also be required. These improvements are expected to solve the present problems with oxide systems.

8. O/W(100) ELECTRONIC STRUCTURE

The embedding approach has also been applied to the study of oxygen-induced features in the O/W(100) surface electronic structure, as experimentally investigated by I.L. Krainsky with inverse photoemission spectroscopy. Fully relativistic calculations with large clusters have been carried out for oxygen adsorption at room and elevated temperatures.

The basic W_{18} substrate cluster used is shown in Fig. 15. It consists of 12 W atoms in the first layer and 6 W atoms in the second layer. According to the results from the ion scattering study by Mullins and Overbury (1989), oxygen adsorbs at room temperature at bridge sites. These are the sites between W1 and W2, W3 and W4, and so on. With all surface sites filled, this leads to a O_8/W_{18} cluster.

At higher temperatures the surface reconstructs to a missing-row structure with adsorption of oxygen above second-layer W atoms (W5, etc.). This structure has been modeled with a $O_6/W_{18}[R]$ cluster, in which the row of W1 and W3 first-layer atoms has been moved to the third layer (now W7 and W8), and 6 O atoms were adsorbed above the 6 second-layer W atoms. Identical potentials have been used for atoms that are equivalent on extended surfaces

FIGURE 15.

W_{18} cluster model (see text).

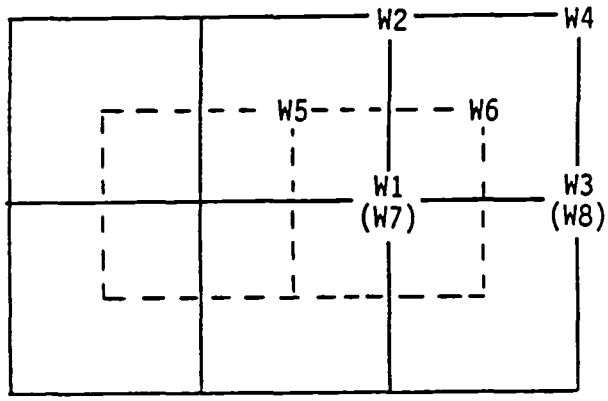

The calculated charge distributions for the three different clusters are given in Table X. The W1 atom in W_{18} (the only one in the first layer for which a potential is optimized) acquires a very small negative charge of -0.05 electrons, while the other atoms show net charges between -0.2 and +0.2 electrons. Adsorption of O at the bridge sites (in O_8/W_{18}) oxidizes the first layer and leads to some charge transfer to the second layer. During reconstruction, the oxygen atoms move to positions above second-layer W atoms, which leads in O_6/W_{18}[R] to additional oxidation of the remaining W2 and W4 first-layer atoms. The net charges on the adsorbed oxygen atoms are of the order of -0.2 to -0.3 electrons.

To study the changes in the unoccupied densities of states that accompany the oxidation and reconstruction processes, density differences (ΔDOS) have been generated. Two types of differences are considered, ΔDOS for all non-equivalent atoms in the clusters and ΔDOS for sets of selected atoms only. The comparison between the two cases will be of importance for judging the validity of the cluster approach. By eliminating the contributions from atoms at the cluster boundary, cluster size and edge effects can be expected to be held at a minimum.

TABLE X.

Net atomic charges q (electrons) for the different oxygen and tungsten atoms in W_{18}, O_8/W_{18} (unreconstructed), and O_6/W_{18}[R] (reconstructed). The numbers for those atoms whose potentials were optimized are printed in bold type.

Atom	Layer	W_{18}	O_8/W_{18}	O_6/W_{18}[R]
q(O1)		.....	**-0.28**	**-0.22**
q(O2)		.....	-0.19	-0.21
q(W1)	I	**-0.05**	**+0.19**	.....
q(W2)	I	-0.01	**+0.38**	**+0.49**
q(W3)	I	+0.20	+0.39	.....
q(W4)	I	+0.08	+0.57	+0.64
q(W5)	II	**+0.11**	**-0.18**	**-0.11**
q(W6)	II	-0.20	-0.68	-1.01
q(W7)	III	.....	.....	**-0.04**
q(W8)	III	.....	.....	+0.56

Fig. 16 shows the differences in the densities of states for room-temperature adsorption (O_8/W_{18}-W_{18}), and Fig. 17 for adsorption at elevated temperatures (O_6/W_{18}[R]-W_{18}) where the surface reconstructs. In the upper panels of these figures, the density differences for all non-equivalent atoms are taken into account and in the lower panels only the density differences O1,W1 - W1 and O1,W2,W5 - W1,W5, respectively. (The density difference O1,W2,W5 - W2,W5 is similar but deviates near E_F from the one shown, and the difference including W1 is preferred because this is the embedded atom in the unreconstructed surface cluster).

The two ΔDOS in Fig. 16 are very similar, while in Fig. 17 there are some differences present because the shape of the substrate cluster changes with reconstruction. The results, in particular of Fig. 16, confirm the validity of the cluster approach in that non-physical edge effects are effectively eliminated already by taking DOS differences, even when edge atoms are included. For changing cluster sizes or shapes, however, the contributions from edge atoms should be excluded. For the DOS plots, a standardized output has been implemented in the fully and quasirelativistic scattered-wave programs.

The oxygen-induced features in the calculated densities of states above the Fermi level agree well with those observed in inverse photoemission spectra. The major effects caused by the temperature-induced reconstruction are (i) changes in the DOS near 1 eV and (ii) the appearance of a double peak around 5 eV. Both effects are clearly seen when the cluster results in Figs. 16 and 17 are compared. A further difference involves the density of states near the Fermi level. In the low-temperature, non-reconstructed case, the density at E_F is largely eliminated and the surface peak just below E_F is shifted to higher binding energy, while in the high-temperature case substantial density remains around E_F and the surface peak does not shift.

FIGURE 16.

Density difference for O/W(100) at room temperature.

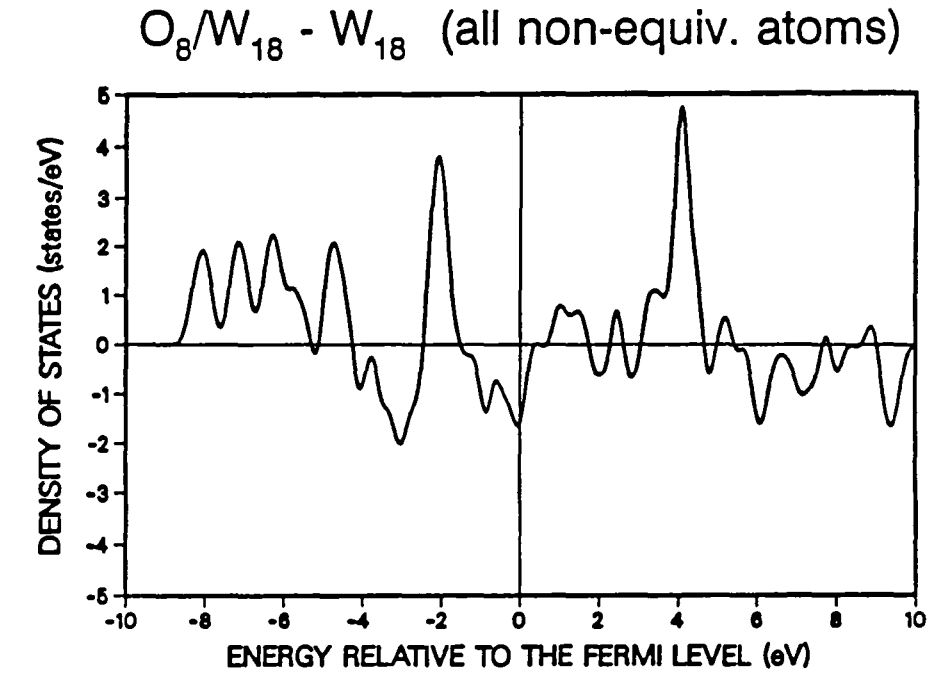

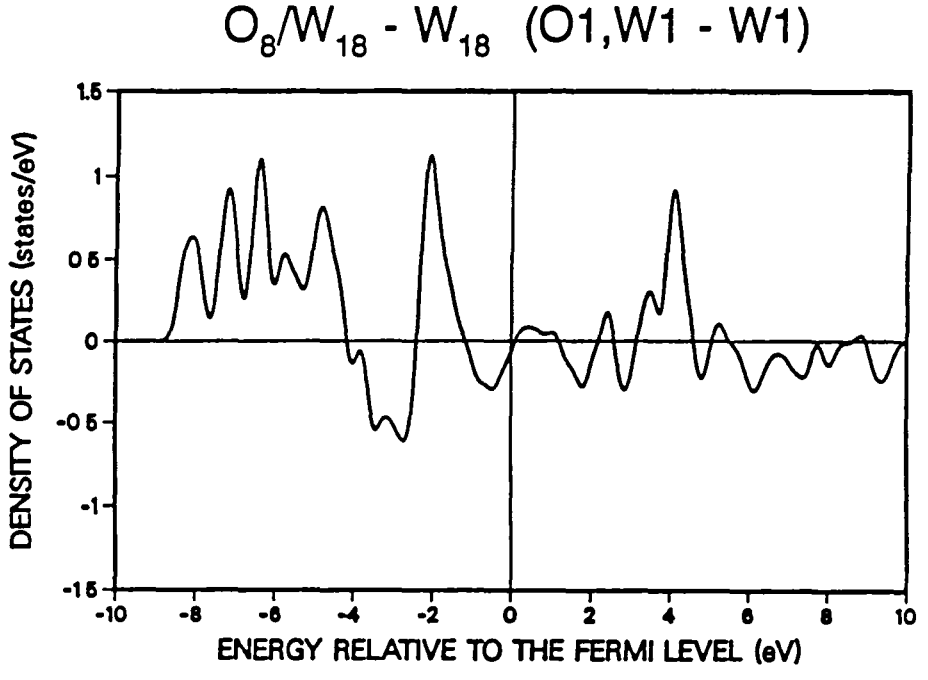

FIGURE 17.

Density difference for O/W(100) at elevated temperatures

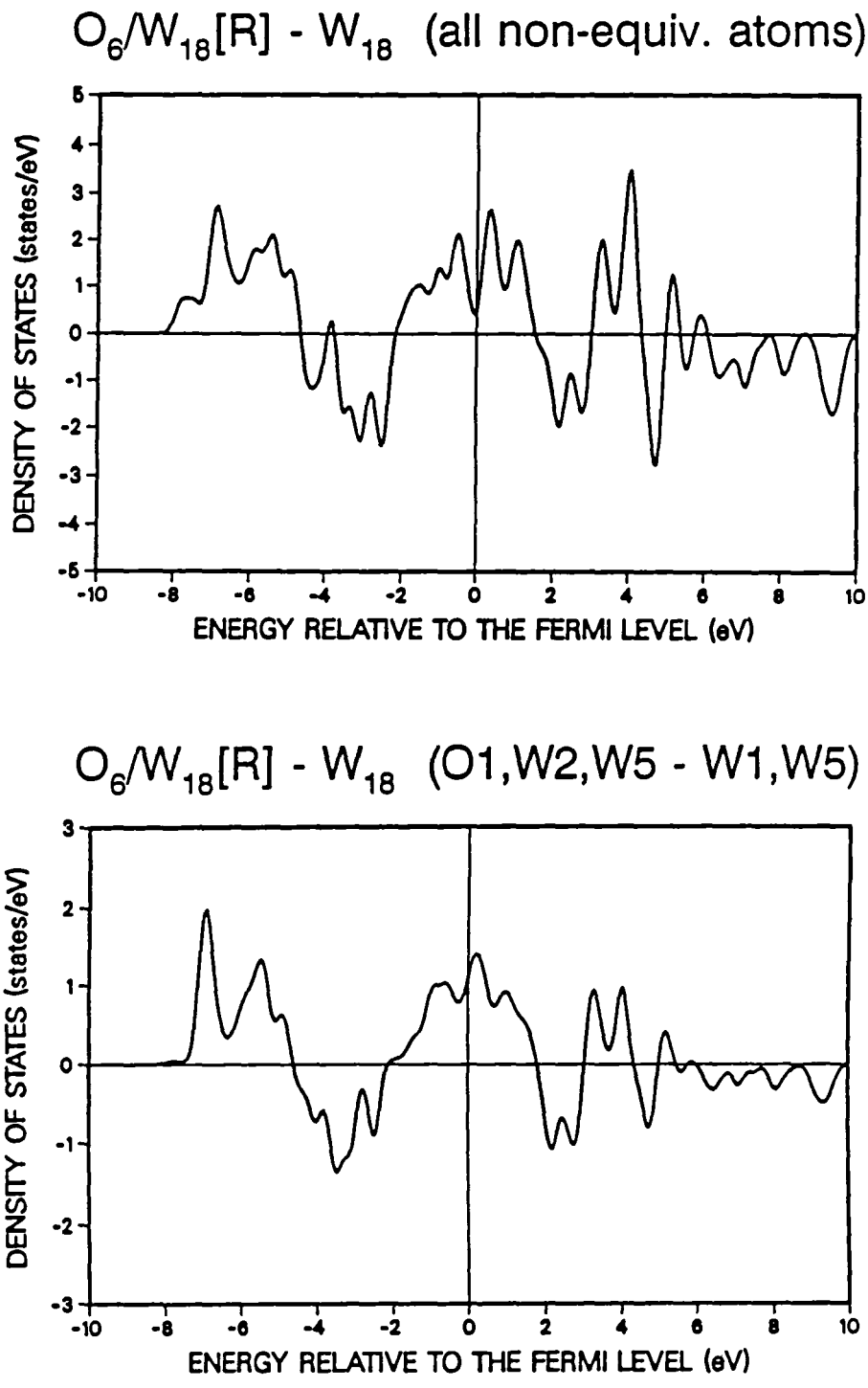

9. YBaCuO SUPERCONDUCTOR RESULTS

The implementation of a population analysis and charge partitioning algorithm in the quasi- and nonrelativistic Xα program has enabled a detailed comparison of the fully, quasi-, and non-relativistic electronic structure of YBaCuO. The calculated valence and conduction band densities of states for the three cases, as derived from a $Y_2Ba_2Cu_{12}O_{18}$ cluster, are shown in Figs. 18-20.

The comparison between the fully and quasirelativistic results in Figs. 18 and 19, respectively, shows a reasonable similarity for the overall DOS, in particular with respect to the dominant double peak below the Fermi level that is observed in photoemission spectra. The atomic decomposition of the DOS, however, reveals significant differences which are due to the missing spin-orbit interaction in the quasirelativistic calculation. (All published results from solid-state calculations have only been at the quasi-relativistic level as well).

The clearly indicated doublets for the localized Cu $3d_{3/2}$ and $3d_{5/2}$ states (at around -3 eV) are not present in the quasi-relativistic DOS, and differences are also seen in the unoccupied Y 4*d* states (between 2 and 4 eV) and Ba 5*d* states (between 4 and 6 eV) in the conduction band DOS. Because details in the Cu 3*d* - O 2*p* interaction likely hold the key to the origin of the mechanism of high-temperature superconductivity, the spin-orbit interaction in the Cu 3*d* states and their coupling to the O 2*p* states deserve further analysis.

While there is a great deal of similarity between the fully and quasirelativistic electronic structure, the nonrelativistic treatment fails to properly represent the complete system. The breakdown is due to the failure to properly describe the valence electronic structure of Ba, which is too heavy to be treated non-relativistically. Fig. 20 shows that the unoccupied Ba 5d states are missing and that substantial Ba-related density is present in the regime below the Fermi level.

The analysis of the charge distribution in Table XI identifies these occupied states as Ba 6p states, which in the nonrelativistic treatment become strongly stabilized relative to the 5d states. It is also noteworthy that the oxidation level of Y and Ba is higher and that of Cu lower in the fully relativistic as compared to the quasirelativistic calculation.

The results from the fully relativistic calculations have been published previously (Müller, 1989).

FIGURE 18.

Total (per unit cell) and partial (atomic) densities of states for fully relativistic $Y_2Ba_2Cu_{12}O_{18}$.

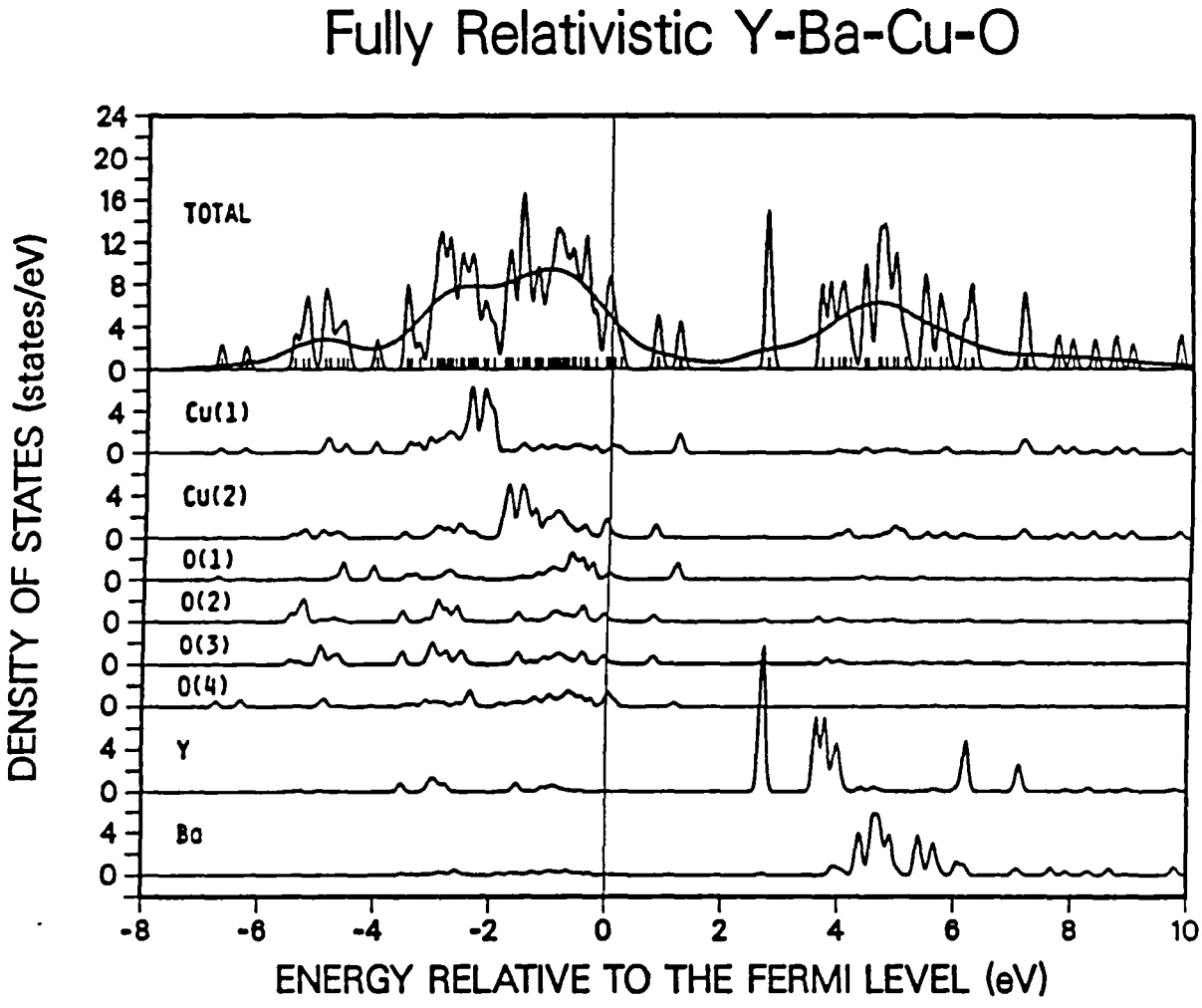

FIGURE 19.

Total (per unit cell) and partial (atomic) densities of states for quasirelativistic $Y_2Ba_2Cu_{12}O_{18}$.

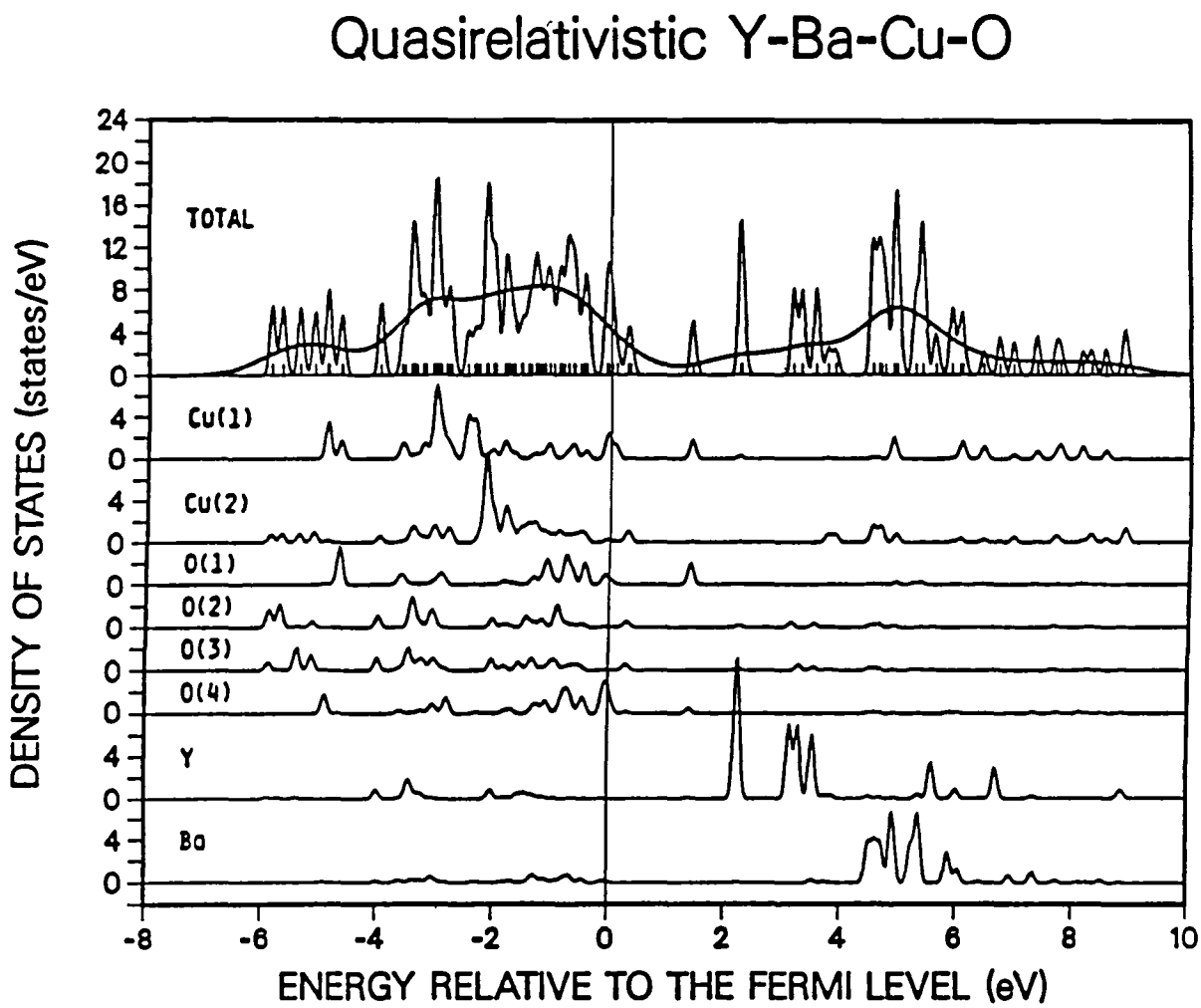

FIGURE 20.

Total (per unit cell) and partial (atomic) densities of states for nonrelativistic $Y_2Ba_2Cu_{12}O_{18}$.

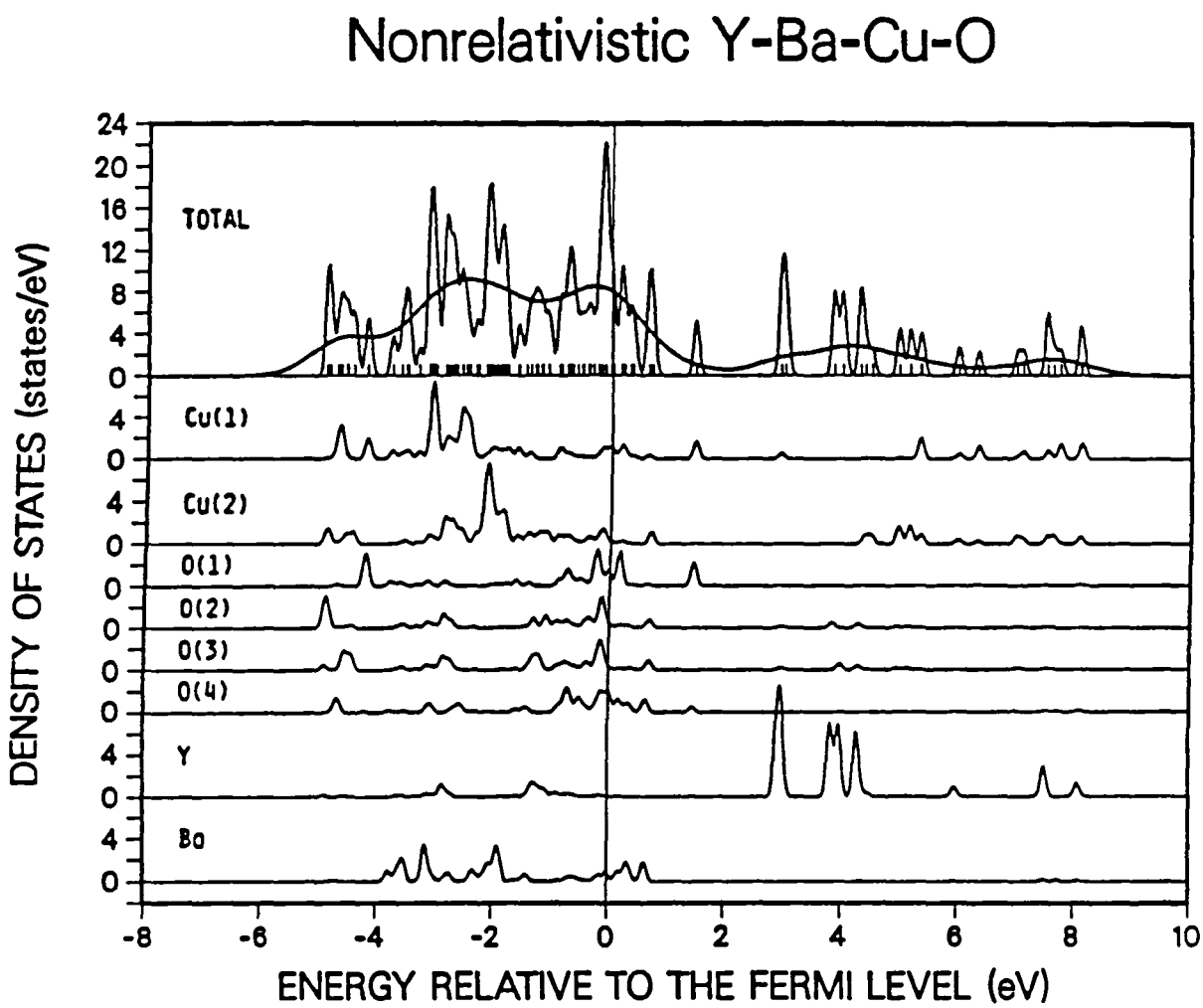

TABLE XI.

Valence charge distribution for a $Y_2Ba_2Cu_{12}O_{18}$ cluster at different levels of Xα scattered-wave calculations.

Atom	*s*	*p*	*d*	sum	net
Fully relativistic					
Y	0.26	0.23	1.41	1.90	+1.10
Ba	0.17	0.27	1.00	1.44	+0.56
Cu1	0.27	0.81	9.28	10.36	+0.64
Cu2	0.30	0.30	9.61	10.21	+0.79
O1	2.03	4.72	....	6.75	-0.75
O2	2.03	4.67	....	6.70	-0.70
O3	2.03	4.67	....	6.70	-0.70
O4	2.06	4.57	....	6.63	-0.63
Quasirelativistic					
Y	0.27	0.24	1.43	1.94	+1.06
Ba	0.19	0.29	1.06	1.54	+0.46
Cu1	0.39	0.73	9.20	10.32	+0.68
Cu2	0.31	0.26	9.62	10.19	+0.81
O1	2.03	4.74	....	6.77	-0.77
O2	2.03	4.66	....	6.69	-0.69
O3	2.03	4.66	....	6.69	-0.69
O4	2.04	4.61	....	6.65	-0.65
Nonrelativistic					
Y	0.25	0.24	1.48	1.97	+1.03
> Ba	0.10	4.85	0.31	5.26	-3.26
Cu1	0.30	0.72	9.12	10.14	+0.86
Cu2	0.30	0.24	9.55	10.09	+0.91
O1	2.03	4.12	....	6.15	-0.15
O2	2.03	4.49	....	6.52	-0.52
O3	2.03	4.49	....	6.52	-0.52
O4	2.04	4.19	....	6.23	-0.23

10. CONCLUSIONS

The scattered-wave cluster approach has proven to be very successful for the determination of the minimum work functions for a large variety of low-work-function surfaces. The relative accuracy is very high when cluster size and shape effects can be minimized by an empirical adjustment or by taking appropriate differences through which undesired cluster-specific effects are largely eliminated.

Remaining problems include possibly too large surface dipoles, a better description of optimum adsorbate coverages, especially for barium, and an improvement in the stability of results based on clusters with different sizes and shapes.

Several approaches have been explored to deal with these questions. Larger clusters with two-dimensional networks of dipoles have been employed for Ba and BaO on W(100), and it is expected that this will solve the optimum coverage problem. Embedded calculations have been used to eliminate cluster shape and edge effects and achieve a better stability of the results with respect to cluster size. Other possible improvements include an adjustment of the cluster Fermi level to more closely resemble the work function of a surface, and the investigation of higher-order effects in the depolarization model.

Another very important area is the determination of interatomic distances and probable surface structures using the ab initio cluster approach. Because of the very high computational requirements, such calculations have so far been limited to small systems.

While very significant progress has been made during the course of this program, more work is needed to further develop the necessary tools and validate the applied models so that predictive capabilities can be achieved. This is required if more complicated systems where reliable experimental data are scarce, such as scandate surfaces, are to be successfully described. It is the goal of this work to advance computational materials science to the point where future materials with improved properties are initially engineered on the computer.

11. REFERENCES

Blaszczyszyn R., Blaszczyszyn M., and Meclewski R., Surface Sci. 51, 396 (1975).

Case D.A. and Yang C.Y., J. Chem. Phys. 72, 3443 (1980).

Cook M. and Case D.A., QCPE 21, 465 (1989).

Fehrs D.L. and Stickney R.E., Surface Sci. 24, 309 (1971).

Haas G.A., Shih A., Marrian C.R.K., Appl. Surface Sci. 16, 139 (1983).

Hemstreet L.A., Chubb S.R., and Pickett W.E., Phys. Rev. B 40, 3592 (1989).

Hopkins B.J. and Smith B.J., J. Chem. Phys. 49, 2136 (1968).

Jansen H.J.F. and Freeman A.J., Phys. Rev. B 30, 561 (1984).

Krainsky I.L., J. Vac. Sci. Technol. A 6, 780 (1988).

Lamouri A. and Krainsky I.L., Surf. Sci. 278, 286 (1992).

Müller W., Final Technical Report: *Theoretical Study of Cathode Surfaces and High-Temperature Superconductors*, NASA CR-195407 (October 1994).

Müller W., Physica C 162-164, 1357 (1989).

Mullins D.R. and Overbury S.H., Surface Sci. 210, 481 (1989).

Petukhov A.G., Lambrecht W.R.L., Segall B., Krainsky I.L., and Lamouri A., Proceedings of the Tri-Service/NASA Cathode Workshop, Cleveland, Ohio (1994).

Schmidt L.D. and Gomer R., J. Chem. Phys. 45, 1605 (1966).

Swanson L.W. and Strayer R.W., J. Chem. Phys. 48, 2421 (1968).

Tuck R.A., Gardiner T.M., Skinner H.B., Norris R., Norman D., Thornton G., Owen I.W., and Richardson C.H., presented at the 1986 Tri-Service Cathode Workshop, Rome Air Development Center, Rome, NY (March 1986).

12. TECHNICAL PRESENTATIONS AND PUBLICATIONS

PRESENTATIONS

- W. Müller, "Work-Function Calculations for Cs, Ba, and BaO Adsorbed on Refractory Metal Surfaces", 8th North Coast Symposium of the American Vacuum Society, Cleveland, Ohio, June 5, 1991.

- W. Müller, "Accurate Work-Function Curves for Adsorbates on Metal Surfaces from Cluster Calculations", International Symposium on the Physics and Chemistry of Finite Systems: From Clusters to Crystals, Richmond, Virginia, October 8-12, 1991.

- W Müller, "Computational Modeling of Dispenser Cathode Emission Properties", International Electron Devices Meeting, Washington, D.C., December 8-11, 1991.

- W. Müller, "Mechanism of Emission Enhancement in Barium Dispenser Cathodes", Tri-Service/NASA Cathode Workshop, Greenbelt, Maryland, March 17-19, 1992.

- W. Müller, "Fundamental Materials Properties for Understanding Cathode Emission Properties", 9th North Coast Symposium of the American Vacuum Society, Cleveland, Ohio, June 4, 1992.

- A. Lamouri, W. Müller, and I.L. Krainsky, "Unoccupied Electronic Energy Levels of a Model Dispenser Cathode", March Meeting of the American Physical Society, Seattle, Washington, March 22-26, 1993.

- A. Lamouri, I.L. Krainsky, and W. Müller, "Electronic Structure and Work Function Study of a Model Dispenser Cathode Surface", 15th Symposium on Applied Surface Analysis, Cleveland, Ohio, June 9-11, 1993.

- W. Müller, "Structure/Property Relationships for Scandate-Type Cathode Surfaces", Tri-Service/NASA Cathode Workshop, Cleveland, Ohio, March 29-31, 1994.

- R.T. Longo, D.R. Dibb, R. Forman, and W. Müller, "Scandate Cathode", Tri-Service/NASA Cathode Workshop, Cleveland, Ohio, March 29-31, 1994.

- A. Lamouri, W. Müller, and I.L. Krainsky, "Geometry and Unoccupied Electronic States of a Model BaO Cathode Surface", Tri-Service/NASA Cathode Workshop, Cleveland, Ohio, March 29-31, 1994.

PUBLICATIONS

- W. Müller, "Computational Modeling of Dispenser Cathode Emission Properties", IEDM Technical Digest, p. 399 (1991).

- W. Müller, "Mechanism of Emission Enhancement in Barium Dispenser Cathodes", Proceedings of the Tri-Service/NASA Cathode Workshop, Greenbelt, Maryland, p. 96 (1992).

- A. Lamouri, I.L. Krainsky, and W. Müller, "Electronic Structure and Work Function Study of a Model Dispenser Cathode Surface", Surf. Interface Anal. 21, 150 (1994).

- A. Lamouri, I.L. Krainsky, and W. Müller, "Geometry and Unoccupied Electronic States of a Model BaO Cathode Surface", Proceedings of the Tri-Service/NASA Cathode Workshop, Cleveland, Ohio, p. 127 (1994).

- A. Lamouri, W. Müller, and I.L. Krainsky, "Geometry and Unoccupied Electronic States of Ba and BaO on W(001)", Phys. Rev. B 50, 4764 (1994).

Technical Summaries have also been submitted to the Numerical Aerodynamic Simulation (NAS) supercomputing program at Ames Research Center for the 1991-92, 1992-93, and 1993-94 operational years. Copies of the NAS reports (pages 48-51) and the journal articles are attached.

ELECTRONIC STRUCTURE OF SUPERCONDUCTORS

Wolfgang Mueller, Principal Investigator
Analatom, Inc. / NASA Lewis Research Center

RESEARCH OBJECTIVE

To investigate the electronic structure of high-temperature superconductors and other materials of technological importance with methods of computational quantum chemistry, to perform theoretical analyses of critical materials properties, and to derive and predict macroscopic properties from calculated microscopic parameters

APPROACH

Electronic structure calculations are carried out for large atomic clusters using self-consistent ab initio and scattered-wave methods, which are based on the Schroedinger and Dirac wave equations.

ACCOMPLISHMENT DESCRIPTION

The relativistic scattered-wave cluster investigation of the electronic structure of Y-Ba-Cu-O has been completed. The validity of the cluster approach has been demonstrated by comparison of the present results with experimental and other theoretical data. For the study of electronic coupling parameters, ab initio calculations have been explored for small Cu-O clusters.

In the area of low-work-function surfaces, a breakthrough has been achieved in the modeling of the electron emission properties of a variety of tungsten-alloy cathode surfaces, which are used in traveling-wave tubes for space communications. The emission enhancement that is observed for alloy relative to pure tungsten substrates has been explained on the basis of calculated surface dipole properties.

A typical calculation requires 10 hours of CPU time on the Cray Y-MP and 4 megawords of memory.

SIGNIFICANCE

The successful modeling of electronic properties of existing materials enables systematic investigations of new materials with improved properties that are initially engineered on the computer.

FUTURE PLANS

Embedded cluster and plane-wave calculations will be carried out to further investigate the electronic structure of superconductors and cathode surfaces. Of particular interest will be differences in the surface and bulk electronic structures and the determination of important electronic coupling parameters.

PUBLICATIONS

Mueller, W. "Computational Modeling of Dispenser Cathode Emission Properties." IEDM Technical Digest (1991): 399-402.

NAS Technical Summary, March 1992 - February 1993

Electronic Structure of Cathode Surfaces

Wolfgang Mueller, Principal Investigator
Analatom, Inc. / NASA Lewis Research Center

Research Objective

To investigate the electronic structure and to derive and predict macroscopic properties of low-work-function cathode surfaces from calculated microscopic parameters.

Approach

Electronic structure calculations are carried out for large atomic clusters in order to determine the charge distribution, surface dipole strengths and dipole interactions on thermionic cathode surfaces by using self-consistent ab initio and scattered-wave methods based on the Schroedinger and Dirac wave equations.

Accomplishment Description

A microscopic explanation has been provided for the variation in electron emission that is observed among the refractory metals and alloys commonly used for the electron emitting surfaces of barium dispenser cathodes. The accompanying figure shows the calculated work function versus coverage curves for BaO adsorbed on different substrates. The sequence and magnitude of the work function minima are accurately described by the calculations. The BaO/Ir-W and BaO/Os-W surfaces exhibit lower work functions than the BaO/W and BaO/Pt surfaces because of the reduced depolarization of the surface dipoles on hexagonal as compared to cubic substrates.

A typical calculation requires 10 hours of CPU time on the Cray Y-MP and 4 megawords of memory.

Significance

Thermionic cathodes are a major component in traveling-wave tubes that are used as amplifiers for satellite communications and as power transmitters to planetary research stations and robotic vehicles. The successful modeling of the electronic properties of existing materials enables systematic investigations of new materials with improved properties that are initially engineered on the computer.

Future Plans

Relativistic embedded cluster calculations will be carried out to determine the geometrical and electronic structure, surface dipole properties, desorption characteristics, and work functions of barium dispenser and scandate cathode surfaces at room and operating temperatures.

Publications

1. Mueller, W. "Mechanism of Emission Enhancement in Barium Dispenser Cathodes." Proceedings of the 1992 Tri-Service/NASA Cathode Workshop, Greenbelt, MD.
2. Mueller, W. "Fundamental Materials Properties for Understanding Cathode Emission Properties." 9th North Coast AVS Symp., Cleveland, OH, June 1992.

Group ID Number: 5273
Project Title: Electronic Structure of Cathode Surfaces
Principal Investigator: Wolfgang Mueller, (216) 433-3512
Discipline: Computational Chemistry
Number of figures: 1

Figure Caption: Work function versus coverage curves for BaO on Pt, W, Ir-W, and Os-W cathode surfaces.

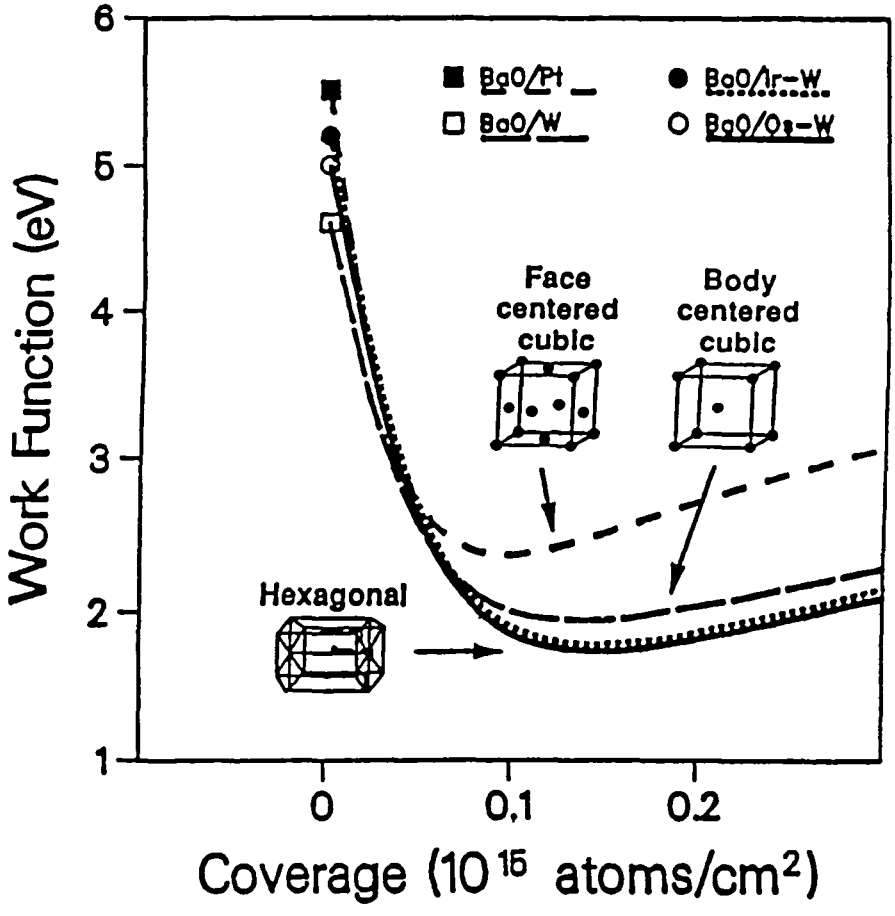

ELECTRONIC STRUCTURE OF CATHODE SURFACES
Wolfgang Mueller, Analatom, Inc.

Research Objective
To investigate the chemical, physical, and electronic structure of low-work-function cathode surfaces and to derive and predict macroscopic properties from calculated microscopic parameters.

Approach
Electronic structure calculations are carried out for large atomic clusters in order to determine the geometry, charge distribution, surface dipole properties, and work functions of thermionic cathode surfaces by using self-consistent ab initio and scattered-wave methods based on the Schroedinger and Dirac wave equations.

Accomplishment Description
The densities of occupied and unoccupied electronic states for barium and barium /oxygen adsorbed on the (001) face of body-centered-cubic tungsten have been calculated for different geometrical arrangements of the adatoms above the surface and compared with photoemission spectra. It was demonstrated that the barium on tungsten system is well described by the calculations for a barium height of 2 38 Angstroms above the surface and that barium and oxygen adsorb in alternating fourfold-hollow sites of the tungsten surface. The surface dipole properties have been analysed and work functions generated for these systems.

A typical calculation requires 20 hours of CPU time on the Cray C-90 and 4 megawords of central memory.

Significance
Thermionic cathodes are major components in traveling-wave tubes that are used as amplifiers for satellite communications and as power transmitters to planetary research stations and robotic vehicles. The successful modeling of the electronic properties of existing materials enables systematic investigations of new materials with improved properties that are initially engineered on the computer.

Future Plans
Ab initio and relativistic embedded cluster calculations will be carried out to determine the surface dipole properties and work functions of barium dispenser and scandate cathode surfaces at room and operating temperatures

Publications
1 Mueller, W Structure/Property Relationships for Scandate-Type Cathode Surfaces. Tri-Service/NASA Cathode Workshop, Paper 3.2, Cleveland, Ohio, March 1994
2 Lamouri, A.; Krainsky, I.L.; and Mueller, W.: Electronic Structure and Work Function Study of a Model Dispenser Cathode Surface. Surface and Interface Analysis, vol. 21, 1994, pp 150-154.
3. Lamouri, A.; Mueller, W.; and Krainsky, I.L.: Geometry and Unoccupied Electronic States of Ba and BaO on W(001). Physical Review B, 1994, accepted for publication.

Additional Information
Group ID Number: 5273
Project Title: Electronic Structure of Cathode Surfaces
Principal Investigator: Wolfgang Mueller, (216) 835-4610
Discipline: General/Chemistry
Keywords: Dispenser cathodes, work function
Animation. None
Figures: 0

COMPUTATIONAL MODELING OF DISPENSER CATHODE EMISSION PROPERTIES

W. Müller

Analatom, Incorporated

Westlake, Ohio 44145, U.S.A.

ABSTRACT

Work function curves for BaO on W, Os, Os-W, and Pt have been derived from calculated initial surface dipoles and their depolarization at higher coverages. An accurate picture is obtained for the minimum work functions of the different materials. The optimum in emission that is observed for the Os-W alloy substrate has its origin in the small depolarization of the surface dipole on hexagonal-close-packed substrates. This important result provides the long-awaited microscopic explanation for the emission enhancement in alloy cathodes. An increase in the surface concentration of W for the Os-W substrate leads to an increase in the calculated work function, which is consistent with the observed emission degradation during the life of the cathode.

INTRODUCTION

The microscopic explanation for the variation in electron emission that is observed among the refractory metals and alloys used for the electron emitting surfaces of barium dispenser cathodes is one of the long outstanding questions in thermionic cathode research [1].

It is well known that the emission from impregnated tungsten cathodes can be significantly enhanced by coating the surface with Re, Os, Os-Ru, or Ir. Similar effects can be achieved by using mixed-metal matrices instead of a pure W matrix. During the activation and early life of the cathode, interdiffusion between W and the other metal(s) occurs and an alloy surface is formed, with a monolayer of adsorbed Ba and O from the impregnant. The best metal coating among the 5d transition metals is Os, followed by Ir, Ru, and Re, while Pt gives rise to a strong degradation of the emission properties [1].

The improvement in emission is caused by a lowering of the work function from ~1.9 eV for tungsten (B-type) to 1.7-1.8 eV for alloy (M-type or mixed-metal) cathodes. A Pt coating, on the other hand, increases the work function to ~2.1 eV [2]. The emission current density J is related to the work function ϕ by the Richardson equation [3]

$$J = A_0 T^2 \exp(-e\phi/kT) \qquad (1)$$

where $A_0 = 1.2\times10^6$ A/m^{-2}K^{-2}, T is the temperature, e the elementary charge, and k the Boltzmann constant. While the effect due to alloy formation is relatively small (about 10 percent of the work function change of ~2.6 eV from clean W to BaO/W), it is technologically very important because a variation in ϕ of 0.2 eV changes the emission current density at 1300 K by a factor of 6. Alternatively, a cathode with a lower work function can be operated at a lower temperature with the same J, thereby increasing the life of the cathode.

It is the purpose of the present investigation to calculate the microscopic electronic properties which are responsible for the lowering of the work function in coated dispenser cathodes, and thereby gain a more thorough understanding of the emission characteristics of different materials. The calculated properties are then used to derive work-function-versus-coverage curves for different substrates, including effects due to alloy formation and changes in the surface composition with aging.

The variation of the work function with coverage is based on the depolarization of the Ba-O-substrate dipole, which is responsible for the lowering of the work function. The two relevant parameters, i.e., the initial surface dipoles at low coverages and their depolarization at higher coverages, are obtained from cluster calculations. It will be shown that the minimum work functions for different cathode surfaces can successfully be modeled and that the optimum in emission for tungsten-alloy substrates is caused by a smaller depolarization of the surface dipole on substrates with the hexagonal-close-packed crystal structure.

CH3075-9/91/0000-0399 $1 00 © 1991 IEEE

DEPOLARIZATION MODEL

The decrease in the work function from 4.5-5.5 eV for the bare metal substrates to around 2 eV for the cathode surfaces is caused by the adsorption of Ba and O and the creation of a Ba-O-substrate surface dipole that lowers the electrostatic potential for electron emission. At small coverages, a linear variation of the work function with adsorbate coverage is observed. At higher coverages, the increasing repulsive interaction between the surface dipoles causes the work-function-versus-coverage curve to deviate from the linear behavior, and a minimum is eventually reached. The work function change, $\Delta\phi = \phi - \phi_0$, is given by the Helmholtz equation [4]

$$\Delta\phi = - e\mu N(2\epsilon_0)^{-1} \qquad (2)$$

where μ is the effective surface dipole at coverage N and ϵ_0 is the permittivity of vacuum.

The effective surface dipole can be expressed as

$$\mu = \mu_0 - \alpha f \qquad (3)$$

where μ_0 is the initial surface dipole at low coverages, α an effective polarizability, and f the electric field resulting from all other dipoles. The electric field f for a simple square network of point-dipoles has been evaluated by Topping [5] and is given by

$$f = 9\mu N^{3/2}(4\pi\epsilon_0)^{-1}. \qquad (4)$$

Substituting f into Eqn. (3), solving for μ and substituting into Eqn. (2) yields

$$\Delta\phi = - 1.88\, e\mu_0 N / (1+c\alpha N^{3/2}) \qquad (5)$$

with μ_0 in debyes (D), α in Å^3, and N in 10^{15} atoms/cm^2. The two important microscopic properties, the initial surface dipole μ_0 and the polarizability α, have been calculated with the cluster approach as described below. Because the constant c depends on the validity of the point-dipole approximation and the actual overlayer formed, it is treated as an adjustable parameter.

Eqn. (5) has experimentally been verified for alkali adsorption on single crystal surfaces of W [6] and was found to be valid up to the work function minimum. For larger coverages, the work function is more and more determined by the properties of the adsorbate itself, which are no longer described by the depolarization model. At sufficiently large coverages the work function of the pure adsorbate is eventually reached.

CLUSTER APPROACH

Relativistic electronic structure calculations, based on the Xα scattered-wave approach [7], have been carried out for BaO adsorbed on W, Os, Pt, and Os-W alloys. The substrate is modeled with atomic clusters representing the body-centered-cubic (bcc) crystal lattice of W, the hexagonal-close-packed (hcp) lattice of Os and the solid solution of W in Os, and the face-centered-cubic (fcc) lattice of Pt.

For W the (100) face is considered, for Os and Os-W the (10$\bar{1}$0) face, and for Pt the (111) face. For Os and Pt these choices represent the dominant crystal faces present on actual cathode surfaces [2]. The substrate of BaO/W cathodes is polycrystalline with many faces present and the (100) orientation has been chosen because of its simple structure. Crystallites with the (110) orientation cover about 50 percent of a typical surface, but its contribution to the overall emission has not yet been clearly established [8].

BaO is assumed to be adsorbed in an upright position with Ba above O. A Ba-O distance of 2.6 Å is used for W and Os, and 2.7 Å for Pt, as suggested by Norman et al. [2]. Ba heights above the surface of 3.2 Å for W and 3.7 Å for all other substrates are used. The substrate clusters typically contain 3 atomic layers and between 12 and 21 substrate atoms.

The initial dipole moments μ_0 have been calculated with clusters containing 2 BaO molecules at a sufficiently large separations (5-6 Å), and the polarizabilities α from clusters with 3 BaO molecules separated by about 3 Å (except for Pt where a smaller cluster with 2 BaO was used). The clusters are described as $[BaO]_{2(3)}/W_{19}(100)$, $[BaO]_{2(3)}/Os_{21}(10\bar{1}0)$, and $[BaO]_2/Pt_{16(12)}(111)$. The BaO/W cluster is shown as an example in Fig. 1. For the solid solution of W in Os two substrate clusters were considered, an Os-rich $Os_{11}W_{10}$ cluster and a W-rich $W_{11}Os_{10}$ cluster.

FIGURE 1. $[BaO]_{2(3)}/W_{19}(100)$ Cluster.

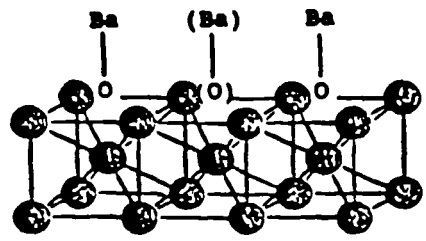

The polarizability α is calculated from the decrease in the cluster dipole moment per adsorbed BaO, $\Delta\mu_c$, according to

$$\alpha = \Delta\mu_c / f_c \qquad (6)$$

where f_c is the (additional) dipole field present in the cluster with the higher surface coverage.

RESULTS AND DISCUSSION

The calculated initial surface dipoles, polarizabilities, work function data, and optimum coverages are given in Table I. The initial surface dipoles μ_0 are found to increase steadily in the series BaO on W(100), Os(10$\bar{1}$0), and Pt(111). The polarizability α, however, shows a minimum for Os(10$\bar{1}$0), while its increase from W to Pt is proportional to the increase in μ_0. The respective results for the W-rich BaO/W-Os and the Os-rich BaO/Os-W alloy clusters are similar to those for BaO/Os. The calculated values for α are much closer to the atomic polarizability of W (10 Å^3) than for Ba (40 Å^3) [9], and reflect the high oxidation level of Ba.

The small depolarization for the Os and Os-alloy substrates with the hcp crystal structure has important consequences for the calculated work function changes. Typically, a large initial dipole, which causes a steep decrease in the initial work function with increasing coverage, is accompanied by a large depolarization. The latter causes the work function curve to deviate earlier from the initial linear decrease, which results in a higher minimum work function, and thereby cancels the benefits from the initially steeper decline to a large extent. The combination of a fairly large initial dipole and small depolarization, as present in the hcp systems, is therefore the ideal condition for very low work functions.

The work function curves have been calculated by use of Eqn. (5) where the constant c has been adjusted such that the experimental minimum of 2.0 eV for BaO/W(100) is reproduced, which yields c=2.41. For BaO/Os(10$\bar{1}$0) this choice of c, however, produces a minimum work function of 1.5 eV, which is believed to be too small. By assuming that an equi-triangular network is formed on the hexagonal substrates (as compared to a square network on the cubic substrates) c changes to $c_{hex} = 11/9\ c_{cubic}$, and N in equation (5) has the dimension $N_{hex} = 2/\sqrt{3}\ N_{cubic}$ (1.15×10^{15} atoms/cm^2) [5].

With the different constants c for the cubic and hexagonal systems and the bare substrate work functions ϕ_0 given in Table I, minimum work functions are obtained which are in excellent agreement with experimental data. The calculated work functions for the Os and Pt systems are, respectively, 0.1 eV and 0.3 eV higher than for BaO/W(poly), and the work function for the Os-rich BaO/Os-W system is 0.14 eV lower. The emission degradation that is observed for Os-coated surfaces with increasing life of the cathode is attributed to the diffusion of Os into the W substrate. This is very well illustrated by the results for the W-rich BaO/W-Os system, the calculated work function of which (1.82 eV) falls in between the values for the Os-rich alloy and polycrystalline W.

The presented theoretical approach is supported by the results for other low-work-function systems like Ba/W and Cs/W, for which the calculated minimum work functions are higher (Ba) and lower (Cs) than those for BaO cathode surfaces.

It should be noted that for Os(10$\bar{1}$0) and Pt(111) the bare metal work functions ϕ_0 are not known and that the polycrystalline values have been used [10]. For the Os-W system no information is available at all and the average (5.0 eV) of the bare metal

TABLE I. Calculated initial surface dipoles μ_0(D), polarizabilities α(Å^3), work function data ϕ(eV), and optimum coverages N_s(10^{15} atoms/cm^2) for BaO on W, Os, Pt, and Os-W alloys. (ϕ_s for BaO/W(100) has been adjusted*).

System	Lattice	μ_0	α	ϕ_0	$\Delta\phi$	ϕ_s	ϕ_s^{exp}	N_s
BaO/W(100)	bcc	31.2	16.6	4.65	-2.65	2.00*	2.0	0.14
BaO/W(poly)	bcc	(31.2)	(16.6)	4.54	-2.65	1.89	1.9	0.14
BaO/Os(10$\bar{1}$0)	hcp	40.5	13.7	5.4	-3.42	1.98	...	0.16
BaO/Pt(111)	fcc	51.9	27.8	5.3	-3.13	2.17	2.1	0.10
BaO/W-Os(10$\bar{1}$0)	hcp	38.4	14.1	5.0	-3.18	1.82	...	0.15
BaO/Os-W(10$\bar{1}$0)	hcp	41.1	15.1	5.0	-3.25	1.75	1.7	0.15

work functions of W and Os is used; this value may be compared with a quoted value of 4.98 eV for a W - 60% Re alloy [11]. The calculated minimum work functions depend, of course, critically on ϕ_0.

The theoretical work-function-versus-coverage curves for BaO on W(poly), Os-(10$\bar{1}$0), Pt(111), and Os-W(10$\bar{1}$0) are shown in Fig. 2. For the BaO/W(poly) curve, μ_0 and α from BaO/W(100) have been used. Experimentally, a minimum is not observed for the work function curves of these cathode surfaces, and ϕ tends to drift very slowly lower toward the work function of the BaO overlayer [12]. Because these effects are not considered in the depolarization model, the curves beyond the minimum and the calculated optimum coverages N_s have probably no significance in real systems.

FIGURE 2.
Calculated Work-Function-Versus-Coverage Curves for BaO on W, Os, Os-W, and Pt.

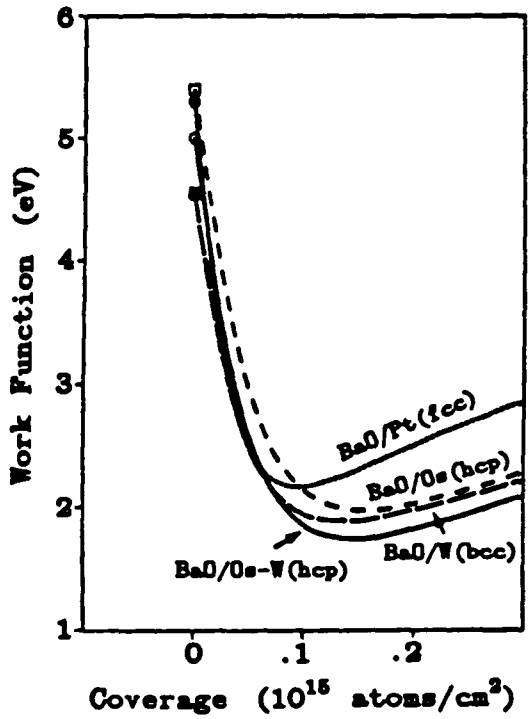

In summary, the increase in the effective work functions for BaO on Os and Pt relative to W has its origin in the increase of the bare metal work function and for Pt additionally in the large increase of the depolarization, while the optimum for the Os-W system results from an interplay between a large initial surface dipole, a small depolarization, and a (possibly) not too large bare work function. Because of the size of the depolarization effect for the hcp systems, this conclusion is also expected to be valid for other geometries of Ba and O above the surface and other substrates with the same crystal structure.

The calculated Ba binding energies, as obtained from the clusters with the higher surface coverage, are 3.0 eV for BaO on Pt and 4.5 to 5.5 eV for BaO on W and Os. The latter results are in good agreement with measured energies of desorption [13].

CONCLUSIONS

The most significant result of the present investigation is the decrease in the polarizability, or depolarization, of the Ba-O-substrate dipole for the hcp crystal structure with the (10$\bar{1}$0) orientation. The reduced depolarization leads to a larger decrease in the work function than for substrates with the cubic crystal structure and provides the long-awaited microscopic explanation for the improved emission from Os-W and other substrates (like Re-W and Ir-W) with the hcp crystal structure.

ACKNOWLEDGEMENT

The author wishes to express his appreciation for many useful discussions with Mr. E.G. Wintucky and Dr. R. Forman. This work is being supported by the Electron Beam Technology Branch at the NASA Lewis Research Center, Cleveland, Ohio under Contract NAS3-25940.

REFERENCES

[1] R.A. Tuck, Vacuum 33, 715 (1983).
[2] D. Norman et al., Phys. Rev. Letters 58, 519 (1987).
[3] A.S. Gilmour, Jr., *Microwave Tubes* (Artech House, Norwood, 1986).
[4] J. Hölzl and K.F. Schulte, *Solid Surface Physics* (Springer, Berlin, 1979).
[5] J. Topping, Proc. Roy. Soc. (London) A 114, 67 (1927).
[6] L.D. Schmidt and R. Gomer, J. Chem. Phys. 45, 1605 (1966).
[7] M. Cook and D.A. Case, QCPE No. 465 (1983).
[8] R.A. Tuck et al., presented at the Tri-Service Cathode Workshop, RADC, Rome, NY, March 1986.
[9] T.A. Miller and B. Bederson, Adv. Atomic and Molec. Phys. 13, 1 (1977).
[10] G.A. Haas, A. Shih, and C.R.K. Marrian, Appl. Surf. Sci. 16, 139 (1983).
[11] T.L. Matskevich, Sov. Phys. - Tech. Phys. 13, 295 (1968).
[12] G.A. Haas and R.E. Thomas, in *Techniques of Metals Research*, Vol. VI, Part 1 (Interscience, New York, 1972).
[13] R. Forman, Appl. Surf. Sci. 29, 127 (1987).

MECHANISM OF EMISSION ENHANCEMENT IN BARIUM DISPENSER CATHODES

Wolfgang Müller
Analatom, Incorporated
Westlake, Ohio 44145, U.S.A.

ABSTRACT

Calculations are presented for the work functions of BaO on W, Os, Pt and alloys of Re-W, Os-W, Ir-W that are in excellent agreement with experiment. The observed emission enhancement for alloy relative to tungsten dispenser cathodes is attributed to properties of the substrate crystal structure and explained by the smaller depolarization of the surface dipole on hexagonal as compared to cubic substrates. The optimum in emission and minimum in the work function for the BaO/Os-W system has its origin in the presence of a large initial surface dipole, a small depolarization, and a not too large initial work function.

1. INTRODUCTION

The microscopic explanation for the variation in electron emission that is observed among the refractory metals and alloys commonly used for the electron emitting surfaces of barium dispenser cathodes has been one of the long outstanding questions in thermionic cathode research.[1] Several attempts have been made to correlate the observed emission with properties of the adsorbed BaO and/or the metal substrate, but effects due to alloy formation in mixed-metal cathodes have never been addressed on the atomic level. It has also been notoriously difficult, in particular, to account for the severe degradation in emission that is observed for Pt-coated surfaces.

In the present theoretical approach, relativistic cluster calculations are employed to investigate the electronic structure and dipole properties of BaO adsorbed on refractory metals and alloys as a function of coverage. The dominant substrate crystal structures and crystallographic orientations as found on actual cathode surfaces and approximate temperature dependencies of the substrate work functions are explicitly taken into account.

2. METHOD

The important calculated microscopic parameters that determine the effective work functions ϕ are (i) the initial surface dipole μ_0 at low coverages and (ii) the polarizability α and resulting depolarization of the dipoles at higher coverages.

The BaO-substrate complex is modeled with atomic clusters containing typically around 20 substrate atoms and either 2 or 3 adsorbed BaO molecules.[2] The clusters with 2 BaO molecules at sufficiently large separations are used to determine the initial surface dipoles μ_0 and the clusters with 3 BaO molecules at smaller separations (higher coverage) the polarizability α of the charge distribution at the BaO site, according to $\alpha = \Delta\mu_c / f_c$, where $\Delta\mu_c$ is the change in the cluster dipole moment, μ_c, per BaO and f_c is the additional dipole field present in the cluster with the higher surface coverage.

Work function curves are then obtained from the equation[2]

$$\phi = \phi_0 - 1.88\, e\mu_0 N / (1+c\alpha N^{3/2}) \qquad (1)$$

where N is the BaO coverage and c a constant which depends on the geometry of the BaO overlayer and the validity of the point-dipole approximation that is used to calculate the field of the dipole network. For the present cluster approach, c is treated as a parameter and has been chosen such that the minimum work function for BaO/W(100) equals 2.0 eV, which gave c=2.41. A square network of BaO dipoles is assumed on cubic substrates and an equi-triangular network on hexagonal substrates. The constants c for the two cases are related by $c_{hex} = 11/9\ c_{cubic}$, and the dimension of N_{hex} is $2/\sqrt{3}\ N_{cubic}$.

A simple dipole approximation is used to estimate the Ba binding energy, $E_{Ba} = (4\pi\epsilon_0)^{-1} q_{Ba}{}^3/(\mu_c-\mu_s)$, where q_{Ba} is the net charge on Ba and μ_s the contribution to μ_c from the bare substrate cluster.

3. RESULTS

Calculations have been carried out for BaO adsorbed on the (100) face of body-centered-cubic W, the (10$\bar{1}$0) faces of hexagonal-close-packed Os, Re-W, Os-W, Ir-W, and the (111) face of face-centered-cubic Pt.

The calculated dipole properties and work function data are given in Table I. The initial surface dipoles μ_0 increase steadily in the series BaO on W, Os, Pt, and those for the alloy systems are similar to the surface dipole for the also hexagonal Os system. The polarizabilities α, however, show a minimum for Os and lie between the values for W and Os for the alloy systems.

TABLE I. Calculated initial surface dipoles μ_0(D), polarizabilities α(Å^3), work function data ϕ(eV) at 1200 K, optimum coverages N_m(10^{15} atoms/cm^2), and Ba binding energies E_{Ba} (eV) for BaO on W, Os, Pt and W alloys. (ϕ_m for BaO/W(100) has been adjusted*).

System	Lattice	μ_0	α	ϕ_0	$\Delta\phi$	ϕ_m	N_m	E_{Ba}
BaO/W(100)	bcc	31.2	16.6	4.65	-2.65	2.00*	0.14	5.4
BaO/W(poly)	bcc	(31.2)	(16.6)	4.6	-2.65	1.95	0.14	...
BaO/Os(10$\bar{1}$0)	hcp	40.5	13.7	5.2	-3.42	1.78	0.16	6.5
BaO/Pt(111)	fcc	51.9	27.8	5.5	-3.13	2.37	0.10	3.6
BaO/Re-W(10$\bar{1}$0)	hcp	41.4	15.4	5.0	-3.23	1.77	0.14	5.9
BaO/Os-W(10$\bar{1}$0)	hcp	41.1	15.1	5.0	-3.25	1.75	0.15	6.0
BaO/Ir-W(10$\bar{1}$0)	hcp	43.1	15.1	5.2	-3.41	1.79	0.15	6.1

FIGURE 1.

Calculated Work Function Curves for B- and M-type Cathodes.

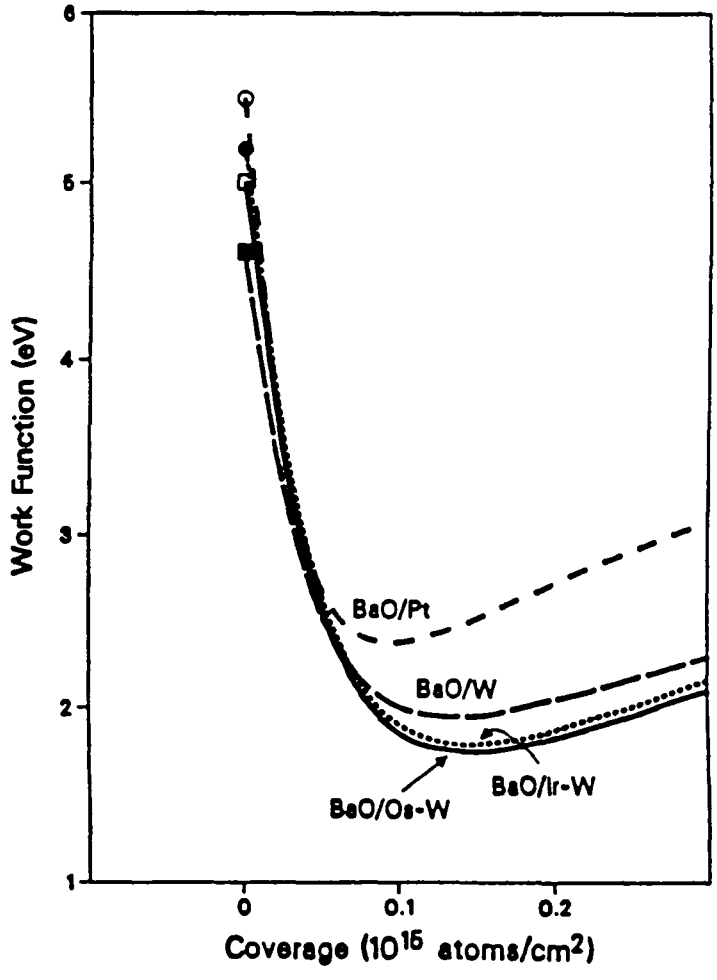

The combination of a sufficiently large initial surface dipole and a small depolarization for the hcp systems gives rise to the largest work function changes $\Delta\phi$ (-3.2 to -3.4 eV). The calculated minimum work functions are in excellent agreement with expectation. The lowest work functions are obtained for the Os-W, Re-W, and Ir-W alloy systems with the hexagonal crystal structure (1.75-1.79 eV), relative to cubic BaO/W (1.95 eV), while the also cubic BaO/Pt system has a substantially higher work function (2.37 eV).

It should be noted that only the work function change $\Delta\phi=\phi-\phi_0$ is obtained from calculated properties and that the minimum work functions depend critically on the bare metal work functions ϕ_0 of the different crystal faces considered. Since accurate values for ϕ_0 are not known in most cases, some assumptions had to be made. The bare metal work functions ϕ_0 given in Table I for a temperature of 1200 K are based on the empirical temperature dependencies of the polycrystalline work functions for the pure metals, which are as follows:[4]

$$
\begin{aligned}
&\text{W}: && \phi_0(T) = 4.52 + 0.6 \times 10^{-4}\, T \\
&\text{Re}: && \phi_0(T) = 4.93 + 0.4 \times 10^{-4}\, T \\
&\text{Os}: && \phi_0(T) = 5.43 - 3.9 \times 10^{-4}\, T \\
&\text{Ir}: && \phi_0(T) = 5.4 - 0.3 \times 10^{-4}\, T \\
&\text{Pt}: && \phi_0(T) = 5.3 + 2.0 \times 10^{-4}\, T\ .
\end{aligned}
$$

Since work functions for the $(10\bar{1}0)$ face of Os and the alloy substrates are not known, the following procedure has been used: For the alloy substrates, first the averages of the polycrystalline metal work functions at 1200 K have been determined and then all work functions for the hcp substrates have been increased by 0.22 eV to account for the differences between the polycrystalline and $(10\bar{1}0)$ values, as taken from the observed increase for hcp Re.[4]

The calculated Ba binding energies (for the clusters with the higher surface coverage) are 5.4 eV for BaO/W(100) and ~6.0 eV for the alloy substrates. This increase of 0.6 eV is in excellent agreement with the observed increase in the energy of desorption for Ba from B- to M-type cathodes,[3] although the experimental energies are about 10% smaller. For the BaO/Pt system, the calculated Ba binding energy drops to 3.6 eV.

4. DISCUSSION

With the successful modeling of the work functions for the different systems, a detailed analysis of the various effects that contribute to the lowering of the work function and the improved emission from dispenser cathodes is now possible. The different factors can be classified as related to (i) properties of the initial work functions of the bare substrates and (ii) the BaO-induced work function changes.

The initial, bare metal, work functions affect the final results by their magnitude and temperature dependence. A high value of ϕ_0 leads to a large charge transfer and a large initial surface dipole μ_0. As expected, the calculated values of μ_0 increase steadily from W to Os and Pt. The large negative temperature coefficient in the temperature dependence of the work function of Os provides an additional benefit for this substrate. Alloying with W, in general, reduces the work functions for Re, Os, Ir, and Pt.

The work function change that is induced by the adsorption of BaO is found to be largest for the hexagonal substrates with the $(10\bar{1}0)$ orientation. The larger $\Delta\phi$ more than compensates for the initially higher work functions of the alloy substrates and leads to minimum work functions that are up to 0.2 eV lower than for BaO/W. The lowering of the work function from B- to M-type cathodes, therefore, has its microscopic origin in the smaller polarizability of the surface dipole on these substrates. The optimum for Os-W cathodes results from the combination of a sufficiently large initial surface dipole μ_0, a small polarizability α, and a not too high initial bare metal work function ϕ_0.

Because of differences in the position of the cluster energy levels as compared to those of an extended surface relative to the adsorbate valence levels, it is likely that the calculated charge transfer and the initial surface dipoles are somewhat too large. This possible artifact is to a large extent, however, compensated by the fact that proportionally smaller μ_0 and α, after readjustment of the parameter c in Eq. (1), mainly affect the calculated coverages and leave the positions of the minimum work functions relative to each other unchanged. Similarly, a different bonding geometry of BaO is not expected to affect the general conclusions.

In summary, the reduced depolarization of the surface dipole on hexagonal as compared to cubic substrates leads to a larger decrease in the work function and provides the long-awaited microscopic explanation for the improved emission from B- to M-type cathodes.

ACKNOWLEDGEMENT

This work has been supported by the NASA Lewis Research Center under Contract NAS3-25940.

REFERENCES

[1] R.A. Tuck, Vacuum 33, 715 (1983).
[2] W. Müller, IEDM Technical Digest, 1991, p. 399.
[3] R. Forman, Appl. Surface Sci. 29, 127 (1987).
[4] G.A. Haas and R.E. Thomas, in *Techniques of Metals Research*, Vol. VI, Part 1 (Interscience, New York, 1972).

SURFACE AND INTERFACE ANALYSIS, VOL. 21, 150–154 (1994)

Electronic Structure and Work Function Study of a Model Dispenser Cathode Surface

A. Lamouri and I. L. Krainsky*
NASA LeRC, 21000 Brookpark Road, Cleveland, OH 44135, USA

W. Muller
Analatom Inc., 29904 Sycamore Oval, Westlake, OH 44145, USA

We have used work function measurements ($\Delta\phi$), Auger electron spectroscopy, low-energy electron diffraction and angle-resolved inverse photoelectron spectroscopy to study the coadsorption of barium and oxygen on tungsten. The experimental two-dimensional band structure was compared with results of embedded cluster model calculations for a c(2 × 2) BaO monolayer on W(001) with barium and oxygen placed on alternate fourfold-hollow sites. Our work function measurements revealed that adsorption of one monolayer of BaO decreased the work function of W(001) (ϕ = 4.63 eV) to ~2.3–2.4 eV regardless of the order of barium and oxygen adsorption on the surface. Inverse photoelectron spectroscopy in the isochromat mode was used to investigate the unoccupied electronic energy levels of one monolayer of BaO on W(001) along two high-symmetry directions of the W(001) surface Brillouin zone Non-dispersing spectral features were observed at 0.6 eV and 3.4 eV above the Fermi level (E_F) and were assigned to transitions into both barium and tungsten d states in good agreement with calculated densities of states.

INTRODUCTION

Ever since it was discovered that alkaline-earth metals reduced the work function of transition metals, adsorption of barium and oxygen on tungsten has received considerable attention because of its importance in thermionic cathodes In recent years, this adsorption system has been investigated extensively Although some of these studies dealt with the electronic structure of the BaO/W system,[1–8] none have been devoted to its unoccupied electronic band structure With the advent of inverse photoelectron spectroscopy (IPS), the unoccupied electronic states that are inaccessible in ordinary photoemission can be probed particularly between the Fermi level and the vacuum level As its name implies, this technique consists of bombarding the surface with a beam of electrons of a known energy and examining the photons emitted through radiative decay [9]

While it has been established for quite some time that the interaction of the barium oxide layer with the tungsten matrix is responsible for reducing the work function and increasing the emission in thermionic dispenser cathodes, the exact coverage and orientation of barium and oxygen on the surface are not well established. The coverage is believed to be between a half and one full monolayer and stoichiometrically very close to BaO,[1,2] with reported work function values ranging from 2 0 to 2 7 eV [3–5] Furthermore, a thorough understanding of the origin of the surface dipole layer is necessary for establishing the mechanism responsible for lowering the work function At present it is not clear whether this dipole layer arises from the polarization of the adsorbed layer or is the result of a partial charge transfer to the substrate.

The objectives of the present study are to determine the variation of the work function of W(001) as a function of barium and oxygen coverages and to investigate the experimental two-dimensional band structure of the empty electronic levels of one monolayer of BaO on the W(001) surface The experimental measurements are compared with the results of fully relativistic embedded cluster model calculations for ordered c(2 × 2) BaO overlayers on the W(001) surface with barium and oxygen occupying adjacent fourfold-hollow sites as shown in Fig 1

EXPERIMENTAL TECHNIQUES

The experiments were performed in an all-stainless-steel ultrahigh vacuum chamber operated in the low

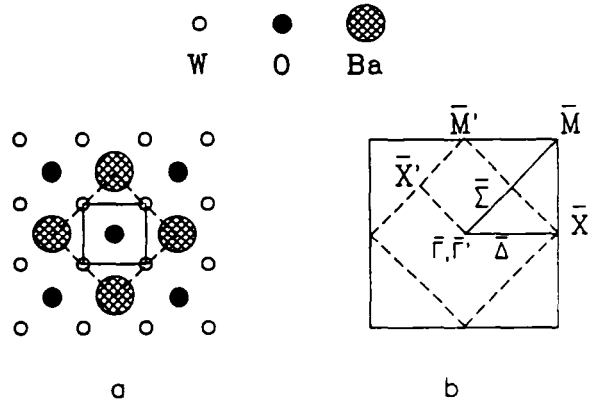

Figure 1 Two-dimensional unit cell of a c(2 × 2) monolayer of BaO on W(001) in (a) real space and (b) reciprocal space

* Author to whom correspondence should be addressed

CCC 0142-2421/94/020150–05

Received 9 June 1993
Accepted 9 September 1993

10^{-11} Torr range This chamber was equipped with a double-pass cylindrical mirror analyzer for Auger monitoring of the surface composition and contaminants, and low-energy electron diffraction (LEED) optics for monitoring the surface structure and orientation.

The IPS spectra were measured in the isochromat mode, i.e. by collecting photons at a fixed photon energy while varying the energy of the incoming electrons. The bandpass photon detector, which was designed after that of Babbe *et al.*,[10] consisted of a CuBe photomultiplier and a CaF_2 window. The combination of the spectral sensitivity of the multiplier and the transmission cut-off of the window created a bandpass detector centered around 9.8 eV with a full width at half-maximum of 0.6 eV.

The low-energy electron gun, which was mounted at 40° relative to the photon detector, used a BaO cathode and was capable of producing a well-focused beam of electrons in the 5–20 eV range The angle of electron beam incidence was varied by rotating the sample. The angular divergence of the electron beam was estimated at better than 3°, giving a momentum resolution of ~ 0.1 Å^{-1}.[11] Count rates of several hundred counts per second were achieved with an electron beam current of 5 μA The overall energy resolution of the spectrometer was of the order of 0.6 eV.

Accurate measurements of the work function were achieved by the diode method. The variation of the target work function was monitored using a feedback loop, which maintained a constant target current while varying the retarding potential The target work function change due to the adsorption was then deduced from the variation of the retarding voltage.

The W(001) crystal was outgassed by electron bombardment at high temperature for several days until the pressure was in the low 10^{-10} Torr range. It was then cleaned in vacuum by repeated heating at 1700 K in an oxygen atmosphere of 6.0×10^{-8} Torr followed by occasional flashing at 2500 K until cleanliness was confirmed by AES, LEED and IPS The target was also flashed before each deposition A full description of the W(001) surface preparation can be found elsewhere.[12]

Oxygen was admitted to the chamber up to pressures in the 10^{-9} Torr range via a variable leak valve, and barium was deposited onto the W(001) surface from a well-outgassed Ba source provided by the Philips Company. Coverages were determined by a combination of work function ($\Delta\phi$), LEED and AES measurements.

RESULTS AND DISCUSSION

Work function measurements

To obtain one monolayer of BaO on W(001), three different preparation methods were used.

In the first method, a monolayer of barium was deposited onto W(001) either by depositing a thick Ba layer and then annealing it at 1100 K for ~3 min as described by Moore and Allison,[12] or by monitoring the change of the W(001) work function as a function of Ba coverage as shown in Fig 2. A c(2 × 2) LEED

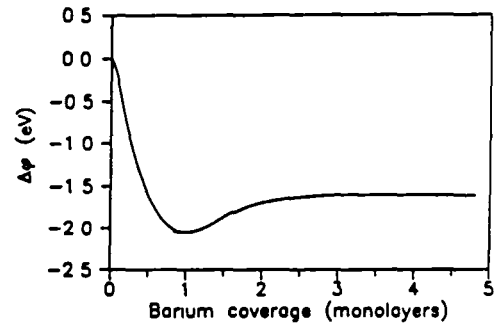

Figure 2. Variation of the work function of W(001) as a function of barium coverage

pattern indicative of an ordered Ba layer was observed at one monolayer coverage. Auger electron spectroscopy analysis showed that the thick barium films were contaminant free. After annealing, however, the films showed a small (< 5%) oxygen contamination

Following the Ba monolayer deposition, the work function of the surface was monitored as a function of oxygen exposure. A graph of the work function change as a function of oxygen exposure is shown in Fig 3 The c(2 × 2) LEED pattern was still observable at an oxygen coverage of ~0.5 L (1 L = 1 Langmuir = 10^{-6} Torr · s), where the work function of the Ba monolayer on W(001) decreased by a maximum value of 0 34 eV. It increased again when oxidation was continued beyond 0.5 L, which is in qualitative agreement with the results of Haas *et al.*[2]

The observed c(2 × 2) LEED pattern at an oxygen coverage of 0.5 L is indicative of a surface where the concentration of the Ba and O atoms is half that of the substrate atoms [cf. Fig 1(a)]. Any deviation from this ratio resulted in a higher work function, as is illustrated in Fig 3. The sharp increase of the work function at coverages higher than 0.5 L of oxygen is interpreted as a possible mechanism for the poisoning of impregnated cathodes Taking into account the work function of W(001) ($\phi = 4.63$ eV)[14] and that of one monolayer of Ba on W(001) ($\phi = 2.63$ eV),[15] we conclude that the work function of one monolayer of BaO on W(001) is $\sim 2.29 \pm 0.1$ eV. This is slightly higher than the values measured thermionically for B-type cathodes, which are typically in the 2.0–2 2 eV range.[16]

In the second method, the W(001) surface was exposed to 0.5 L of oxygen before the barium deposition was performed. A break in the slope of the $\Delta\phi$

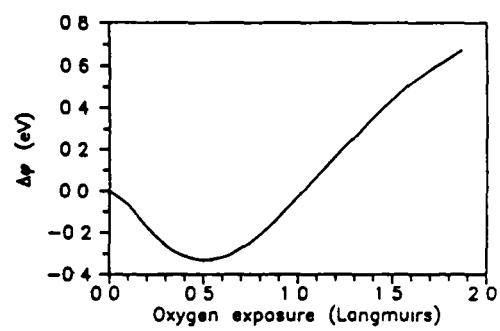

Figure 3. Variation of the work function of one monolayer of barium on W(001) as a function of oxygen exposure

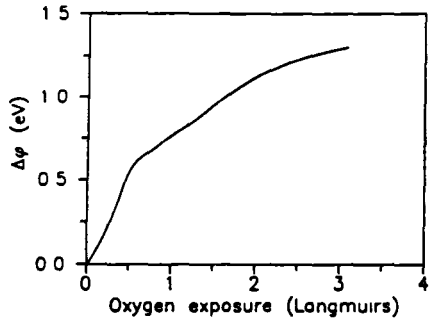

Figure 4 Variation of the work function of W(001) as a function of oxygen exposure

curve and a p(4 × 1) LEED pattern were observed at an oxygen exposure of 0 5 L As shown in Fig 4, the work function of W(001) increased by ~0 6 eV at this coverage, which is consistent with other studies.[17,18]

Following the oxygen exposure, the work function of the surface was monitored as a function of Ba coverage as shown in Fig 5 A maximum drop of 2 79 eV relative to the work function of the O/W(001) surface and a c(2 × 2) LEED pattern were observed at a barium coverage corresponding to the minimum work function. Hence, the work function of one monolayer of BaO on W(001) when using this order of deposition is 2 44 ± 0.1 eV

Finally, one monolayer of BaO on W(001) was obtained by completely oxidizing a thick barium film and then annealing the oxidized film at 1100 K for ~3 min

Auger electron spectroscopy of our monolayer BaO films showed a barium-to-oxygen Auger line intensity ratio of 1 2, which is in good agreement with other studies [3,19] The Auger intensity ratio, LEED structure, work function value and IPS measurements for one monolayer of BaO on W(001) were nearly independent of the order in which barium and oxygen were adsorbed on the surface

Calculated densities of states (DOS) and IPS measurements

To carry out the theoretical calculations, the W(001) substrate was modeled with a 25-atom tungsten cluster consisting of a surface layer with a 4 × 4 array and a subsurface layer with a 3 × 3 array Barium and oxygen were placed on alternate fourfold-hollow sites of the surface layer as shown in Fig 1(a) The barium and oxygen heights corresponding to this adsorption geometry have been optimized by Hemstreet *et al* [5] by calculating the full-potential linearized augmented plane wave (FLAPW) total energy of a c(2 × 2) BaO overlayer placed on both sides of a five-layer W(001) film Projected local DOS were generated for the central W, Ba and O surface atoms by convoluting the energies of the individual states of the cluster with Gaussian functions with full widths at half-maxima of 0 2 eV A more detailed description of the theoretical approach can be found elsewhere.[20]

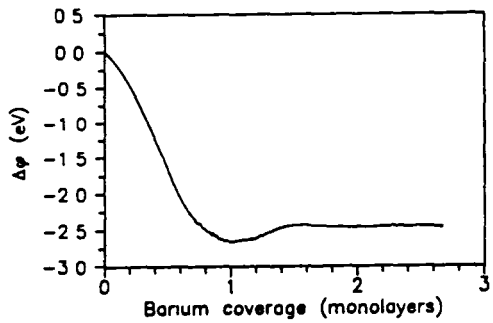

Figure 5 Variation of the work function of 0 5 L of oxygen on W(001) as a function of barium coverage

Inverse photoelectron spectra for one monolayer of BaO on W(001) at different angles of electron incidence in the $\bar{\Gamma}\bar{\Delta}\bar{X}$ [$\bar{\Gamma}'\bar{\Sigma}'\bar{M}'$] and $\bar{\Gamma}\bar{\Sigma}\bar{M}$ [$\bar{\Gamma}'\bar{\Delta}'\bar{X}'$] directions of the surface Brillouin zone (SBZ) of the p(1 × 1) W(001) [c(2 × 2) BaO/W(001)] surface are given in Fig 6 The spectra along the $\bar{\Gamma}\bar{\Delta}\bar{X}$ line were taken in the (001) mirror plane and those in the $\bar{\Gamma}\bar{\Sigma}\bar{M}$ direction were taken in the (011) mirror plane of the unreconstructed tungsten surface [cf Fig 1(b)] A spectrum for one monolayer of Ba on W(001) taken at normal incidence is also shown at the bottom of Fig 6(a) The Fermi edge was determined from the onset of photon emission

The two-dimensional band structure, as derived from the spectra of Fig 6, along with the calculated DOS for a c(2 × 2) BaO layer on W(001) are shown in Fig 7 The component of the wave vector of the incoming electron parallel to the surface ($k_{\parallel}$) was determined from the formula

$$hk_{\parallel} = [8\pi^2 m(E_i - \phi)]^{1/2} \sin\alpha$$

where α is the angle of electron incidence measured from the surface normal, E_i is the electron's initial energy measured from E_F, and ϕ is the work function of the surface being studied A value of 2 37 eV corresponding to the average of the measured work functions was used to analyze the IPS data The solid line on the right panel of Fig 7 represents the calculated total DOS, while the long dashes represent the oxygen and the short dashes the barium contributions

Upon adsorption of one monolayer of BaO, the W(001) surface states[12,21] seemed to have been completely quenched and new peaks appeared At normal incidence, only two features were observed above the Fermi level. One was located at 0 6 eV and the other at 3 4 eV, which was 1 0 eV above the vacuum level (E_V)

The peak near E_F appeared to be reminiscent of the Ba peak observed for one monolayer of Ba on W(001)[15,20] and could only be followed up to a polar angle of 10° in either direction. It showed strong sensitivity to surface contamination and was totally quenched with oxygen adsorption exceeding 1 0 L This, and the calculated DOS shown on the right panel of Fig 7, helped us assign this peak to transitions mainly into Ba d and W d surface states The band derived from this peak was completely flat along the $\bar{\Gamma}\bar{\Delta}\bar{X}$ direction and showed very little dispersion along $\bar{\Gamma}\bar{\Sigma}\bar{M}$ A similar band was observed for one monolayer of Ba on W(001), where it appeared at the center of the SBZ near 0.6 eV above E_F, dispersed upward in the $\bar{\Gamma}\bar{\Delta}\bar{X}$ direction losing intensity and disappeared when $k_{\parallel}$ reached 0.4 $Å^{-1}$.[15]

Inverse photoelectron spectroscopy data for 0 5 L of oxygen on W(001) revealed several oxygen-induced

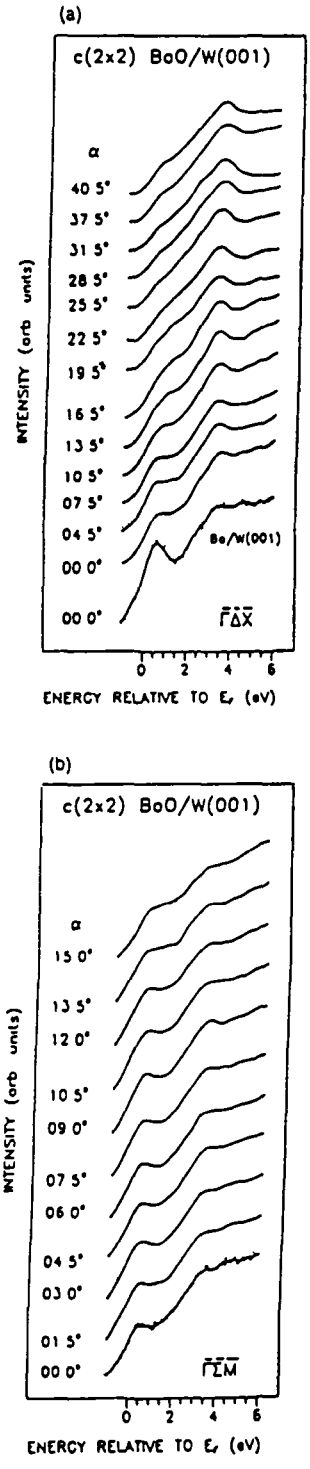

Figure 6 (a) Inverse photoelectron spectra of a c(2 × 2) BaO overlayer on W(001) at different angles of electron incidence α in the $\bar{\Gamma}\bar{\Delta}\bar{X}$ direction of the SBZ of the unreconstructed W(001) surface (b) Inverse photoelectron spectra of a c(2 × 2) BaO overlayer on W(001) at different angles of electron incidence α in the $\bar{\Gamma}\bar{\Sigma}\bar{M}$ direction of the SBZ of the unreconstructed W(001) surface

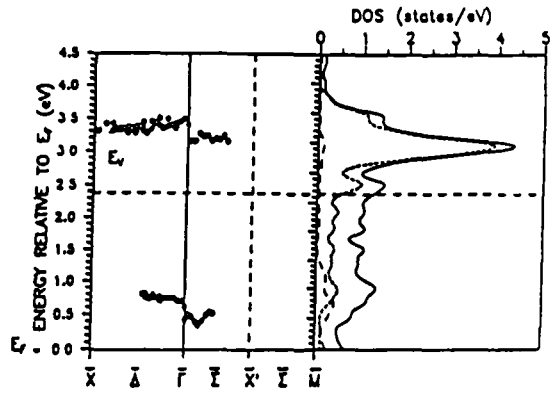

Figure 7. (*Left panel*) Experimental two-dimensional band structure of a c(2 × 2) BaO overlayer on W(001) in the $\bar{\Gamma}\bar{\Delta}\bar{X}$ and the $\bar{\Gamma}\bar{\Sigma}\bar{M}$ directions of the unreconstructed W(001) surface (*Right panel*) Fully relativistically calculated DOS (solid line) The long dashes represent the oxygen and the short dashes the barium contributions

states above the Fermi level [22] However, almost no unoccupied oxygen states were observed for one monolayer of BaO on W(001), as indicated by the calculated DOS of Fig 7 Therefore, we believe that the absence of unoccupied oxygen levels in the case of BaO on W(001) is due to a charge transfer from the barium atom to the oxygen atom, a conclusion that is supported by the calculated charge distribution in the cluster As a result, the barium unoccupied d states become more localized and lose their dispersion. In addition, a Ba–O surface dipole is created. This dipole opposes the W–O dipole and is believed to contribute to the reduction of the surface work function.

The peak located at 3 4 eV, on the other hand, showed little sensitivity to surface contamination Previously, a similar peak was observed for the c(2 × 2) Ba/W(001) surface and was attributed to transitions into tungsten bulk bands.[15] This conclusion was based on the fact that this peak showed little sensitivity to surface contamination and on FLAPW calculations, which predicted a feature in the DOS at 3.5 eV above E_F originating from the inner layers of a 19-layer film [23] However, recent IPS data appeared to indicate that this state also comprised a large Ba component Barium on W(001) coverage-dependent data[24] taken along the $\bar{\Gamma}\bar{\Sigma}\bar{M}$ line of the W(001) unreconstructed surface revealed a Ba-related feature near 3.4 eV for $\alpha = 34°$, a region where no unoccupied W(001) states were observed [21] The intensity of this state increased with Ba coverage Therefore, we now assign this state to transitions into both Ba d states and W d bulk states. This is consistent with FLAPW calculations by Hemstreet *et al* [25] for a c(2 × 2) Ba monolayer placed on both sides of a five-layer W(001) film, which revealed a strong enhancement of a tungsten bulk peak located 3 2 eV above E_F upon adsorption of barium. Our calculated DOS, however, showed that the contribution to the peak near 3 4 eV seems to come almost entirely from Ba d states This apparent discrepancy is due to the fact that the employed cluster contains only two layers of tungsten atoms, none of which is representative of tungsten bulk atoms.

Overall, our IPS measurements were confirmed by the fully relativistically calculated DOS for a c(2 × 2) BaO monolayer on the W(001) face with barium and oxygen placed on alternate fourfold-hollow sites

In summary, we observed the formation of a c(2 × 2) LEED pattern associated with the adsorption of one monolayer of BaO on W(001) The work function of

W(001) (ϕ = 4 63 eV) decreased to a minimum value of 2 3–2 4 eV at this coverage. By investigating the electronic states above the Fermi level at this coverage, we were able to identify both Ba d and W d states The absence of oxygen unoccupied states in the presence of Ba on the W(001) surface can be explained by a charge transfer from barium to oxygen This charge transfer creates a surface dipole that more than compensates for the dipole created by the adverse charge transfer from tungsten to oxygen The resulting net dipole is believed to be responsible for reducing the work function and enhancing emission in dispenser cathodes

Acknowledgements

We would like to thank Lou Maschak for his assistance with the experimental set-up and Ben Ebihara for designing the Ba source This work was supported by the NASA Lewis Research Center under contract NAS3-25940 and the National Research Council

REFERENCES

1 D Brion, J C Tonnerre and A. M Shroff, *Appl Surf Sci* **16**, 55 (1983)
2 G A Haas, A Shih and C R K Marrian, *Appl Surf Sci* **16**, 139 (1983)
3 G A Haas, C R K Marrian and A Shih, *Appl Surf Sci* **24**, 430 (1985)
4 R Forman *J Appl Phys* **47**, 5272 (1976)
5 L A Hemstreet, S R Chubb and W E Pickett, *Phys Rev B* **40**, 3592 (1989)
6 J A. T Verhoeven and H van Doveren, *Appl Surf Sci* **5**, 361 (1980)
7 G Thornton, I W Owen, C H Richardson, D Norman, R A Tuck, H B Skinner, P J Wadsworth and T M Gardiner, *Vacuum* **38**, 401 (1988)
8 W Muller, *IEEE Trans Electron Devices* **36**, 180 (1989)
9 J B Pendry, *J Phys C* **14**, 1381 (1981), D P Woodruff, *J Vac Sci Technol A* **1**, 1104 (1982), V Dose, *Surf Sci Rep* **5**, 337 (1985), N V Smith and D P Woodruff, *Prog Surf Sci* **21**, 295 (1986), P D Johnson and S L Hulbert, *Rev Sci Instrum* **61**, 2277 (1990)
10 N Babbe, W Drube, I Schäfer and M Skibowsky, *J Phys E* **18**, 158 (1985)
11 I L Krainsky, *Rev Sci Instrum* **62**, 1746 (1991).
12 I L. Krainsky, *J Vac Sci Technol A* **5**, 735 (1987)
13 G E Moore and H W Allison, *J Chem Phys* **23**, 1609 (1955)
14 R L. Billington and T N Rhodin, *Phys Rev Lett* **41**, 1602 (1978)
15 A Lamouri and I L Krainsky, *Surf Sci* **278**, 286 (1992)
16 B C Lamartine, K G Eyink, J v Czarnecki, W V Lampert and T W Haas, *Appl Surf Sci* **24**, 575 (1985)
17 E Bauer, H Poppa and Y Viswanath, *Surf Sci* **58** 517 (1976)
18 H M Kramer and E Bauer, *Surf Sci* **92**, 53 (1980)
19 D Mueller, A. Shih, E Roman, T Madey, R Kurtz and R Stockbauer, *J Vac Sci Technol A* **6**, 1067 (1988)
20 A. Lamouri, W Muller and I L Krainsky, *Phys Rev B* (to be published)
21 A. Lamouri and I L. Krainsky, *Surf Sci* (to be published)
22 I L. Krainsky, *J Vac Sci Technol A* **6**, 780 (1988)
23 L F Mattheiss and D R Hamann, *Phys Rev B* **29**, 5372 (1984)
24 A. Lamouri and I L Krainsky (unpublished)
25 L. A. Hemstreet and S R Chubb, *Phys Rev B* **47**, 10748 (1993)

GEOMETRY AND UNOCCUPIED ELECTRONIC STATES OF A MODEL BAO CATHODE SURFACE

A. Lamouri
Case Western Reserve University, Cleveland, Ohio 44106
I. L. Krainsky
NASA LeRC, 21000 Brookpark Road, Cleveland, Ohio 44135
W. Müller
Analatom Inc., 29904 Sycamore Oval, Westlake, Ohio 44145

INTRODUCTION

Ever since it was discovered that alkaline-earth metals reduced the work function of transition metals, adsorption of barium and oxygen on tungsten has received considerable attention because of its importance in thermionic cathodes. Although some of these studies dealt with the electronic structure of the BaO/W system[1-8], none have been devoted to its unoccupied electronic band structure With the advent of Inverse Photoelectron Spectroscopy, the unoccupied electronic states which are inaccessible in ordinary photoemission can be probed, particularly between the Fermi level and the vacuum level.

EXPERIMENTAL

The experiments were performed in an all stainless steel ultra-high vacuum chamber which operated in the low 10^{-11} Torr range. This chamber was equipped with a double pass cylindrical mirror analyzer for Auger monitoring of the surface composition and contaminants, and LEED optics for monitoring the surface structure and orientation. IPS spectra were measured in the isochromat mode, by collecting photons at a fixed photon energy using a photon detector (designed after Babbe et al.[9]) while varying the energy of the incoming electrons. The low energy electron gun, which was mounted at 40° relative to the photon detector, used a BaO cathode and was capable of producing a well-focused beam of electrons in the 5 to 20 eV range [10] The angle of electron beam incidence was varied by rotating the sample. Measurements of the work function were conducted employing the diode method. The variation of the target work function was monitored using a feedback loop which maintained a constant target current while varying the retarding potential. The target was cleaned before each deposition. A full description of the W(001) surface preparation can be found elsewhere.[11] Oxygen was admitted to the chamber up to pressures in the 10^{-9} Torr range via a variable leak valve and barium was deposited onto the W(001) surface from a Ba source provided by the Philips Company Coverage was determined by a combination of $\Delta\phi$, LEED, and AES measurements.

WORK FUNCTION MEASUREMENTS

To obtain one monolayer of BaO on W(001) three different preparation methods were used

In the first method, a monolayer of barium was deposited onto W(001) either by depositing a thick Ba layer and then annealing it at 1100 K for approximately 3 minutes as described by Moore and Allison,[12] or by monitoring the change of the W(001) work function as a function of Ba coverage as shown in Fig.1. A c(2x2) LEED pattern indicative of an ordered Ba layer was observed at one monolayer coverage.

Following the Ba monolayer deposition, the work function of the surface was monitored as a function of oxygen exposure. A graph of the work function change as a function of oxygen exposure is shown in Fig. 2. The c(2x2) LEED pattern was still observable at an oxygen coverage of approximately 0.5 L (1 L=1 Langmuir=10^{-6} Torr sec.) where the work function of the Ba monolayer on W(001) decreased by a maximum value of 0.34 eV. It increased again when oxidation was continued beyond 0.5 L which is in qualitative agreement with the results of Haas et al.[2]

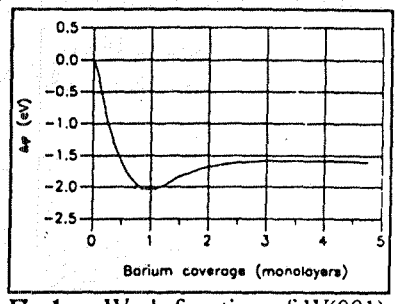

Fig.1. Work function of W(001) vs. Ba coverage

The observed c(2x2) LEED pattern at an oxygen coverage of 0.5 L corresponded to a surface with the concentration of the Ba and O atoms equal ½ that of the substrate atoms (cf. Fig. 3(a,b)). Any deviation from this ratio resulted in a higher work function, as is illustrated in Fig. 2. Taking into account the work function of W(001) (ϕ=4.63 eV)[13] and that of one monolayer of Ba on W(001) (ϕ=2.63 eV),[14] we conclude that the work function of one monolayer of BaO on W(001) is $\phi \approx 2.29 \pm 0.1$ eV. This is slightly higher than the values measured thermionically for B-type cathodes which are typically in the 2.0 to 2.2 eV range.[15]

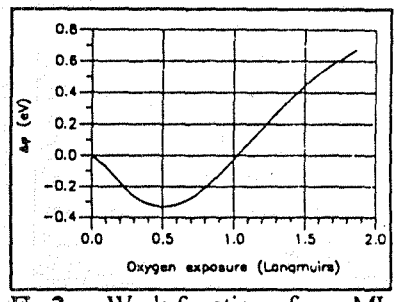

Fig.2. Work function of one ML of Ba on W(001) vs. oxygen exposure

In the second method, the W(001) surface was exposed to 0.5 L of oxygen before the barium deposition was performed. A break in the slope of the $\Delta\phi$ curve and a p(4x1) LEED pattern were observed at an oxygen exposure of 0.5 L. As shown in Fig. 4, the work function of W(001) increased by approximately 0.6 eV at this coverage which is consistent with other studies.[16,17] Following the oxygen exposure, the work function of the surface was monitored as a function of Ba coverage as shown in Fig. 5. A maximum drop of 2.79 eV relative to the work function of the O/W(001) surface and a c(2x2) LEED pattern were observed at a barium coverage corresponding to the minimum work function. Hence the work function of one monolayer of BaO on W(001) when using this order of deposition is ϕ=2.44±0.1 eV.

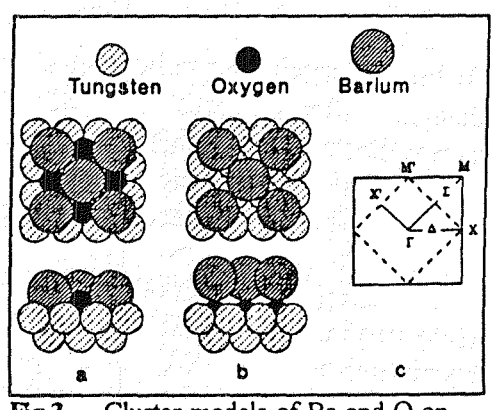

Fig.3. Cluster models of Ba and O on W(001) in (a) tilted and (b) upright configurations. (c)- SBZ of the clean (solid line) and coated W(001) surface.

Finally, one monolayer of BaO on W(001) was obtained by completely oxidizing a thick barium film and then annealing the oxidized film at 1100 K for approximately 3 minutes.

AES analysis of our monolayer BaO films showed a barium to oxygen Auger line intensity ratio of 1:2 which is in good agreement with other studies.[3,18] The Auger intensity ratio, LEED structure, work function value and IPS measurements for one monolayer of BaO on W(001) were nearly independent of the order in which barium and oxygen were adsorbed on the surface.

CALCULATED DOS AND IPS MEASUREMENTS

To carry out the theoretical calculations, the W(001) substrate was modeled with a 25-atom tungsten cluster consisting of a surface layer with a 4x4 array and a sub-surface layer with a 3x3 array Barium and oxygen were placed on alternate fourfold-hollow sites of the surface layer as shown in Fig 3(a) The barium and oxygen heights corresponding to this adsorption geometry have been optimized by Hemstreet et al [5] Projected local densities of states were generated for the central W, Ba, and O surface atoms by convoluting the energies of the individual states of the cluster with Gaussian functions with full widths at half maxima of 0 2 eV.

The two-dimensional band structure, as derived from the IPS spectra[19], along with the calculated DOS for a c(2x2) BaO layer on W(001) are shown in Fig 6

Upon adsorption of one monolayer of BaO, the W(001) surface states[12,21] seemed to have been completely quenched and new peaks appeared At normal incidence, only two features were observed above the Fermi level One was located at 0.6 eV and the other at 3.4 eV, which was 1.0 eV above the vacuum level (E_V).

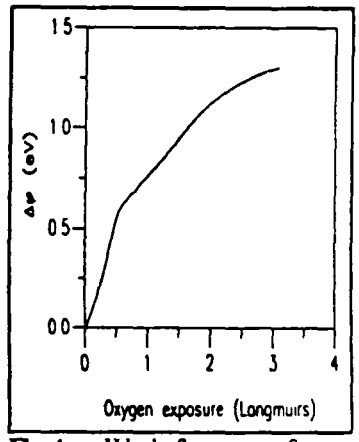

Fig.4. Work function of W(001) as a function of oxygen exposure

The peak near E_F appeared to be reminiscent of the Ba peak observed for one monolayer of Ba on W(001)[14,19] and could only be followed up to a polar angle of 10° in either direction It showed strong sensitivity to surface contamination and was totally quenched with oxygen adsorption exceeding 1.0 L. This, and the calculated DOS shown on the right panel of Fig 6, helped us assign this peak to transitions mainly into Ba and W d surface states.

IPS data for 0.5 L of oxygen on W(001) revealed several oxygen-induced states above the Fermi level.[20] However, almost no unoccupied oxygen states existed in the calculated DOS for one monolayer of BaO on W(001) as it is shown in Fig. 6. Therefore, we believe that the absence of unoccupied oxygen levels in the case of BaO on W(001) is due to a charge transfer from the barium atom to the oxygen atom, a conclusion which is supported by the calculated charge distribution in the cluster. As a result, the barium unoccupied d states become more localized and lose their dispersion. In addition, a Ba-O surface dipole is created. This dipole opposes the W-O dipole and is believed to contribute to the reduction of the surface work function.

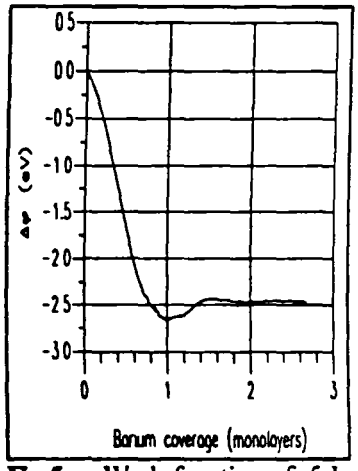

Fig.5. Work function of 5 L of oxygen on W(001) vs Ba coverage

The peak located at 3.4 eV, on the other hand, showed little sensitivity to surface contamination. Previously, a similar peak was observed on the c(2x2) Ba/W(001) surface and was attributed to transitions into W bulk bands [14] This conclusion was based also on LAPW calculations which predicted a feature in the DOS at 3.5 eV above E_F originating from the inner layers of a 19-layer film.[21] However, our IPS data appeared to indicate that this state also comprised a large Ba component. The intensity of this state increased with Ba coverage We now assign this state to transitions into both Ba d states and W d bulk states. This is consistent with FLAPW calculations by Hemstreet et al [22] for a c(2x2) Ba monolayer placed on both sides

of a 5-layer W(001) film which revealed a strong enhancement upon adsorption of barium of a tungsten bulk peak located at 3.2 eV above E_F. Our calculated DOS, however, showed that the contribution to the peak near 3.4 eV seems to come almost entirely from Ba d states. This apparent discrepancy is due to the fact that the employed cluster contains only two layers of W atoms, none of which is representative of W bulk atoms

Overall, our IPS measurements were confirmed by the fully-relativistically calculated DOS for a c(2x2) BaO monolayer on the W(001) face with barium and oxygen placed on alternate fourfold-hollow sites.

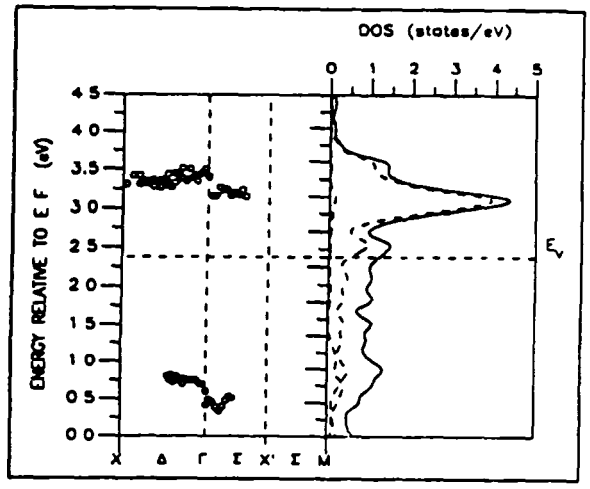

Fig. 6. Left panel Experimental 2-D band structure of a c(2x2) BaO overlayer on W(001) in ΓΔX and ΓΣM directions of W(001) Right panel Fully-relativistic total DOS (solid line) with oxygen and barium contributions represented by dashed and dotted lines respectively

REFERENCES

1 D Brion, J.C. Tonnerre and A.M. Shroff, *Appl Surf Sci* **16**, 55 (1983).
2 G.A Haas, A. Shih and C.R.K. Marrian, *Appl Surf Sci* **16**, 139 (1983).
3 G A. Haas, C.R.K. Marrian and A. Shih, *Appl Surf Sci* **24**, 430 (1985).
4 R. Forman, *J Appl Phys* **47**, 5272 (1976).
5 L.A. Hemstreet, S R. Chubb and W.E. Pickett, *Phys Rev B* **40**, 3592 (1989).
6 J A.T Verhoeven and H. van Doveren, *Appl. Surf Sci* **5**, 361 (1980).
7 G. Thornton, I.W. Owen, C.H. Richardson, D. Norman, R.A. Tuck, H.B Skinner, P J Wadsworth and T.M. Gardiner, *Vacuum* **38**, 401 (1988).
8 W. Müller, *IEEE Trans Elec Dev* **36**, 180 (1989).
9 N mBabbe, W. Drube, I Schäfer and M. Skibowsky, *J. Phys E* **18**, 158 (1985).
10 I L. Krainsky, *Rev Sci Instrum.* **62**, 1746 (1991).
11. I.L. Krainsky, *J Vac Sci Technol A* **5**, 735 (1987).
12. G E. Moore and H.W. Allison, *J. Chem. Phys* **23**, 1609 (1955).
13. R.L. Billington and T.N. Rhodin, *Phys. Rev Lett.* **41**, 1602 (1978).
14. A. Lamouri and I.L. Krainsky, *Surf Sci* **278**, 286 (1992).
15 B.C Lamartine, K.G. Eyink, J. v. Czarnecki, W.V. Lampert and T.W. Haas, *Appl. Surf Sci* **24**, 575 (1985).
16. E. Bauer, H. Poppa and Y. Viswanath, *Surf. Sci.* **58**, 517 (1976).
17. H.M. Kramer and E. Bauer, *Surf. Sci.* **92**, 53 (1980).
18. D. Mueller, A. Shih, E. Roman, T. Madey, R. Kurtz and R. Stockbauer, *J Vac Sci Technol A* **6**, 1067 (1988).
19. A. Lamouri, W. Müller and I.L. Krainsky, *Surf. & Int. Anal* (to be published).
20. I.L. Krainsky, *J. Vac. Sci Technol A* **6**, 780 (1988).
21. L.F. Mattheiss and D.R. Hamann, *Phys. Rev. B* **29**, 5372 (1984).
22. L.A. Hemstreet and S.R. Chubb, *Phys. Rev. B* **47**, 10748 (1993).

Geometry and unoccupied electronic states of Ba and BaO on W(001)

A Lamouri
NASA Lewis Research Center, 21000 Brookpark Road, Cleveland, Ohio 44135

W. Müller
Analatom Inc, 29904 Sycamore Oval, Westlake, Ohio 44145

I L Krainsky
NASA Lewis Research Center, 21000 Brookpark Road, Cleveland, Ohio 44135

(Received 19 October 1993, revised manuscript received 23 March 1994)

A study aimed at understanding the geometrical and electronic properties of barium and oxygen coadsorbed on the tungsten (001) surface has been carried out by means of work-function measurements ($\Delta\phi$), Auger-electron spectroscopy, low-energy electron diffraction, inverse photoelectron spectroscopy, and relativistic-electronic-structure calculations A report of the experimental measurements and a comparison with theoretical results from embedded-cluster-model calculations are presented. Our experimental studies show that the work function of the W(001) surface (ϕ=4.63 eV) is lowered to approximately 2 3–2 4 eV by coadsorption of 1 ML of Ba and O regardless of the order of deposition of these two species The technique of IPS in the isochromat mode was used to determine the unoccupied electronic-energy band structure for ordered $c(2\times2)$ Ba and O layers on W(001) Several spectral features are observed above the Fermi level (E_F), which we assign to transitions into Ba and W d states The measured two-dimensional electronic band structure is independent of the order of Ba and O deposition Using embedded-cluster-model calculations, we investigated two possible adsorption configurations of an ordered $c(2\times2)$ adlayer of Ba and O on W(001) "tilted," where Ba and O are placed on alternate fourfold-hollow sites, and "upright," where the adsorbed atoms lay above the same site with Ba outermost The calculated densities of states for the tilted geometry show distinct peaks above E_F originating from Ba and W d orbitals and are in good agreement with the experimental results

I. INTRODUCTION

Barium dispenser cathodes are widely used in microwave power devices because of their reliability, long life, and high current densities At operating temperatures of approximately 1300 K, these cathodes achieve current densities of up to 100 A/cm^2 by maintaining a low work-function surface composed of Ba and O on a W matrix [1,2] It is also widely accepted that the active layer of these cathodes is composed of Ba and O that is stoichiometrically very close to BaO (Ref. 3) with a coverage for the Ba and O layers believed to be between .5 ML and 1 ML [4,5] However, it is not clear whether Ba and O are adsorbed as a BaO molecule or if BaO dissociates completely on the surface [6,7]

The lowering of the work function of transition metals by adsorption of alkaline-earth metals can be attributed to the formation of a surface-dipole layer resulting from charge transfer from the adsorbate to the substrate. Recent full-potential linearized augmented-plane-wave (FLAPW) calculations for $c(2\times2)$ Ba overlayers on W(001),[8] however, lead to the conclusion that, for ML coverages, the bonding is not ionic but rather metallic covalent, with the dipole layer residing in the polarized Ba valence electrons, much like for the adsorption of alkali metals on transition metals [9,10]

In order to understand the adsorbate-substrate interaction, a thorough knowledge of the arrangement of the Ba and O adatoms on the surface is necessary. Several papers with conflicting results have been published on this subject. While some groups propose a model with a standing-up adsorption layer in which Ba is outermost,[11,12] others produce experimental and theoretical data consistent with a more coplanar adsorption geometry where Ba and O occupy alternate fourfold-hollow sites [13,14] These conflicting results and the interest in understanding the mechanism of operation of thermionic dispenser cathodes have generated several research programs in the last few decades. New and improved cathodes rely heavily on these studies and on a thorough understanding of not only the geometrical but also the electronic structure of alkaline-earth oxides adsorbed on transition metals

To date, most of the studies of the adsorption of BaO on W(001) were aimed at understanding the geometrical structure of the adsorbate Although some of these studies dealt with the electronic structure of the BaO/W system, none have been devoted to its unoccupied electronic band structure. Only two theoretical studies of this system, the FLAPW (Ref. 13) and the cluster-model[15] calculations, have been reported to date, both of which lack a thorough investigation of the unoccupied densities of states (DOS).

To carry out the research, a model surface is necessary

since actual dispenser cathode surfaces are polycrystalline and porous In addition, their mechanism of activation and operation is complex, involving diffusion of Ba and O from the impregnant and desorption of the adsorbates from the surface Experimental measurements by Haas, Shih, and Marrian[3] have shown that a reasonable model consists of 1 ML of Ba and O on the W(001) surface Using low-energy electron-diffraction (LEED) and work-function measurements, they established that a $c(2\times2)$ structure and a minimum work-function value are achieved at this coverage

In the present work, the experimental two-dimensional band structure of the unoccupied electronic levels for 1 ML of Ba and O on W(001) is presented The measurements are compared with embedded-cluster-model calculations

This paper is organized as follows First, the experimental techniques and the computational details of the fully relativistic embedded-cluster-model approach are briefly described The experimental results are then compared with the calculated DOS Finally, the conclusions from the present study are summarized

II. EXPERIMENTAL TECHNIQUES

The experimental work was carried out in an all stainless-steel ultrahigh-vacuum chamber operated in the low 10^{-11}-Torr range This system is equipped with a double-pass cylindrical mirror analyzer for Auger monitoring of the surface composition and with LEED optics for monitoring the surface structure and orientation A detailed description of the experimental setup can be found elsewhere[16,17] and only its most important features are described here

Inverse photoelectron spectroscopy (IPS) measurements were performed in the isochromat mode at a photon energy of 9 8 eV by means of a photon detector designed after that of Babbe *et al* [18] and a low-energy electron gun, which was built for this experiment [19] The electron gun used a BaO cathode and was mounted at 40° relative to the detector The angle of electron incidence was varied by rotating the sample Count rates of several hundred counts per second were achieved with an electron-beam current of 5 μA The electron-beam angular divergence was estimated at better than 3°, giving a momentum resolution of approximately 0 1 Å^{-1}. The overall energy resolution of the spectrometer was approximately 0 6 eV

The W(001) crystal was cleaned in vacuum by repeated heating at 1700 K in an oxygen atmosphere of $6\ 0\times10^{-8}$ Torr followed by occasional flashing at 2500 K until cleanliness was confirmed by Auger-electron spectroscopy (AES), LEED, and IPS The target was also flashed before each deposition Ba was deposited onto the W(001) surface from a well-outgassed Ba source provided by the Philips Company Coverages were determined by a combination of $\Delta\phi$, LEED, and AES measurements Accurate measurements of the work-function change were performed using the retarding field method as described in Ref 17

Three methods were used to prepare 1 ML of BaO on W(001). These methods have been described in detail elsewhere [20]

In the first method, 1 ML of barium was adsorbed on the W(001) surface followed by exposure to 0 5 L (1 L = 1 Langmuir $=10^{-6}$ Torr sec) of oxygen at room temperature The work function of W(001) ($\phi=4$ 63 eV) (Ref 21) decreased to a minimum value of 2 29 eV at this coverage. In addition, a $c(2\times2)$ LEED pattern and an O to Ba Auger-line intensity ratio of 2 1 were obtained [3]

In the second method, the target was exposed to 0 5 L of oxygen at room temperature before the barium deposition was performed A work-function minimum value of 2 44 eV was obtained in this case. The room-temperature $p(4\times1)$ O/W(001) LEED structure was replaced by a $c(2\times2)$ structure at a Ba coverage corresponding to the minimum work function The O to Ba Auger ratio was similar to the one obtained in the first method In fact, we obtained a similar LEED structure and AES intensity ratio from BaO films on W(001), which were obtained by completely oxidizing a thick barium film and then annealing it at 1100 K for approximately 3 min, as described by Mueller *et al* [22]

In the third method, we exposed the W(001) surface to 0 5 L of oxygen at approximately 1100 K before performing the barium deposition We obtained a work-function minimum value of 2 38 eV, in the same range as for the previous methods In contrast to the first and second methods where a ML of Ba and O on the W(001) surface created a $c(2\times2)$ structure, the ML here retained the $p(2\times1)$ LEED structure of the first adsorbed annealed oxygen layer

To summarize, adsorption of 1 ML of BaO reduced the work function of the W(001) surface by approximately the same amount, regardless of the Ba and O deposition order and temperature treatment However, films obtained by annealing the O layer produced a completely different LEED pattern from those of the unannealed samples Therefore, the relationship between the geometrical structure and the work function is not unique in this case

In real space two adsorption geometries, tilted and upright, corresponding to the $c(2\times2)$ LEED pattern have been considered for the unannealed surface By comparing our experimental measurements with the results of embedded-cluster-model calculations, the structure of Ba and O adsorbed on W(001) can be determined

III. THEORETICAL APPROACH

We used fully relativistic embedded-cluster calculations to investigate the surface electronic structure of $c(2\times2)$ Ba and BaO on W(001). The computational approach employed was the Dirac-Slater scattered-wave method, which was originally developed by Yang, Rabii, and Case [23–25]

In the fully relativistic scattered-wave method, the Dirac wave equation is solved for muffin-tin potentials All electrons are treated self-consistently in a fully relativistic fashion The formalism includes the mass-velocity and Darwin corrections to the energy, as well as spin-orbit interaction through the use of spin-angular,

four-component wave functions in the framework of double-group theory Quasirelativistic calculations (without spin-orbit interaction) were carried out for comparison Slater's statistical $X\alpha$ local-density functional[26] was used for the treatment of exchange and correlation effects

The W(001) substrate was modeled with an atomic cluster consisting of 25 W atoms in two layers a 4×4 array was used for the surface layer and a 3×3 array for the subsurface layer A ML of Ba on W(001) was modeled by positioning the Ba atoms in the fourfold-hollow sites of the surface layer in a $c(2\times2)$ arrangement, resulting in a $Ba_5/W_{16}W_9$ cluster Three different heights for the Ba atom above the W(001) surface were investigated $z_{Ba}=4\ 31a_0$, $4\ 50a_0$, and $4.69a_0$ corresponding to 2 28, 2.38, and 2 48 Å, respectively ($a_0=0\ 5292$ Å) For Ba and O on W(001), two different adsorption sites were considered for oxygen In the first case, O was adsorbed in the vacant fourfold-hollow sites of the Ba/W(001) surface with $z_O=2\ 88a_0$ and $z_{Ba}=4\ 63a_0$, leading to a $Ba_5O_4/W_{16}W_9$ cluster In the second case, O was assumed to be adsorbed directly below Ba with $z_O=0\ 89a_0$ and $z_{Ba}=5\ 38a_0$, leading to a $Ba_5O_5/W_{16}W_9$ cluster These clusters are illustrated in Figs 1(a) and 1(b) The Ba and O heights were those optimized by Hemstreet, Chubb, and Pickett[13] using thin-film FLAPW calculations

The radii of the atomic spheres for the central atoms in each layer were chosen as 88% of the sphere radii, as determined in the standard fashion from the superposition of nonrelativistic atomic charge densities [27] The sphere radii of the surrounding atoms were set equal to those of the central atoms to simulate the equivalences of an extended surface The numerical potentials of the inner atoms were converged in an environment of identical potentials for the surrounding atoms This was accomplished by transferring the potentials from the inner to the outer atoms of the cluster at each iteration By using this approach, the inner atoms of the cluster were embedded in an additional shell of atoms that enforced a proper local environment representative of an extended surface

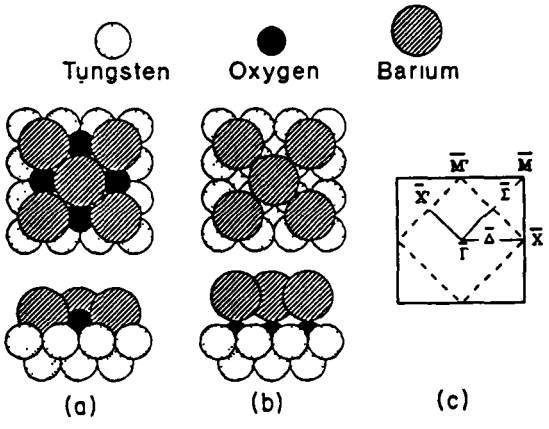

FIG 1 Top and side views of cluster models for a $c(2\times2)$ ML of Ba and O on W(001) in the (a) tilted and (b) upright configurations (c) illustrates the SBZ of the clean W(001) surface (solid square) and that of the $c(2\times2)$ BaO/W(001) system (dashed square)

Projected local densities of states were generated for the inner atoms by convoluting the calculated energies of the individual states with Gaussian functions with full widths at half maxima of 0 2 eV The DOS shown below for Ba and BaO and W include the contributions from one central Ba, O (for BaO/W), and W atom of the top layer of the cluster Although the unit cell for $c(2\times2)$ coverages contains one adatom per two tungsten atoms, the one-to-one ratio was chosen because the contributions from the atomic layers to the experimentally observed spectra are expected to decay rapidly below the uppermost adsorbed layer

IV. RESULTS

In this section, we present the results of our experimental measurements and theoretical calculations for the adsorption of 1 ML of Ba and O on W The IPS spectra were taken at different angles of electron incidence along the $\bar{\Gamma}\bar{\Delta}\bar{X}$ and $\bar{\Gamma}\bar{\Sigma}\bar{M}$ symmetry lines of the surface Brillouin zone (SBZ) of the clean unreconstructed W(001) surface, corresponding to the $\bar{\Gamma}'\bar{\Sigma}'\bar{M}'$ and $\bar{\Gamma}'\bar{\Delta}'\bar{X}'$ directions of the SBZ of the $c(2\times2)$ structure, respectively [cf Fig 1(c)] The spectra along the $\bar{\Gamma}\bar{\Delta}\bar{X}$ line were taken in the (001) mirror plane and those along $\bar{\Gamma}\bar{\Sigma}\bar{M}$ were taken in the (011) mirror plane of the W(001) $p(1\times1)$ structure The Fermi edge was determined from the onset of photon emission

To derive the experimental two-dimensional band structures, the component of the wave vector of the incoming electron parallel to the surface ($k_\parallel$) was determined using the equation

$$\hbar k_\parallel=[2m(E_i-\phi)]^{1/2}\sin\alpha\ ,$$

where α is the angle of electron incidence measured from the surface normal, E_i is the initial energy of the electron measured from E_F, and ϕ is the work function of the surface being studied A value of $\phi=2\ 63$ eV was used for 1 ML of Ba on W(001) and $\phi=2\ 37$ eV for 1 ML of Ba and O on W(001)

A. Ba on W(001)

IPS spectra for 1 ML of Ba on W(001) along the $\bar{\Gamma}\bar{\Delta}\bar{X}$ and $\bar{\Gamma}\bar{\Sigma}\bar{M}$ directions are shown in Figs. 2(a) and 2(b), respectively Upon adsorption of Ba, all the W(001) surface states[16,28] seem to have been completely quenched and new features appear above E_F

Along the $\bar{\Gamma}\bar{\Delta}\bar{X}$ symmetry line these features include two well-defined peaks located at 0 6 and 3 4 eV and two shoulders located at 2 3 and 2.7 eV above E_F A full description of these features can be found elsewhere [17]

Along the $\bar{\Gamma}\bar{\Sigma}\bar{M}$ symmetry line only two features are observed above E_F, one well-defined peak located at 0 6 eV and a broad peak near 3.4 eV. Both of these features appear only between $\alpha=0°$ and 28.5°. The peak located immediately above E_F shows a slight upward dispersion, while the one above the vacuum level (E_V) disperses

slightly downward in this symmetry direction

Calculated DOS for Ba heights of 2 28, 2 38, and 2 48 Å above the W substrate are shown in Fig 3 With the exception of differences associated with states possessing energies greater than 2 eV above E_F, it is found that the DOS is changed insignificantly as the Ba height is varied Although technically the only meaningful states associated with the calculations have energies less than the experimental vacuum level (2 7 eV), it is useful to monitor the behavior of states that have energies greater than the experimental vacuum level but smaller than the cluster vacuum level, provided these kinds of states have the potential to couple to the IPS process and can be observed as resonances We believe that a comparison between theory and experiment for states immediately above the experimental vacuum level is possible in this case, since the position of the calculated states with respect to the Fermi level is found to be insensitive to the separation between the vacuum level and the calculated Fermi level The final-state energy shifts due to the occupation of the empty electronic levels are found to be small (+0 1 eV)

Figure 4 shows the dispersion of all the observed peaks as a function of $k_{\parallel}$ in the left panel, and the theoretically calculated DOS for a Ba height of 2 38 Å above the W substrate in the right panel In contrast to *s* and *p* surface states that are observed with inverse photoemission for alkali-metal adsorption on transition metals,[29-31] the states in our case do not have free-electron-like dispersions Instead, all of the observed unoccupied states, with the exception of the one immediately above E_F, seem to possess little or no dispersion as is expected for states with significant *d* character Our theoretical analysis reveals that the state immediately above E_F contains a large Ba *d* contribution near 0 6 eV and a dominating W contribution in its dispersive part up to 1 6 eV

The peaks located at or below the vacuum level show strong sensitivity to surface contamination and are, therefore, assigned to transitions into Ba and W *d* surface states, a conclusion which is supported by the calculated cluster DOS The peak located near 3 4 eV above E_F, on the other hand, changes only slightly as a result of oxygen adsorption Therefore, we believe that this state comprises a W bulk component This is consistent with

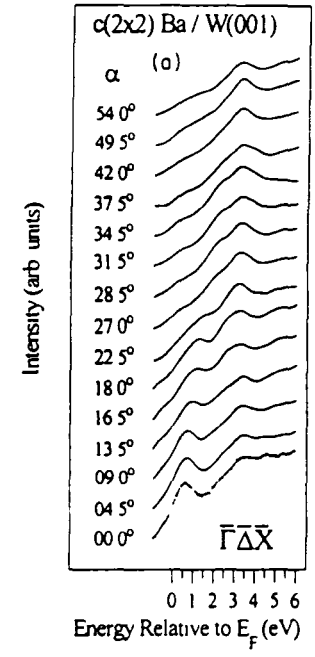

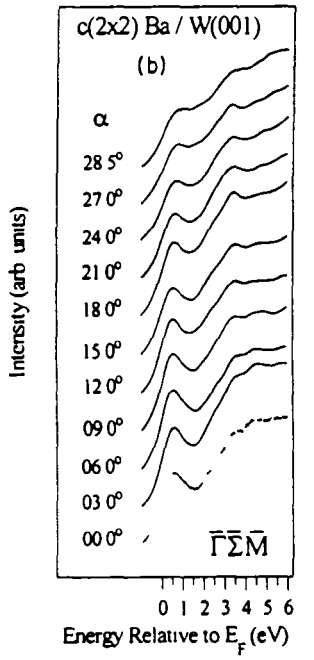

FIG 2 IPS spectra for a $c(2\times2)$ Ba overlayer on W(001) at different angles of incidence α taken along (a) the $\bar{\Gamma}\,\bar{\Delta}\,\bar{X}$ and (b) the $\bar{\Gamma}\,\bar{\Sigma}\,\bar{M}$ directions of the SBZ of clean W(001)

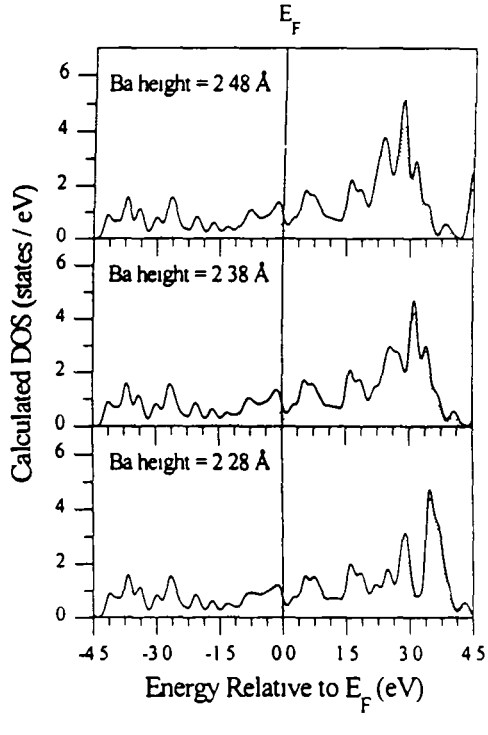

FIG 3 Fully relativistically calculated DOS for an ordered $c(2\times2)$ Ba adlayer on W(001) for three different Ba heights above the surface The total DOS are represented by solid lines and the Ba contributions by dotted lines

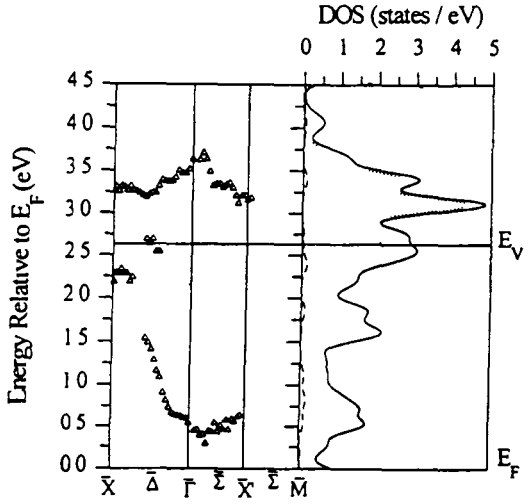

FIG 4 Left panel Experimental two-dimensional band structure for a $c(2\times2)$ Ba overlayer on W(001) along the $\bar{\Gamma}\bar{\Delta}\bar{X}$ and $\bar{\Gamma}\bar{\Sigma}\bar{M}$ symmetry lines of the unreconstructed W(001) surface Right panel Fully relativistically calculated DOS for a Ba height of 2 38 Å The solid line represents the total DOS, the dashed and dotted lines represent the Ba $s+p$ and d contributions, respectively

the DOS from LAPW calculations for a 19-layer W(001) film, which predict a strong feature near 3 5 eV above E_F originating from the inner layers of the film.[32] Furthermore, a bulklike state was observed near 3 5 eV in our IPS measurements of the clean unreconstructed tungsten surface The band from the unreconstructed surface and the one from 1 ML of Ba on W(001) overlap over large segments of the $\bar{\Gamma}\bar{X}$ and $\bar{\Gamma}\bar{M}$ lines [16,28] However, recent Ba on W(001) coverage-dependent data[33] taken in the $\bar{\Gamma}\bar{\Sigma}\bar{M}$ direction for angles close to 35° reveal a Ba-induced feature in the IPS spectra near 3.4 eV, a region where no tungsten unoccupied states are observed.[28] We therefore attribute the band near 3.4 eV to transitions into both Ba d and W bulk d states This is consistent with the DOS based on the present cluster model and also on FLAPW calculations by Hemstreet and Chubb[8] for a $c(2\times2)$ Ba adlayer placed on both sides of a five-layer W(001) film, which show a strong enhancement of the W-related peaks at 3 2 eV after adsorption of barium. Although our IPS measurements appear to indicate that both Ba and W contribute to the state near 3.4 eV above E_F, the cluster DOS seem to attribute this state almost entirely to Ba d orbitals. This apparent discrepancy is due to the fact that the employed cluster contains only two layers of W atoms, none of which is representative of bulk atoms

Overall, our experimental and theoretical results are in good agreement with the calculations of Hemstreet and Chubb[8] in that the same features are obtained above the Fermi level Their calculations confirm that the surface states and resonances of W(001) acquire significant admixture of Ba d surface states in the vicinity of E_F. In close agreement with the cluster results, their calculated DOS show broad peaks around 0 6 and 1 3 eV above E_F Their dominant Ba-related peak (for a Ba height of 2 48 Å) is located at 2 7 eV and virtually coincides with the cluster result for the same height (cf Fig 3) However, in our experimental spectra a peak at this energy appears only as a shoulder of the main peak at 3 5 eV; it is therefore likely that the Ba height of 2.48 Å is slightly too large.

B. BaO on W(001)

The IPS spectra for 1 ML of Ba and O on W(001) along the $\bar{\Gamma}\bar{\Delta}\bar{X}$ and $\bar{\Gamma}\bar{\Sigma}\bar{M}$ symmetry lines are shown in Figs 5(a) and 5(b), respectively. Spectra corresponding

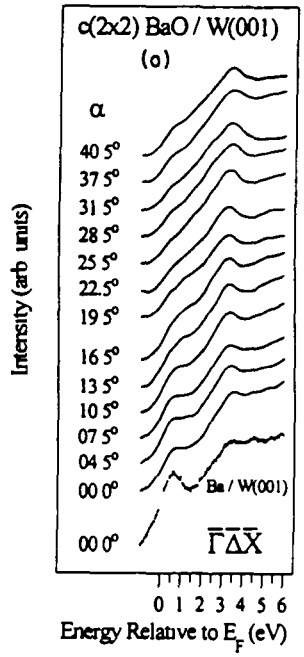

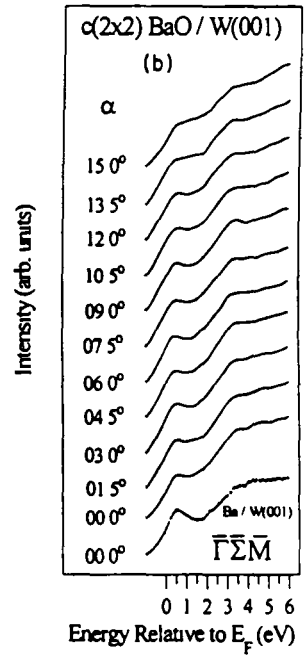

FIG 5 IPS spectra for a $c(2\times2)$ BaO overlayer on W(001) at different angles of incidence α taken along (a) the $\bar{\Gamma}\bar{\Delta}\bar{X}$ and (b) the $\bar{\Gamma}\bar{\Sigma}\bar{M}$ directions of the SBZ of clean W(001)

to a $c(2\times2)$ Ba monolayer on W(001) taken at normal incidence are shown at the bottom of Figs 5(a) and 5(b) for comparison Like the work-function results, the IPS spectra were also independent of the order of Ba and O adsorption on the surface at room temperature. Since IPS is a surface-sensitive technique, this suggests that the arrangement of the adatoms on the surface at room temperature is unique regardless of the order of deposition

Figure 6 illustrates the fully relativistically calculated cluster DOS for the upright and tilted geometries for the $c(2\times2)$ BaO adlayer on W(001) For comparison, we have also included the quasirelativistic DOS (without spin-orbit interaction) for the tilted geometry. Because the fully and quasirelativistic results for the tilted configuration differ significantly, only the fully relativistic treatment is appropriate

The experimental two-dimensional band structure is presented in Fig 7 along with the fully relativistically calculated DOS for the tilted configuration Only two features are observed above E_F for the BaO monolayer One is located near 0 6 eV and the other near 3 4 eV above E_F, which is 1 eV above E_V

The agreement with experiment for the lower-energy peaks located at 0 5 and 0 75 eV appears to be better for the upright configuration, as can be seen by comparing Figs 6 and 7 However, there is a disparity between the experimental results and the DOS for the upright configuration in that the major calculated peak at 1 5 eV is not observed along the two high-symmetry directions ($\bar{\Gamma}\bar{\Delta}\bar{X}$ and $\bar{\Gamma}\bar{\Sigma}\bar{M}$) probed experimentally Since it is very unlikely that the calculated peak centered around

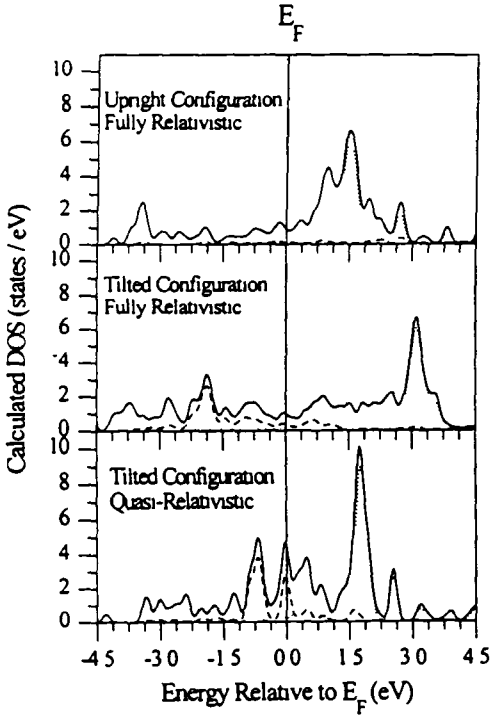

FIG 6 Quasirelativistically and fully relativistically calculated DOS for a $c(2\times2)$ BaO layer on W(001) for two different adsorption configurations (tilted and upright) Solid lines represent the total DOS, dashed and dotted lines represent the oxygen and barium contributions, respectively

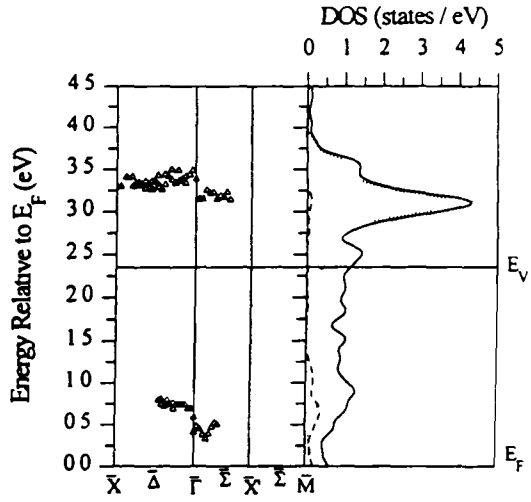

FIG 7 Left panel Experimental two-dimensional band structure for a $c(2\times2)$ BaO overlayer on W(001) along the $\bar{\Gamma}\bar{\Delta}\bar{X}$ and $\bar{\Gamma}\bar{\Sigma}\bar{M}$ symmetry lines of the unreconstructed W(001) surface Right panel Fully relativistically calculated DOS for BaO on W(001) in the tilted configuration The solid line represents the total DOS, the dashed and dotted lines represent the oxygen and barium contributions, respectively

1 5 eV has a component that would not be observed experimentally along high-symmetry directions, we believe that the tilted fully relativistic calculation provides the most suitable model This conclusion is supported by the appearance of a peak in the calculated DOS near the resonance observed experimentally at 3 4 eV

While the band near 3 4 eV changed only slightly after adsorption of oxygen, which is consistent with this state having a W bulk component, the band near 0 6 eV changed significantly In contrast to Ba on W(001), the band near 0 6 eV does not disperse in the $\bar{\Gamma}\bar{\Delta}\bar{X}$ direction It is totally quenched with oxygen adsorption exceeding 1.0 L IPS data for 0.5 L of oxygen on W(001) reveal several oxygen-induced unoccupied states [34] However, the calculated DOS for 1 ML of BaO on W(001) show only small O contributions in the 0.5–1 0-eV energy range We believe that the absence of dispersion of the observed Ba states and the relatively small contributions of O unoccupied states above E_F, in the case of Ba and O on the W(001) surface, are the result of electronic charge transfer from W and Ba to O. This charge transfer causes these states to become more localized and, therefore, less dispersive. In addition, a Ba-O surface dipole resulting from the charge transfer from barium to oxygen is created This dipole opposes and more than compensates for the W-O dipole and is believed to contribute to the net surface dipole responsible for lowering the work function of the surface.

Finally, the nondispersing bands, which were observed for 1 ML of Ba on W(001) at 2 3 and 2 6 eV, are totally quenched after adsorption of O, presumably due to them being moved above the vacuum level as a result of the slight reduction of the work function and due to the consolidation of the different Ba peaks into one major feature in the case of BaO on W (cf. Figs 4 and 7)

V. SUMMARY AND CONCLUSIONS

The chemisorption of Ba and O on W(001) was studied with inverse photoelectron spectroscopy and relativistic cluster calculations Adsorption of Ba and BaO created $c(2\times2)$ LEED structures at ML coverages The behavior of the unoccupied electronic states above E_F was investigated at this coverage It is shown that the observed unoccupied states possess strong Ba d character The states between 0 5 and 2 5 eV contain contributions from Ba and W surface states The state near 3 5 eV, which is observed for both Ba and BaO on W(001), is believed to originate from transitions into Ba d surface and W d bulk states

Oxygen adsorption quenches the Ba/W(001) states located at 2 3 and 2 7 eV and causes the loss of dispersion in the feature near 0 6 eV This, and the absence of unoccupied O levels, can be explained by electronic charge transfer from Ba and W to O The additional Ba-O dipole counteracts the W-O dipole, and is believed to be responsible for reducing the work function and enhancing emission from the BaO/W(001) surface relative to Ba/W(001)

The work function of W(001) ($\phi=4$ 63 eV) was reduced to 2 3–2 4 eV upon adsorption of 1 ML of Ba and O The value of the work function, the LEED structure, and the IPS spectra are independent of the order of Ba and O deposition at this coverage

Overall, the fully relativistically calculated DOS for $c(2\times2)$ Ba and BaO (in the tilted configuration) on W(001) are found to be in reasonably good agreement with the experimental results

ACKNOWLEDGMENTS

We would like to thank Lou Maschak for his assistance with the experimental setup and Ben Ebihara for designing the Ba source We would also like to thank Dr L A Hemstreet for sending us a copy of his work on Ba/W(001) before publication. This work was supported by NASA under Contract No NAS3-25940 and the National Research Council

[1]G A Haas, H F Gray, and R E Thomas, J Appl Phys **46**, 3293 (1975)
[2]R Forman, Appl Surf Sci **2**, 258 (1979)
[3]G A Haas, A Shih, and C R K Marrian, Appl Surf Sci **16**, 139 (1983)
[4]D Brion, J C Tonnerre, and A M Shroff, Appl Surf Sci **16**, 55 (1983)
[5]G A Haas, C R K Marrian, and A Shih, Appl Surf Sci **24**, 430 (1985)
[6]R Forman, J Appl Phys **47**, 5272 (1976)
[7]G A Haas, R E Thomas, C R K Marrian, and A Shih, Appl Surf Sci **40**, 277 (1989)
[8]L A Hemstreet and S R Chubb, Phys Rev B **47**, 10748 (1993), L A Hemstreet (private communication)
[9]E Wimmer, A J Freeman, J R Hikes, and A M Karo, Phys Rev B **28**, 3074 (1983)
[10]D M Riffe, G K Wertheim, and P H Citrin, Phys Rev Lett **64**, 571 (1990)
[11]D Norman, R A Tuck, H B Skinner, P J Wadsworth, T M Gardiner, I W Owen, C H Richardson, and G Thornton, Phys Rev Lett **58**, 519 (1987)
[12]G Thornton, I W Owen, C H Richardson, D Norman, R A Tuck, H B Skinner, P J Wadsworth, and T M Gardiner, Vacuum **38**, 401 (1988)
[13]L A Hemstreet, S R Chubb, and W E Pickett, Phys Rev B **40**, 3592 (1989), J Vac Sci Technol A **6**, 1063 (1988)
[14]A Shih, C Hor, W Elam, J Kirkland, and D Mueller, Phys Rev B **44**, 5818 (1991)
[15]W Muller, IEEE Trans Electron Devices **36**, 180 (1989), J Vac Sci Technol A **6**, 1072 (1988)
[16]I L Krainsky, J Vac Sci Technol A **5**, 735 (1987)
[17]A Lamouri and I L Krainsky, Surf Sci **278**, 286 (1992)
[18]N Babbe, W Drube, I Schafer, and M Skibowsky, J Phys E **18**, 158 (1985)
[19]I L Krainsky, Rev Sci Instrum **62**, 1746 (1991)
[20]A Lamouri, I L Krainsky, and W Muller, Surf Interface Anal **21**, 150 (1994)
[21]R L Billington and T N Rhodin, Phys Rev B **41**, 1602 (1978)
[22]D Mueller, A Shih, E Roman, T Madey, R Kurtz, and R Stockbauer, J Vac Sci Technol A **6**, 1067 (1988)
[23]C Y Yang and S Rabii, Phys Rev A **12**, 362 (1975)
[24]C Y Yang, J Chem Phys **68**, 2626 (1978)
[25]D A Case and C Y Yang, J Chem Phys **72**, 3443 (1980)
[26]J C Slater, Adv Quantum Chem **6**, 1 (1972)
[27]J G Norman, Jr , Mol Phys **31**, 1191 (1976)
[28]A Lamouri and I L Krainsky, Surf Sci **303**, 341 (1994)
[29]W Jacob, E Bertel, and V Dose, Phys Rev B **35**, 5910 (1987)
[30]D Heskett, K H Frank, E E Koch, and H J Freund, Phys Rev B **36**, 1276 (1987)
[31]R Dudde, K H Frank, and B Reihl, Phys Rev B **41**, 4897 (1990)
[32]L F Mattheiss and D R Haman, Phys Rev B **29**, 5372 (1984)
[33]A Lamouri and I L Krainsky (unpublished)
[34]I L Krainsky, J Vac Sci Technol A **6**, 780 (1988)

REPORT DOCUMENTATION PAGE

Form Approved
OMB No 0704-0188

1 AGENCY USE ONLY (*Leave blank*)	2. REPORT DATE	3. REPORT TYPE AND DATES COVERED
	August 1995	Final Contractor Report

4 TITLE AND SUBTITLE

Theoretical Study of Cathode Surfaces and High-Temperature Superconductors

5. FUNDING NUMBERS

WU-235-01-03-0A
C-NAS3-25940

6 AUTHOR(S)

Wolfgang Mueller

7 PERFORMING ORGANIZATION NAME(S) AND ADDRESS(ES)

Analatom, Inc
29904 Sycamore Oval
Westlake, Ohio 44145

8 PERFORMING ORGANIZATION REPORT NUMBER

E-9839

9 SPONSORING/MONITORING AGENCY NAME(S) AND ADDRESS(ES)

National Aeronautics and Space Administration
Lewis Research Center
Cleveland, Ohio 44135-3191

10. SPONSORING/MONITORING AGENCY REPORT NUMBER

NASA CR-198379

11 SUPPLEMENTARY NOTES

Project Manager, Edwin G Wintucky, Space Electronics Division, NASA Lewis Research Center, organization code 5620, (216) 433-3510.

12a DISTRIBUTION/AVAILABILITY STATEMENT

Unclassified - Unlimited
Subject Categories 23 and 76

This publication is available from the NASA Center for Aerospace Information, (301) 621-0390

12b DISTRIBUTION CODE

13 ABSTRACT (*Maximum 200 words*)

Calculations are presented for the work functions of BaO on W, Os, Pt, and alloys of Re-W, Os-W, and Ir-W that are in excellent agreement with experiment The observed emission enhancement for alloy relative to tungsten dispenser cathodes is attributed to properties of the substrate crystal structure and explained by the smaller depolarization of the surface dipole on hexagonal as compared to cubic substrates. For Ba and BaO on W(100), the geometry of the adsorbates has been determined by a comparison of inverse photoemission spectra with calculated densities of unoccupied states based on the fully relativistic embedded cluster approach. Results are also discussed for models of scandate cathodes and the electronic structure of oxygen on W(100) at room and elevated temperatures A detailed comparison is made for the surface electronic structure of the high-temperature superconductor $YBa_2Cu_3O_7$ as obtained with non-, quasi-, and fully relativistic cluster calculations.

14 SUBJECT TERMS

Dispenser cathodes; Emission enhancement, Work function calculations; Electronic structure calculations, High-temperature superconductors

15 NUMBER OF PAGES
82

16 PRICE CODE
A05

17 SECURITY CLASSIFICATION OF REPORT	18 SECURITY CLASSIFICATION OF THIS PAGE	19. SECURITY CLASSIFICATION OF ABSTRACT	20. LIMITATION OF ABSTRACT
Unclassified	Unclassified	Unclassified	

End of Document